NASA
Technical
Paper
2918

1989

Effect of Milling Machine Roughness and Wing Dihedral on the Supersonic Aerodynamic Characteristics of a Highly Swept Wing

Christine M. Darden
Langley Research Center
Hampton, Virginia

NASA
National Aeronautics and Space Administration
Office of Management
Scientific and Technical Information Division

Summary

An experimental investigation was conducted to assess the effect of surface finish on the longitudinal and lateral aerodynamic characteristics of a highly swept wing at supersonic speeds. The investigation also included a study of the effects of wing dihedral. Included in the tests were four wing models: three models having 22.5° of outboard dihedral, identical except for surface finish; and a zero-dihedral, smooth model of the same planform for reference. Of the three dihedral models, two were taken directly from the milling machine without smoothing—one having a maximum scallop height of 0.002 in. and the other a maximum scallop height of 0.005 in. The third dihedral model was hand finished to a smooth surface.

Tests were conducted in Test Section 1 of the Langley Unitary Plan Wind Tunnel over a range of Mach numbers from 1.8 to 2.8, a range of angles of attack from −5° to 8°, and at a Reynolds number per foot of 2×10^6. Selected data were also taken at a Reynolds number per foot of 6×10^6. Drag coefficient increases, with corresponding lift-drag ratio decreases, were the primary aerodynamic effects attributed to increased surface roughness due to milling machine grooves. These drag and lift-drag ratio increments due to roughness increased as Reynolds number increased.

Introduction

Subscale wind-tunnel models require precision in definition and in fabrication to accurately replicate the surface of a full-scale configuration. Precise definition of a model is simplified considerably when the model is numerically defined and then machined by a numerical control (NC) milling machine—a computerized system in which the path of the cutting tool is controlled by the previously stored numerical description of the three-dimensional model. When these machines were introduced into the model fabrication process, they produced considerable savings of time and money by eliminating the usual trial and error machining process (refs. 1 and 2). Typically, the NC machinist makes use of spherical cutting tools to machine the complex curved surface found on most models. The spherical cutting tools only cut to the desired model surface at the center of the tool and leave ridges or scallops to either side of the center. The size of the cutting tool and the spacing between each cutting pass determine the number of passes necessary to cut a given area and the height of the scallops left in the metal. Thus, for a given size cutting tool, a smaller step size between passes leaves smaller scallops in the metal but requires more passes to cut the same area.

Even though a new era of model construction was introduced with the NC milling machine, the entire process was not automated. Aerodynamicists required a smooth surface finish within a small tolerance to the required measurements. This smooth surface is typically generated by final hand sanding and filing of the model to the required surface finish. This final step in the process still requires many man-hours to complete. Conversations with experienced model makers indicate that, on steel models of approximately 2.5 ft^2 reference area, this final smoothing requires an estimated 300 to 400 man-hours or about one-third to one-half of the total model construction time. The amount of time required for the filing and sanding in this final step is a function of the height of the remaining scallops. Since the entire model fabrication process is optimized by doing as much work as possible on the NC machine, even when final finishing is required, the number of passes is increased to minimize the resulting scallop heights. If the hand finishing of the models could be entirely eliminated, a considerable savings of time and money would result.

This study investigates the effect of model surface finish obtained during the model milling process on wind-tunnel force data. Three highly swept models, which contained dihedral of 22.5° on the outer wing panel, and which were identical except for surface finish (two with different scallop heights and one smooth), were tested over Mach numbers ranging from 1.8 to 2.8, and the results of force tests for each model are compared. The effect of Reynolds number was investigated by conducting tests at Reynolds numbers per foot of 2×10^6 and 6×10^6. As a further investigation in the test, a fourth model with zero-dihedral and a smooth surface was tested to compare results with the smooth dihedral model to assess dihedral effects on this highly swept planform.

Schlieren, vapor-screen, and oil flow photographs are also included. Preliminary results of this study were published in reference 3.

Symbols

Force and moment data are referenced to the body-axis system except for lift and drag, which are referenced to the stability-axis system. The moment reference center for the model is located 1.431 ft from the nose. The symbols in parentheses are used in the data tables of appendix D.

b		wing span, 2 ft
bal		balance
C_A	(CA)	axial-force coefficient, $\frac{\text{Axial force}}{qS}$
	(CAC)	axial-force coefficient due to model balance-housing pressure coefficient
C_D	(CD)	drag coefficient, $\frac{\text{Drag}}{qS}$
	(CDC)	drag coefficient due to model balance-housing chamber pressure coefficient
C_L	(CL)	lift coefficient, $\frac{\text{Lift}}{qS}$
C_l		rolling-moment coefficient, $\frac{\text{Rolling moment}}{qSb}$
C_{l_β}		roll-stability parameter, per degree, $\frac{C_l\|_{\beta=3^\circ} - C_l\|_{\beta=0^\circ}}{3}$
C_m	(CM)	pitching-moment coefficient, $\frac{\text{Pitching moment}}{qS\bar{c}}$
C_N	(CN)	normal-force coefficient, $\frac{\text{Normal force}}{qS}$
C_n		yawing-moment coefficient, $\frac{\text{Yawing moment}}{qSb}$
C_{n_β}		directional-stability parameter, per degree, $\frac{C_n\|_{\beta=3^\circ} - C_n\|_{\beta=0^\circ}}{3}$
C_Y		side-force coefficient, $\frac{\text{Side force}}{qS}$
C_{Y_β}		side-force parameter, per degree, $\frac{C_Y\|_{\beta=3^\circ} - C_Y\|_{\beta=0^\circ}}{3}$
$\bar{c}$		wing reference chord, 1.6861 ft
H_o		total pressure, psf
L/D	(L/D)	lift-drag ratio, C_L/C_D
M	(MACH)	Mach number
q	(DYN PRS)	dynamic pressure, psf
R/ft	(R/FT)	Reynolds number per foot
S		reference area, 2.5375 ft^2
T_o		total temperature, °F
x		longitudinal distance from nose of model (see fig. 1), ft
y		coordinate in spanwise direction (see fig. 1), ft
z		coordinate in vertical direction (see fig. 1), ft
α	(ALPHA)	angle of attack, deg

β	angle of sideslip, deg
β'	$\sqrt{M^2 - 1}$
Λ	local leading-edge sweep angle, deg

Description of Models

The planform used in this study is characterized by a complex leading-edge shape with generally high sweep. A similar planform has been tested previously in references 4 and 5. The planform is shown in figure 1 and described in table I. Note that the leading-edge sweep angles vary with spanwise position and for Mach 2.4 (the design Mach number) produce velocity components normal to the leading edge that vary from low subsonic over much of the inboard region to nearly sonic for the outboard region. A minimum body with a feathered (i.e., no base area) base was included to house the strain-gage balance and support sting.

Table I. Model Planform Definition

Spanwise stations	Leading edge	Trailing edge
$0 \leq y \leq 0.3$	$x = 12y^2$	$x = 1.388097y^2 + 2.58618$
$0.3 \leq y \leq 0.6$	$x = 0.6377349 + 2.523619(y - 0.2692869)^{1/2}$	$x = 0.83286(y - 0.3) + 2.71111$
$0.6 \leq y \leq 0.95$	$x = 2.19418(y - 0.6) + 2.08901$	$x = 0.83286(y - 0.3) + 2.71111$
$0.95 \leq y \leq 1.0$	$(x - 3.106973)^2 + (y - 0.3971721)^2 = 0.3634$	$x = 0.83286(y - 0.3) + 2.71111$

The investigation included tests of four uncambered models. Three of the models were used to investigate roughness effects and were identical except for surface finish and contained dihedral of 22.5° on the outboard panel of the wing. To investigate effect of dihedral, a fourth, zero-dihedral model with a smooth finish was included. All models had a 3-percent-thick parabolic arc airfoil.

The three dihedral models were cut with a 1-in.-diameter milling tool. The cutting-path spacing was varied so that the maximum resulting scallop heights were 0.005 in. and 0.002 in. for the first two models, and the third was hand finished to a smooth surface. The model with maximum scallop height of 0.005 in. and the smooth model were the same model tested before and after smoothing. The model with the maximum scallop height of 0.002 in. was a separately constructed model. The method of determining the maximum step size allowable between tool passes and the number of passes required to cut each model is included in appendix A. The model with maximum scallops of 0.005 in. will be referred to as the "rough" model. The model with maximum scallops of 0.002 in. will be referred to as the "medium" model. The third model, which had been hand finished, will be referred to as the "smooth" model. The models were cut along a constant percent chord, with 220 passes necessary to cut the rough model and 347 passes necessary to cut the medium model. The number of passes is determined by the maximum scallop height at longest chord, and thus the scallop height on the outboard portions of the wing is an order of magnitude smaller because of the smaller step size between passes.

Photographs of the wind-tunnel models are shown in figures 2(a) through 2(e). Note in figures 2(c), 2(d), and 2(e) that the scallops left by the milling tool follow a constant percent chord and thus vary with their local orientation to the wind—in some places nearly aligned and in others nearly perpendicular. A very noticeable difference in the scallops between the medium and rough models can be observed in the region near the centerline, where, because of the cutting path, the scallops reach their maximum heights for the two models. Note that the scallop orientation is nearly streamwise on the top of the minimum balance housing.

Test Program and Apparatus

Wind-tunnel tests were conducted in Test Section 1 of the Langley Unitary Plan Wind Tunnel. The cross section dimensions of the test section are 4 ft by 4 ft, and the allowable Mach number range is from 1.47 to 2.87. Further information on this tunnel is available in reference 6.

Tests were conducted at Mach numbers ranging from 1.8 to 2.8, angles of attack ranging from $-5°$ to $8°$, and at a Reynolds number per foot of 2×10^6 with selected data taken at a Reynolds number per foot of 6×10^6. A 0.063-in.-wide strip of No. 50 Carborundum grit was applied and sized according to reference 7 and was located 0.4 in. aft of the model leading edge in the streamwise direction. Tests were conducted during several different tunnel entries over a period of several years. Total temperature differences between tests were sometimes necessary because of power availability and outside temperatures. Specific test conditions for the tests can be found in appendix B.

Aerodynamic forces and moments were measured by means of a six-component strain-gage balance contained within the model. The balance was attached through a supporting sting to the permanent strut support system in the wind tunnel. Model balance chamber pressures were measured by means of two tubes routed along the sting and connected to two pressure tranducers outside the tunnel. These pressures were measured throughout the test program in order to correct the data to a condition of free-stream static pressure acting over the total model base area. The data were also corrected for deflections of the balance-sting combination due to aerodynamic loads and for test-section flow angularity.

Because the aerodynamic loads differed by approximately a factor of three between $R/\text{ft} = 2 \times 10^6$ and 6×10^6, two different balances were employed to provide similar levels of aerodynamic coefficient accuracy. The coefficient is based on a balance accuracy of one-half of one percent of the full-scale capacity of each of the six components. The coefficient accuracy for each of the test conditions is found in appendix C.

Vapor-screen, oil flow, and schlieren photographs were obtained at several Mach numbers and several angles of attack. For vapor-screen photographs, model preparation consisted of painting one coat of flat black paint over a coat of zinc chromate primer to reduce the glare. White dots (reference marks) were painted on the model upper-surface centerline at locations where vapor-screen data were desired. A high-intensity mercury vapor light source mounted outside the tunnel was used to produce a thin light sheet across the tunnel test section. The light sheet was oriented normal to the flow and was positioned so that the model could be moved longitudinally to align the light sheet with the white dot reference positions. Photographs were taken by a camera mounted to the ceiling inside the tunnel and located approximately 3 ft downstream from the model. For further information on the procedure for obtaining vapor-screen photographs, see reference 8.

For the oil flow photographs, the model surfaces were painted flat black and then brushed with a mixture of 90-weight oil and yellow fluorescent dye. The model was illuminated by ultraviolet lamps, and photographs were taken through the window of the test section by using two cameras mounted outside the tunnel. Photographs were taken with the model rolled 90° (wings vertical). After the model was positioned in the tunnel, approximately 3 to 4 minutes were required for the oil flow pattern to develop. Normally, three or four different angles of attack could be photographed before the oil needed replenishment. Additional information on the oil flow technique can be found in reference 9.

Schlieren photographs of the flow field were made for several of the test conditions. A complete description of the schlieren system and its principles of operation may be found in references 6 and 10.

Boundary-Layer Considerations

It is expected that the largest increments in the aerodynamic coefficients between the three different surface finishes would occur for the drag. These increments in drag could result from (1) protuberance drag—drag that results from the scallop ridges protruding through the boundary layer; (2) roughness drag due to the scallops acting like an equivalent roughness, which increases the skin friction drag (see ref. 11); (3) wave drag—drag due to the slight increase in volume caused by the scallop ridges; and (4) transition effects—variations in skin friction drag due to different locations of boundary-layer transition. It is beyond the scope of this paper to determine the exact extent to which protuberance, roughness, and wave drag affect the drag increments. In order to minimize transition effects, a transition grit strip was employed. According to references 7, 12, and 13, No. 50 Carborundum grit, located 0.4 in. downstream from the leading edge, is of sufficient height to ensure immediate transition for $R/\text{ft} = 6 \times 10^6$ at all Mach numbers tested. However, at the lower test Reynolds number, only references 7 and 12 predict transition at the transition grit strip. In reference 13, studies conducted on a 55° delta wing measured transition at Mach 2.4 at about 1 in. behind the transition grit and at Mach 2.8 at about 2 in. behind the grit strip for $R/\text{ft} = 2 \times 10^6$. The greater sweep of the present model would likely promote additional crossflow-induced boundary instabilities that would promote earlier transition. Hence it is assumed that the boundary-layer transition is sufficiently close to the grit strip such that transition effects on drag variation are negligible. Therefore, at a given Reynolds number, differences in drag may occur because of differences in proturberence drag, roughness drag, and/or wave drag.

Presentation of Data

A schedule of the tabulated data and tunnel conditions is located in appendix B and the tabulated data for the tests are located in appendix D. Plots of the longitudinal aerodynamic characteristics of the models are given in figures 3 through 9. Lateral-directional stability parameter plots are given in figure 10. Flow visualization results are presented in figures 11 to 21.

Results and Discussion

Because two balances and two different Reynolds numbers were used in the tests in addition to models with varying surface finishes, the data will initially be examined for differences due to balance accuracy and Reynolds number effects. Differences due to surface finish and the effect of dihedral will then be examined at $R/\mathrm{ft} = 2 \times 10^6$.

Balance Accuracy Effects

The effect of balance accuracy on the longitudinal aerodynamic characteristics for the rough model at $R/\mathrm{ft} = 2 \times 10^6$ is shown in figures 3 and 4. See appendix C for balance accuracy values. Note that for the drag polar shown on figure 3(a), there is essentially no difference (less than one count) in the drag level indicated for the two balances between $C_L = -0.18$ and $C_L = 0.14$. Near $C_L = 0.22$, the drag measured by balance 845 is 5 to 7 counts higher than that for balance 740. The agreement between the L/D curves from the two different balances displays the same trend—excellent agreement up to $C_L = 0.14$, and slight deviations beyond.

The pitching-moment data from the two balances show excellent agreement throughout the lift range shown on figure 3(b). Some variation of the results from the two balances again becomes evident in the lift curve where at both negative angles of attack and positive angles of attack the lift measured with balance 740 has a slightly larger magnitude than that measured with balance 845, but this variation is on the order of the accuracy of the two balances.

Comparisons of balance effects at Mach 2.4 (fig. 4) are similar to those shown at Mach 2.0. At $R/\mathrm{ft} = 2 \times 10^6$, the results from the two balances agree up to the higher lift coefficients, where for the drag polar, balance 845 gives slightly higher values of drag. Similarly, differences occur on the lift curve at the higher angles of attack.

These results indicate that comparisons can be made reliably between data from balances 740 and 845 at low lift and angles of attack. When evaluating the data at higher lift coefficients and angles of attack, the previously considered balance accuracy effects must be considered.

Reynolds Number Effects

The effect of Reynolds number on lift, drag, and pitching moment is also shown in figures 3 and 4. On the drag polar, results for moderate lift coefficients are 3 to 5 counts lower in drag for the rough model, due only to Reynolds number changes. Reynolds number effects on L/D are fairly significant between $C_L = 0.04$ and 0.18, with a smaller effect at the negative lift coefficients. The tests at $R/\mathrm{ft} = 6 \times 10^6$ were made with balance 845, and the tests at $R/\mathrm{ft} = 2 \times 10^6$ were made with balance 740. At Mach 2.0, shown on figure 5, the drag of the smooth model at $R/\mathrm{ft} = 2 \times 10^6$ varies from about 2 counts less than that on the rough model near $C_L = 0$ to approximately the same level at both the higher and lower values of C_L. At $R/\mathrm{ft} = 6 \times 10^6$, near $C_L = 0$, the smooth model is about 7 counts lower in drag than the rough model.

Because of the presence of the turbulent boundary layer, the external flow is displaced. This displacement thickness is inversely proportional to the Reynolds number and, therefore, is larger for $R/\mathrm{ft} = 2 \times 10^6$ than for 6×10^6. Flat plate turbulent boundary-layer approximations (refs. 14 and 15) indicate that the displacement thickness for $R/\mathrm{ft} = 6 \times 10^6$ exceeds the maximum scallop height at a distance of about 2 to 3 times farther downstream from the leading edge than for $R/\mathrm{ft} = 2 \times 10^6$.

Hence, a greater protuburence and roughness type drag would likely result at the higher Reynolds number. Further information would be required to determine the exact cause of the difference in the drag increments between the rough and smooth models at the two Reynolds numbers, but clearly the scallop heights have a greater effect on drag at $R/\text{ft} = 6 \times 10^6$. The effect of Reynolds number tends to disappear at both the lower and higher lift coefficients.

There is essentially no difference in the L/D curves for the rough and smooth models at $R/\text{ft} = 2 \times 10^6$ throughout the investigated lift range. As shown in figure 5(b), the pitching-moment and angle-of-attack curves exhibit very little effect of Reynolds number, balance, or roughness except for a slight variation in lift at the highest and lowest angles of attack, which may be due to the previously discussed balance accuracy limitations.

Figure 6 shows the comparison of the rough and smooth models at the two Reynolds numbers for a Mach number of 2.4. Again, the Reynolds number effects on drag differences are quite apparent. At $R/\text{ft} = 6 \times 10^6$, there is a significant difference in the drag levels and the L/D levels of the smooth and the rough models. At $R/\text{ft} = 2 \times 10^6$, however, the differences in the results range up to about 2 drag counts near $C_L = 0$. Though there appears to be some scatter in the data for the smooth model at $R/\text{ft} = 6 \times 10^6$, the trend of these data generally agrees with that at Mach 2.0.

The pitching-moment data, like those at Mach 2.0, show no effect of roughness, balance, or Reynolds number. In the C_L versus angle of attack curve, it is assumed that the deviation in the data at high angles of attack may be attributed to the different balances, as seen in figures 3 and 4.

Results of data taken at the two Reynolds numbers indicate that there is a significant effect of Reynolds number on the surface roughness induced drag and on the L/D differences. Surface finish becomes more critical at the higher Reynolds numbers. The remainder of the force plots show the results of data from the smooth model, the medium model (maximum scallop height of 0.002 in.), and the rough model (maximum scallop height of 0.005 in.) at the test Reynolds number per foot of 2×10^6 with balance 740. Results from the zero-dihedral, smooth model are also included on these figures but will be discussed in the section on dihedral effects.

Surface Finish Effects

The drag polars for the three dihedral models at Mach 2.0 , shown on figure 7(a), are essentially the same, as are the L/D curves. On figure 7(b), the pitching-moment curve has essentially the same slope throughout the lift range shown. The pitching moment for the medium model differs slightly from the other dihedral models at the negative lift coefficients, but because the rough and smooth models give practically the same values, this difference is probably not attributable to surface finish. The same trend is observable for the lift curve shown in figure 7(b). All the results show the same general lift curve slope; however, there are differences of up to 0.3° for a given value of lift.

Results for Mach 2.4 are shown on figure 8. The drag and L/D values for the three dihedral models again agree very well except at the negative lift coefficients, where the results for the medium model show slightly higher levels of drag and slightly higher levels of L/D. Again, the rough and smooth models have excellent agreement at these lift coefficients. Near $C_L = 0$, where the effects of roughness had shown up previously, the three models differ by only 1 to 2 drag counts, which is within the accuracy of the balance.

The pitching-moment and lift curves on figure 8(b) display the same general trends as at Mach 2.0, except that the pitching-moment curve for the medium model is consistently higher than for the other two models by about 0.002. Results for Mach 2.8, shown in figure 9, show excellent agreement for all three dihedral models.

Figure 10 shows the effect of scallop height on the lateral-directional stability parameters as a function of angle of attack. There is no apparent effect of the scallop height on any of the stability results, either for angle of attack or with Mach number for the ranges tested.

Generally, the results shown on figures 7 to 10 would indicate that at a test Reynolds number of 2×10^6, any differences in force data between the models are within the accuracy of the balance at the model test conditions. In the instances where the rough and smooth models have better agreement than the medium and smooth, it would appear that the reasons are attributable either to some slight difference in test condition for the medium model or to the fact that the rough and smooth models were the same model, tested before and after smoothing, and the medium model was a separate model, but not to the surface finish of the model itself.

Dihedral Effects

Dihedral effects can be assessed by comparing results from the flat, zero-dihedral wing with those from the smooth dihedral wings. The effects on the longitudinal data are shown in figures 7, 8, and 9 and those on the lateral-directional stability parameters in figure 10. Generally the same trend in longitudinal data between the flat wing and the dihedral wings is evident at the three Mach numbers shown. Near $C_L = 0$, drag levels for the flat wing vary from the same levels as the dihedral wings to 1 to 2 counts lower. The most significant difference occurs at the higher lift coefficients where the flat wing drag is approximately 4 counts lower than the dihedral wing drag at Mach 2.0. This difference increases to approximately 8 counts for Mach 2.8. Comparable increases in L/D for the flat wing occur at the higher lift coefficients.

The largest effect of dihedral is apparent in the lateral-directional stability parameters shown in figure 10. The yawing-moment derivative increases because of dihedral, and the rolling-moment derivative and the side-force derivative decrease because of dihedral.

Flow Visualization Photographs

In addition to longitudinal- and lateral-force data and derivatives, flow visualization provides valuable information to the aerodynamicist. Through the use of oil flow, schlieren, and vapor-screen photographs, the researcher is able to identify flow phenomena such as separation, leading-edge vortices, and shocks, all of which affect the resulting forces and moments on the aircraft. If meaningful flow visualization is hampered by the milling machine scallops, then these models are not acceptable to the aerodynamicist.

Oil Flow Photographs

To assess the effect of the scallops on oil flow visualization, several photographs are included (figs. 11 through 17). Oil flow visualization photographs were not obtained for the smooth or medium dihedral models. They were, however, obtained for the rough dihedral at both Reynolds numbers at Mach 2.0 and Mach 2.4. Photographs were taken of the top and bottom of the model at several angles of attack. To provide a comparison, oil flow photographs of the smooth flat model at two angles of attack are included. A schedule of the oil flow photographs is included in table II.

Table II. Oil Flow Photograph Schedule

Figure	Model	Angle of attack, deg	Mach number	Reynolds number	Side viewed
11(a)	Flat	0	2.4	2×10^6	Top
(b)		5			
12(a)	Rough	−5	2.4	2×10^6	Bottom
(b)		0			
(c)		5			
13(a)	Rough	−5	2.4	2×10^6	Top
(b)		0			
(c)		5			
14(a)	Rough	−5	2.0	6×10^6	Bottom
(b)		0			
(c)		5			
15(a)	Rough	−5	2.0	6×10^6	Top
(b)		0			
(c)		5			
16(a)	Rough	−5	2.4	6×10^6	Bottom
(b)		0			
(c)		5			
17(a)	Rough	0	2.4	6×10^6	Top
(b)		5			

Oil flow photographs of the flat uncambered wing are shown in figure 11 at $\alpha = 0°$ and $5°$. The flow types shown in these figures are representative of those expected on both the flat and dihedral models. As shown in figure 11(a), when the flat wing is at $\alpha = 0°$, the flow across the wing is smooth and attached. At $\alpha = 5°$, several types of flow can be seen on the model, including (1) a leading-edge vortex that originates near the apex and sweeps across the wing, and (2) separation at the wing tips. This type of flow pattern is expected on the dihedral wing when it is tested near these conditions.

Since dihedral tests were made at two Reynolds numbers, oil flow photographs representative of each Reynolds number are included in figures 12 through 17. Since the dihedral wing, unlike the flat wing, is different on the upper and lower surfaces, photographs of both surfaces are also included. Most oil flow studies were performed at Mach 2.4, but to explore the effect of Mach number, several were conducted at Mach 2.0 and are also included. Figure 12(a) is an oil flow photograph of the rough dihedral at $R/\mathrm{ft} = 2 \times 10^6$, Mach 2.4, and shows the bottom of the model at $\alpha = -5°$. For this angle, the bottom surface is the leeward surface and a vortex, originating near the apex, sweeps outboard slightly as it progresses down the body. There is a slight spanwise tendency in the flow near the rear center portion of the body, where the scallop heights are greatest and are nearly perpendicular to the flow.

As the model angle of attack is increased from $-5°$ to $0°$, the vortex, discussed above, disappears. The center portion of this model does not have the nice uniform streamwise flow that occurred on the flat model. The oil appears to be trapped between the scallops and forced into a slightly spanwise direction. The region near the centerline of the model appears to have no oil. At $\alpha = 5°$, the flow on this windward side of the model appears similar to that which occurs at $\alpha = 0°$.

The top side of the model under the same test conditions as figure 12 is shown in figure 13. At $\alpha = -5°$ the flow on the outboard wing upper surface is attached and streamwise. Streaks of oil appear near the center of the model. The flow at $\alpha = 0°$ shows essentially the same pattern as at $\alpha = -5°$. When the model angle of attack is increased to $5°$ (see fig. 13(c)), the vortex can be seen sweeping across the wing. Also, strong spanwise flow on the outboard sections of the rear portion of the wing is obvious. As stated previously, minimal oil patterns appear near the center portion.

Figures 14 and 15 present oil flow photographs of the rough model at $R/\mathrm{ft} = 6 \times 10^6$ and Mach 2.0. The bottom of the model is shown in figure 14 and the top in figure 15. The flow patterns are very similar to those at $R/\mathrm{ft} = 2 \times 10^6$, with a vortex originating near the nose and coming back across the wing. This vortex again disappears when the model is raised to $\alpha = 0°$, but a streak of oil does run tangential to the center portion of the wing. The flow patterns do not change substantially from $\alpha = 0°$ to $\alpha = 5°$.

The top of the rough dihedral model at $R/\mathrm{ft} = 6 \times 10^6$ and Mach 2.0 is shown in figure 15. At $\alpha = -5°$, there are some streaks of oil but the flow is mostly attached and streamwise on the outboard portions of the wing. At $\alpha = 0°$, some of the oil streaks disappear near the mid portion of the wing and the outboard flow remains smooth and attached. At $\alpha = 5°$, the vortex from the nose appears, and there is strong spanwise flow near the trailing edge of the wing. As at the lower Reynolds number, the center portions of the wing, where the scallops are nearly perpendicular to the flow, seem to contain very little oil. Figures 16 and 17 show the rough model at $R/\mathrm{ft} = 6 \times 10^6$ and Mach 2.4. The oil flows for these conditions show essentially the same features as at the lower Mach number.

Though the oil near the center portions of the wing seems to disappear more quickly for the scalloped model at the test conditions shown, the features usually determinable by oil flow techniques, such as separation and vortices, are still very visible on this model.

Schlieren Photographs

Figures 18 and 19 present schlieren photographs for the rough dihedral and the smooth dihedral, respectively. The rough model is shown for Mach numbers of 1.8, 2.4, and 2.8, and the smooth model is shown for Mach numbers 2.0, 2.4 and 2.8. Both models are shown for $\alpha = 5°$ and $R/\mathrm{ft} = 2 \times 10^6$. In figure 18, the bow and trailing-edge shocks are very noticeable. Note, weak waves that appear to emanate from the scallops of the model are evident between the bow and trailing-edge shocks, but these waves have little effect on the resulting data. These embedded shock-like disturbances are more easily seen in figure 18(a), where the shock angle is not quite so steep. The smooth dihedral model is shown in figure 19. Slight disturbances in the flow can be observed in the photograph shown in figure 19(a), perhaps from the transition grit; however, these are not as strong at the shocks emanating from the rough model.

Vapor-Screen Photographs

Vapor-screen photographs of the flat and dihedral models are shown in figures 20 and 21. The vapor-screen photograph of the flat model shown in figure 20 is presented for reference. For the test conditions indicated, a fairly strong nose vortex is visible. Since a consistent set of vapor-screen photographs with the rough and smooth models at these same conditions does not exist, several photographs are shown for conditions that are as close as could be attained. Figure 21(a) contains photographs of the smooth dihedral model at two different locations and of the rough dihedral at one location. Note that the smooth model is at $\alpha = 5°$ and that two well-established vortices are observed at each location. The rough dihedral is at a lower angle of attack, but one can distinguish a separation bubble forming near the leading edge of the model.

Figure 21(b) contains photographs of the smooth and rough dihedral models at $x = 28$ in. The two top photographs are for the same Mach numbers, but the rough dihedral model is at $\alpha = 6°$. At this location on the model, the dihedral of the wing is causing the vortex to be buried in the shadows and barely visible.

Figure 21(c) shows the vapor screen located at $x = 40$ in.; this is downstream of the base of the model. Note that the tip vortices, the leading-edge vortex, and the trailing-edge shock are all seen in the photographs for both the rough and smooth models. Generally, the degree of surface finish did not significantly impact the observance of the most significant flow features with the vapor-screen technique.

Concluding Remarks

An experimental investigation was conducted to assess the effect of surface finish on the longitudinal and lateral aerodynamic characteristics of a highly swept wing at supersonic speeds. The investigation included tests of four wing models: three models having 22.5° of outboard dihedral, identical except for surface finish; and a flat smooth model of the same planform for reference. Of the three dihedral models, one was taken directly from the milling machine after being cut so that the maximum scallop height was 0.005 in., the second cut so that its maximum scallop height was 0.002 in.; and the third hand finished to a smooth surface. Tests were conducted in Test Section 1 of the Langley Unitary Plan Wind Tunnel over a range of Mach numbers from 1.8 to 2.8, a range of angles of attack from $-5°$ to $8°$, and a Reynolds number per foot of 2×10^6. Selected data were also taken at a Reynolds number per foot of 6×10^6.

For all test Mach numbers, drag coefficient increases, with the corresponding lift-drag ratio decreases, were the primary aerodynamic effects attributed to increased surface roughness due to the milling machine scallops. These drag and lift-drag ratio increments due to roughness increased as Reynolds number increased. The degree of surface finish did not significantly impact the results of the flow visualization techniques.

NASA Langley Research Center
Hampton, VA 23665-5225
June 2, 1989

References

1. Dyke, R. M.: *Numerical Control.* Prentice-Hall, Inc., c.1967.
2. Pressman, Roger S.; and Williams, John E.: *Numerical Control and Computer-Aided Manufacturing.* John Wiley & Sons, Inc., c.1977.
3. Darden, Christine M.: The Effect of Model Roughness Caused by Numerical-Control Milling Machines on Wind-Tunnel Force Data. *J. Natl. Tech. Assoc.*, vol. 61, no. 4, Apr. 1988, pp. 49–55.
4. Robins, A. Warner; Carlson, Harry W.; and Mack, Robert J.: *Supersonic Wings With Significant Leading-Edge Thrust at Cruise.* NASA TP-1632, 1980.

5. Robins, A. Warner; Lamb, Milton; and Miller, David S.: *Aerodynamic Characteristics at Mach Numbers of 1.5, 1.8, and 2.0 of a Blended Wing-Body Configuration With and Without Integral Canards.* NASA TP-1427, 1979.
6. Jackson, Charlie M., Jr.; Corlett, William A.; and Monta, William J.: *Description and Calibration of the Langley Unitary Plan Wind Tunnel.* NASA TP-1905, 1981.
7. Braslow, Albert L.; and Knox, Eugene C.: *Simplified Method for Determination of Critical Height of Distributed Roughness Particles for Boundary-Layer Transition at Mach Numbers From 0 to 5.* NACA TN 4363, 1958.
8. Morris, Odell A.; Corlett, William A.; Wassum, Donald L.; and Babb, C. Donald: *Vapor-Screen Technique for Flow Visualization in the Langley Unitary Plan Wind Tunnel.* NASA TM-86384, 1985.
9. Loving, Donald L.; and Katzoff, S.: *The Fluorescent-Oil Film Method and Other Techniques for Boundary-Layer Flow Visualization.* NASA MEMO 3-17-59L, 1959.
10. Liepmann, H. W.; and Roshko, A.: *Elements of Gasdynamics.* John Wiley & Sons, Inc., c.1957.
11. Czarnecki, K. R.: *The Problem of Roughness Drag at Supersonic Speeds.* NASA TN D-3589, 1966.
12. Braslow, Albert L.; Hicks, Raymond M.; and Harris, Roy V., Jr.: *Use of Grit-Type Boundary-Layer-Transition Trips on Wind-Tunnel Models.* NASA TN D-3579, 1966.
13. Stallings, Robert L., Jr.; and Lamb, Milton: *Effects of Roughness Size on the Position of Boundary-Layer Transition and on the Aerodynamic Characteristics of a 55° Swept Delta Wing at Supersonic Speeds.* NASA TP-1027, 1977.
14. Yuan, S. W.: *Foundations of Fluid Mechanics.* Prentice-Hall, Inc., c.1967.
15. Eckstrom, D. J.: *Engineering Analysis of Boundary Layers and Skin Friction on Bodies of Revolution at Zero Angle of Attack.* TM 55-21-21, Lockheed Missiles & Space Co., May 1965.

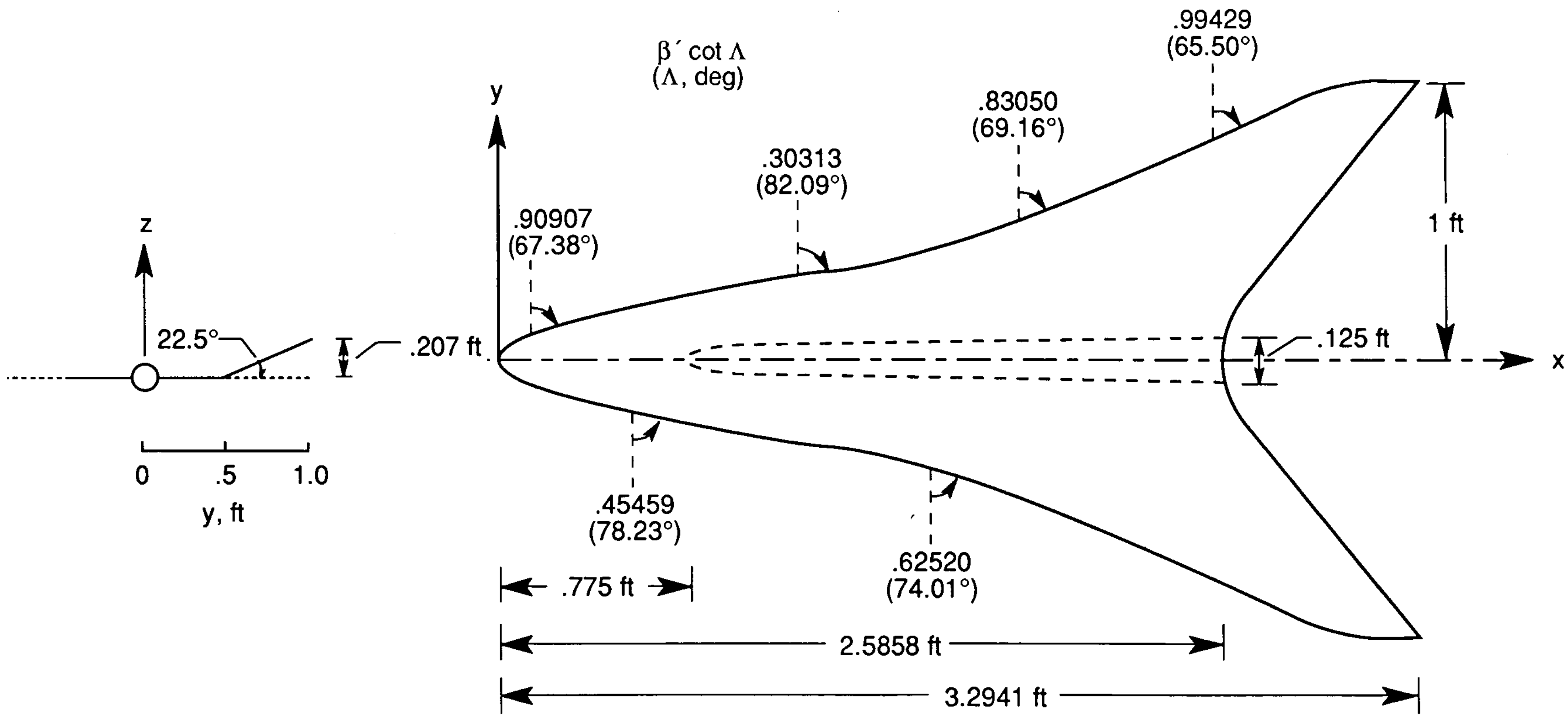

Figure 1. Wing planform and dihedral. Wing area = 2.5375 ft^2.

ORIGINAL PAGE
BLACK AND WHITE PHOTOGRAPH

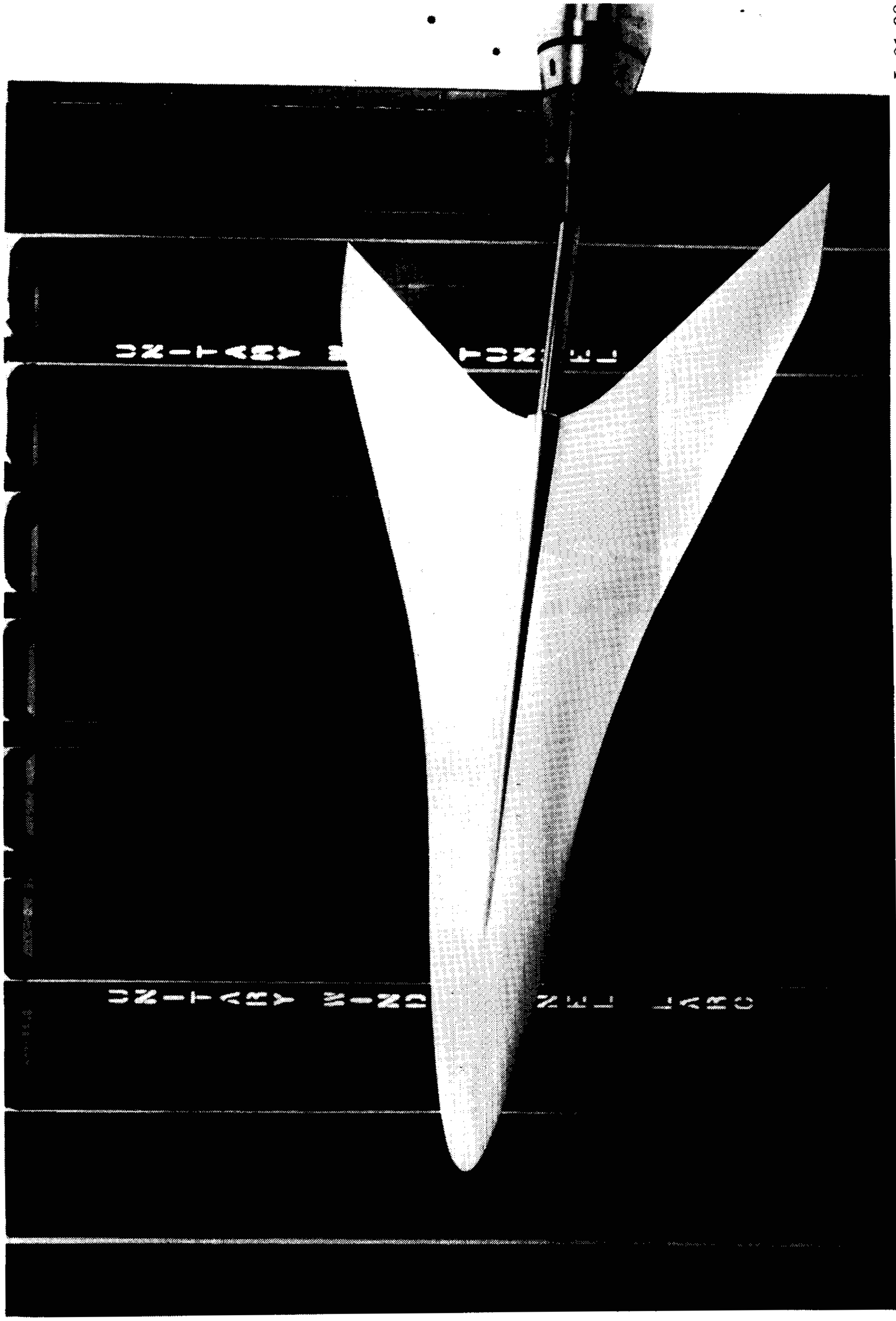

L-81-98

(a) Flat smooth model.

Figure 2. Photographs of test models.

ORIGINAL PAGE
BLACK AND WHITE PHOTOGRAPH

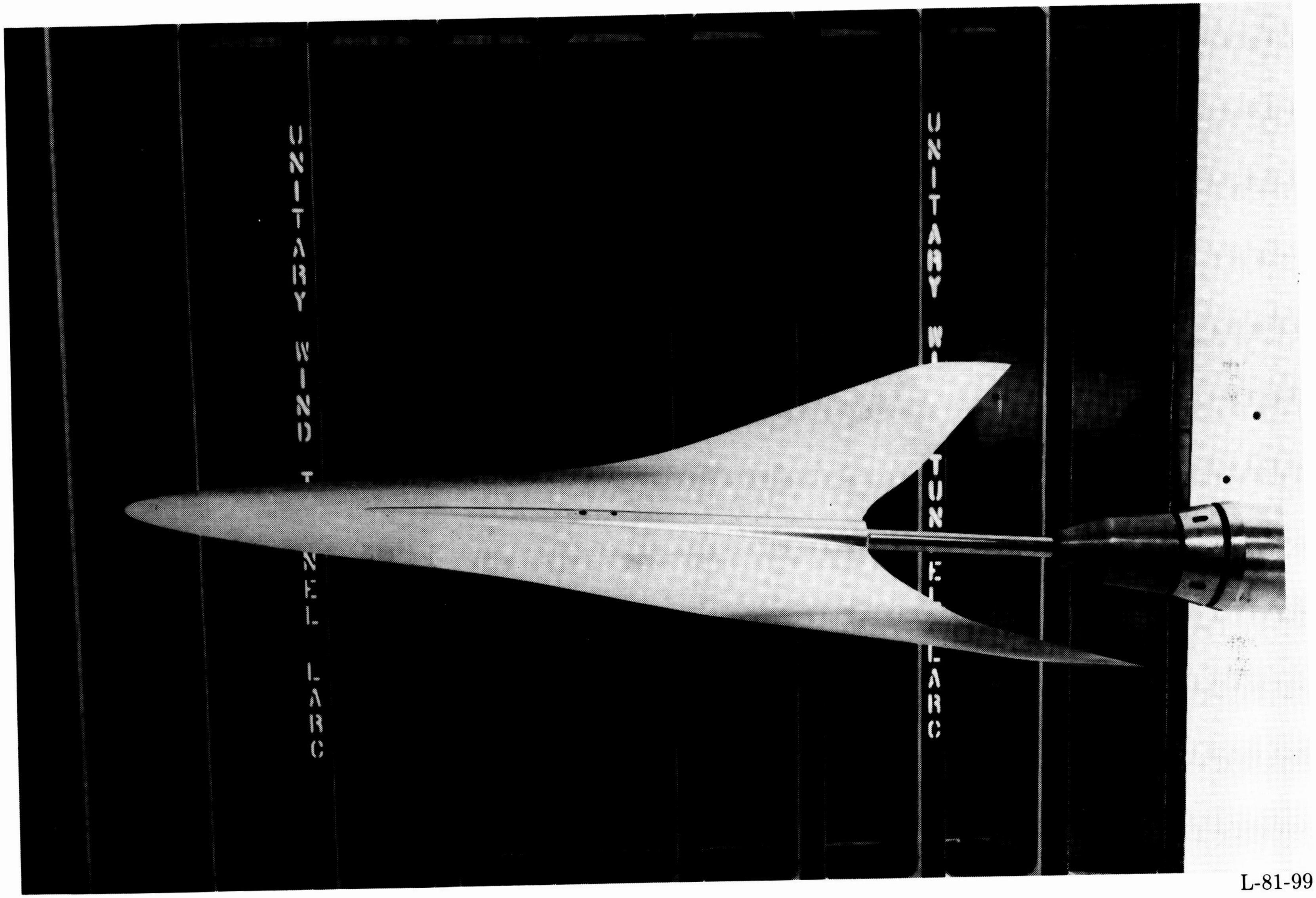

L-81-99

(b) Smooth dihedral.

Figure 2. Continued.

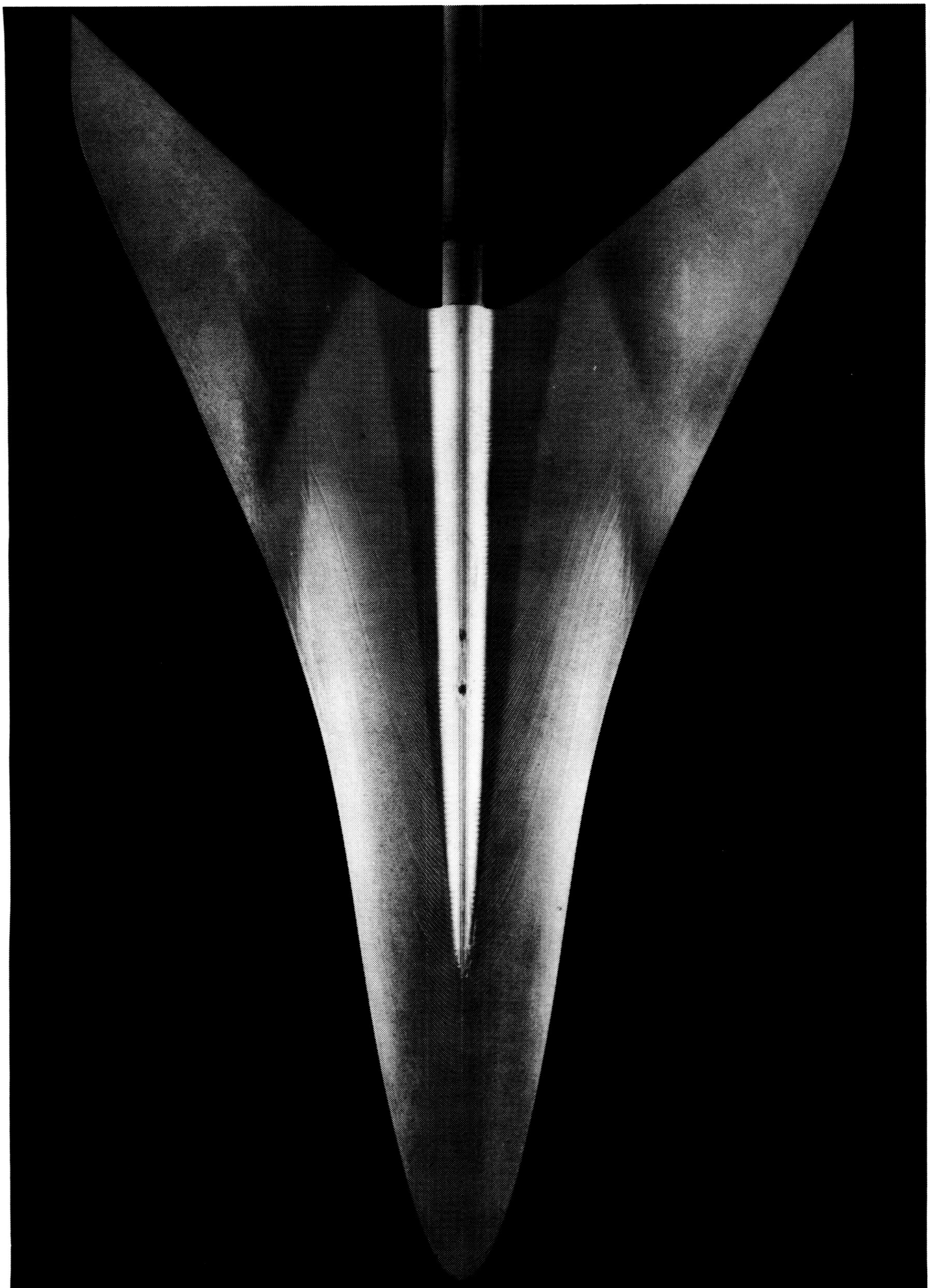

L-84-3756

(c) Medium dihedral.

Figure 2. Continued.

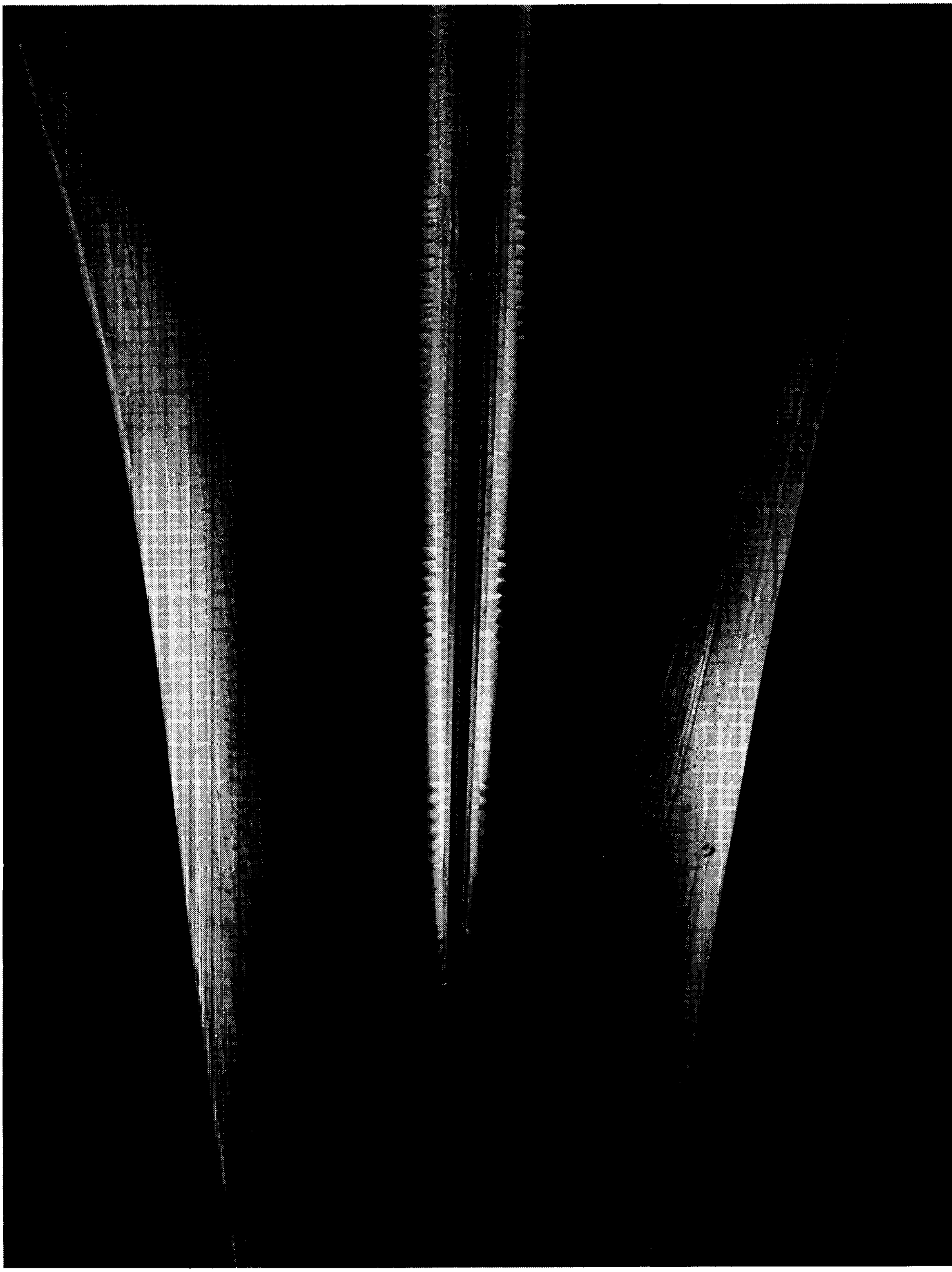

(d) Close-up of medium dihedral.

Figure 2. Continued.

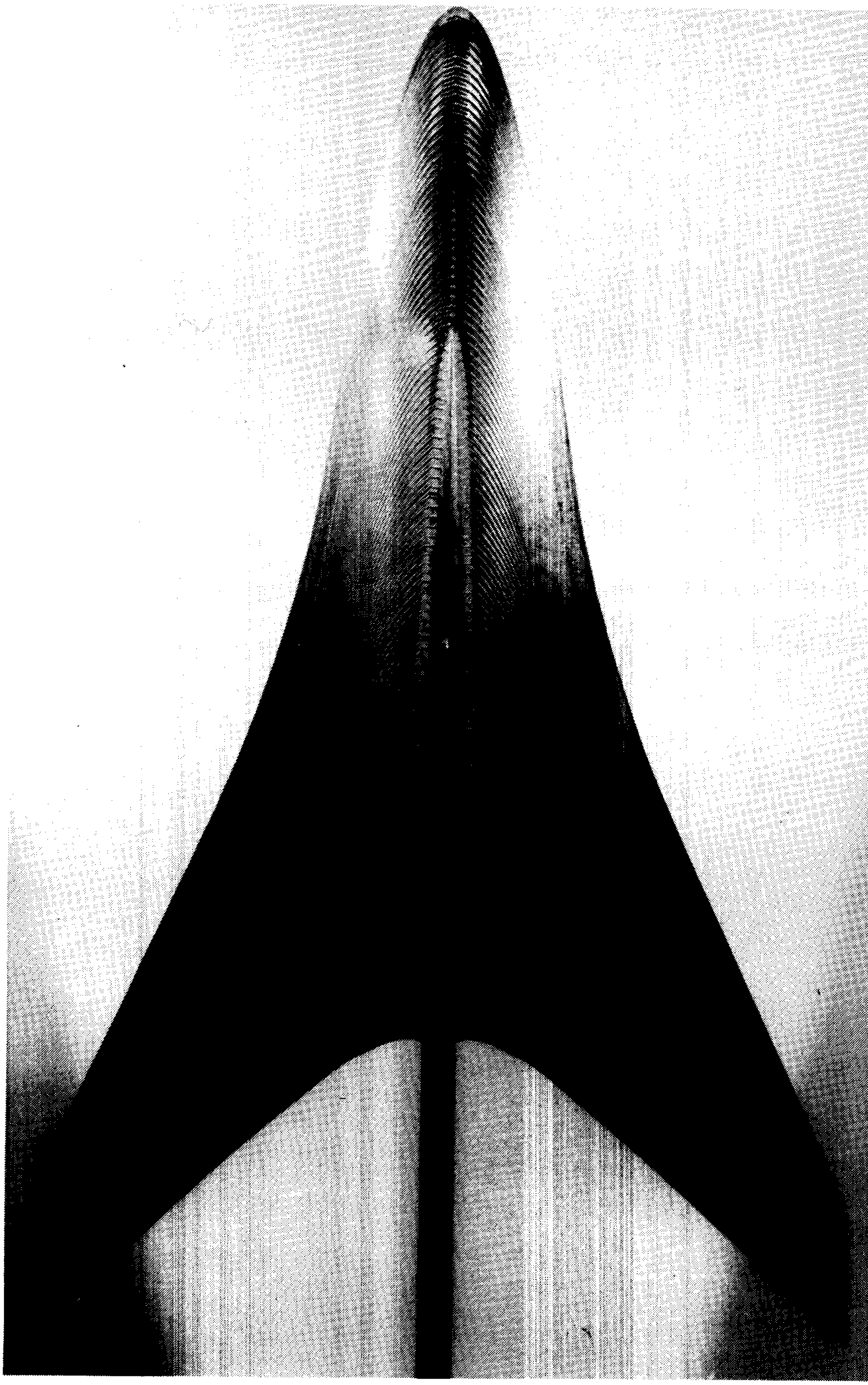

L-79-4234

(e) Rough dihedral.

Figure 2. Concluded.

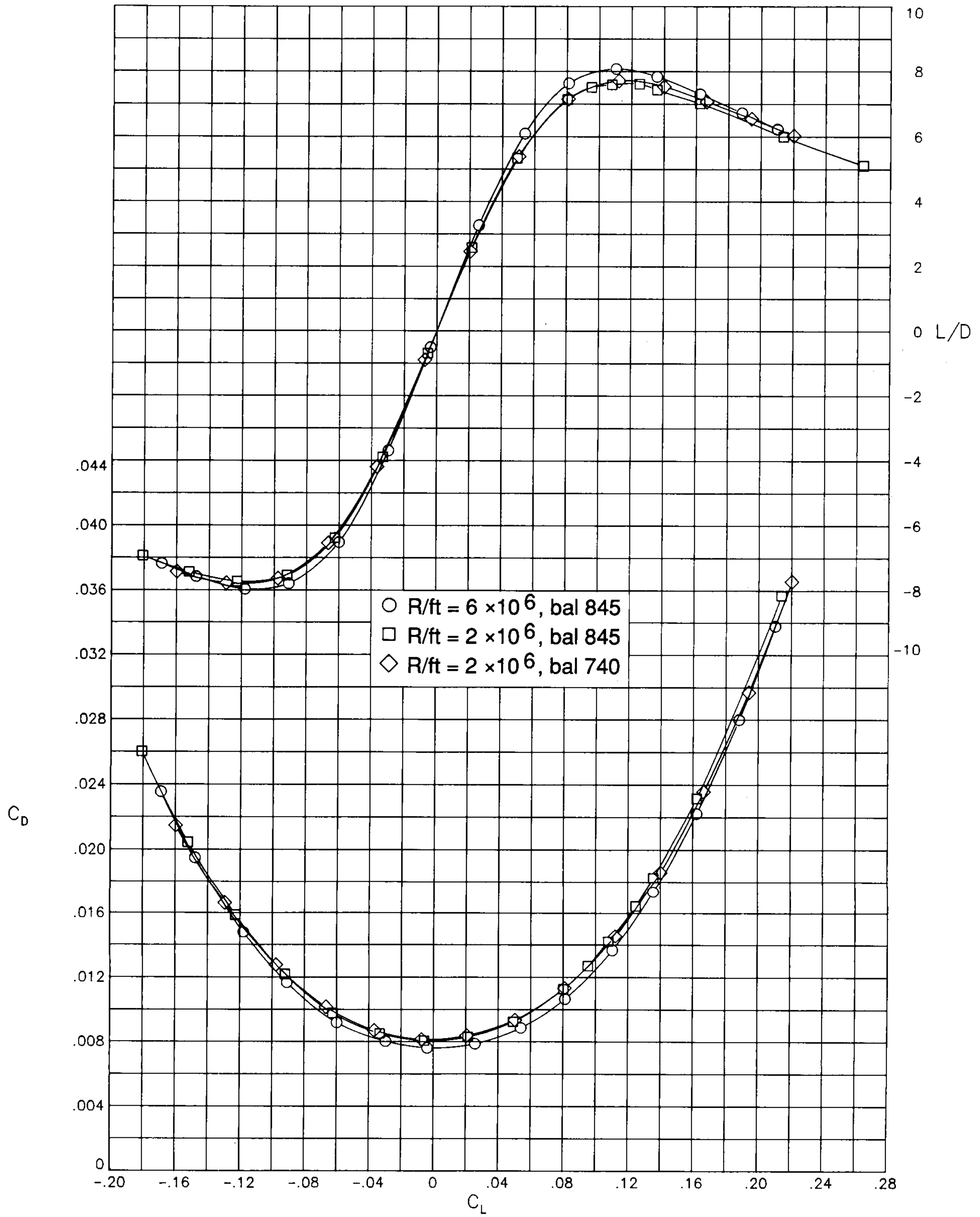

(a) Drag and performance as a function of lift.

Figure 3. Balance and Reynolds number effects on rough dihedral; $M = 2.0$.

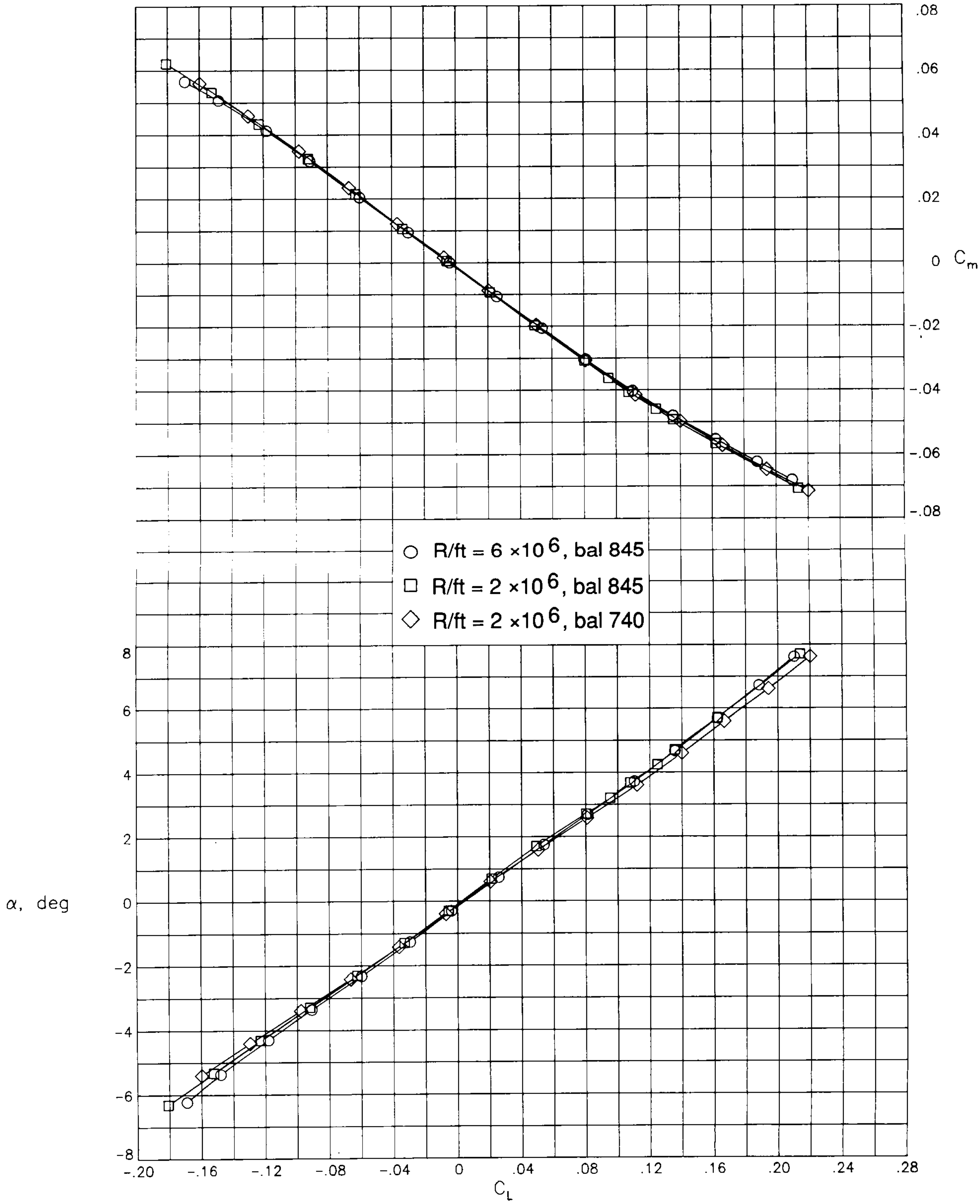

(b) Angle of attack and pitching moment as a function of lift.

Figure 3. Concluded.

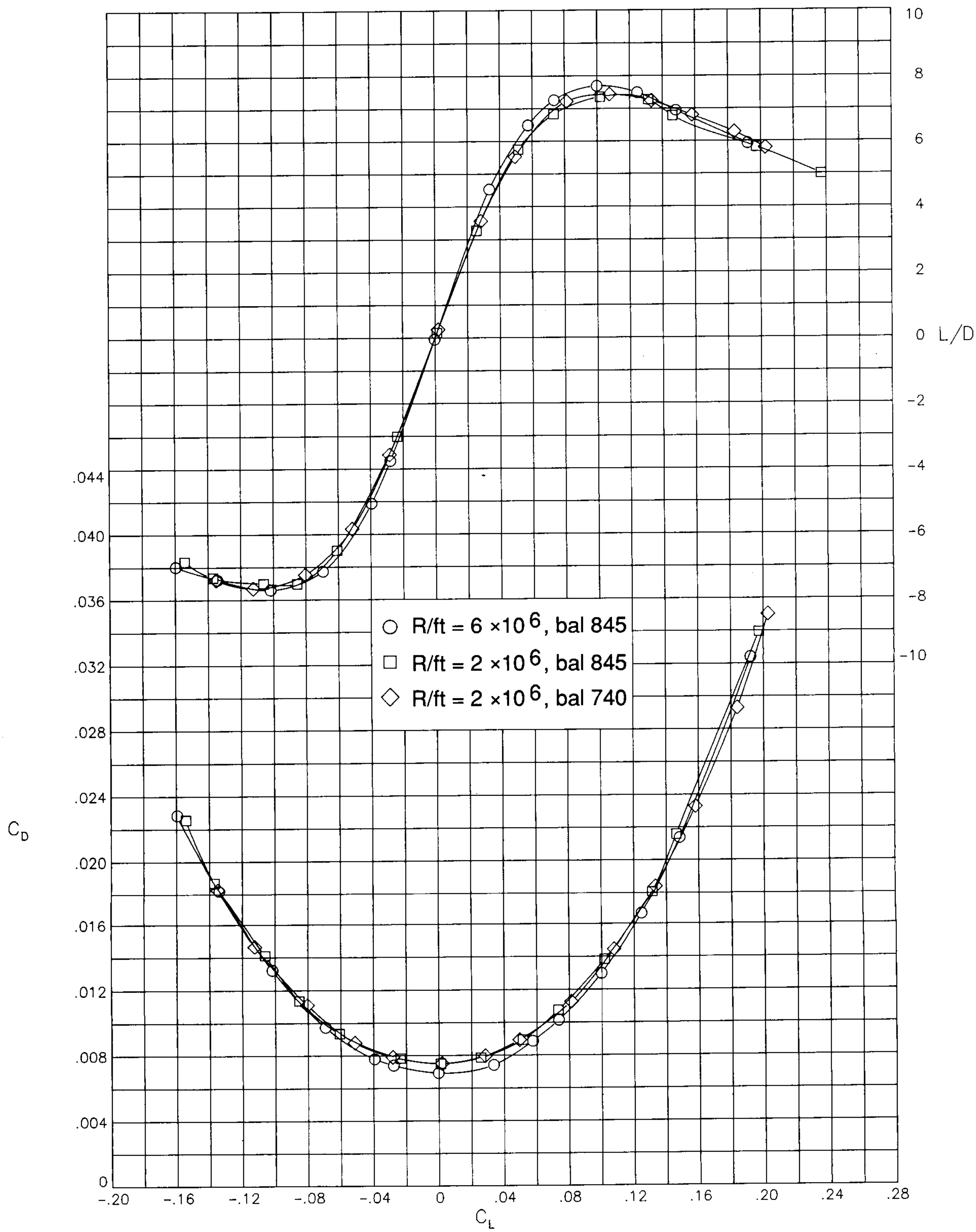

(a) Drag and performance as a function of lift.

Figure 4. Balance and Reynolds number effects on rough dihedral; $M = 2.4$.

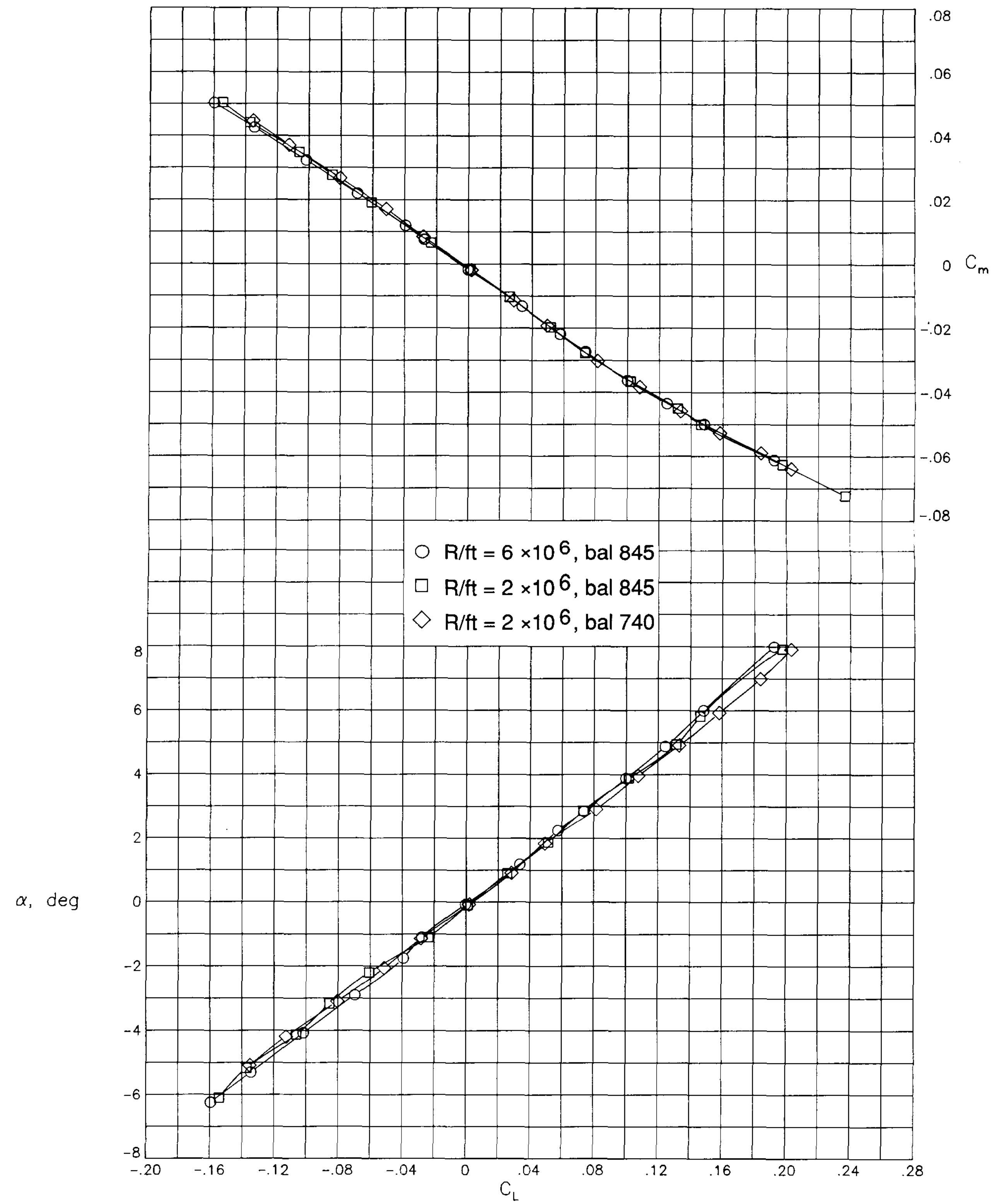

(b) Angle of attack and pitching moment as a function of lift.

Figure 4. Concluded.

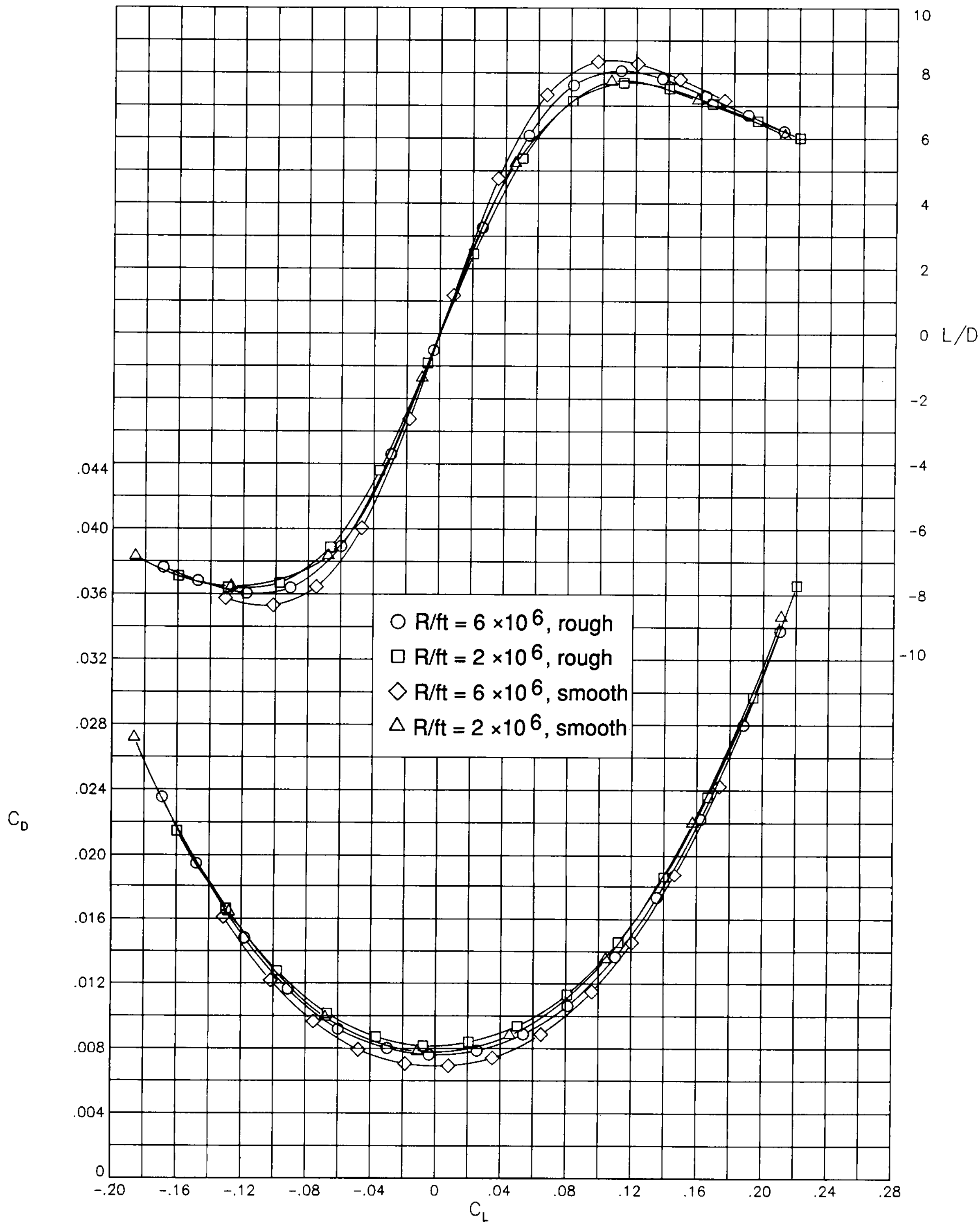

(a) Drag and performance as a function of lift.

Figure 5. Reynolds number effect on rough and smooth models; $M = 2.0$.

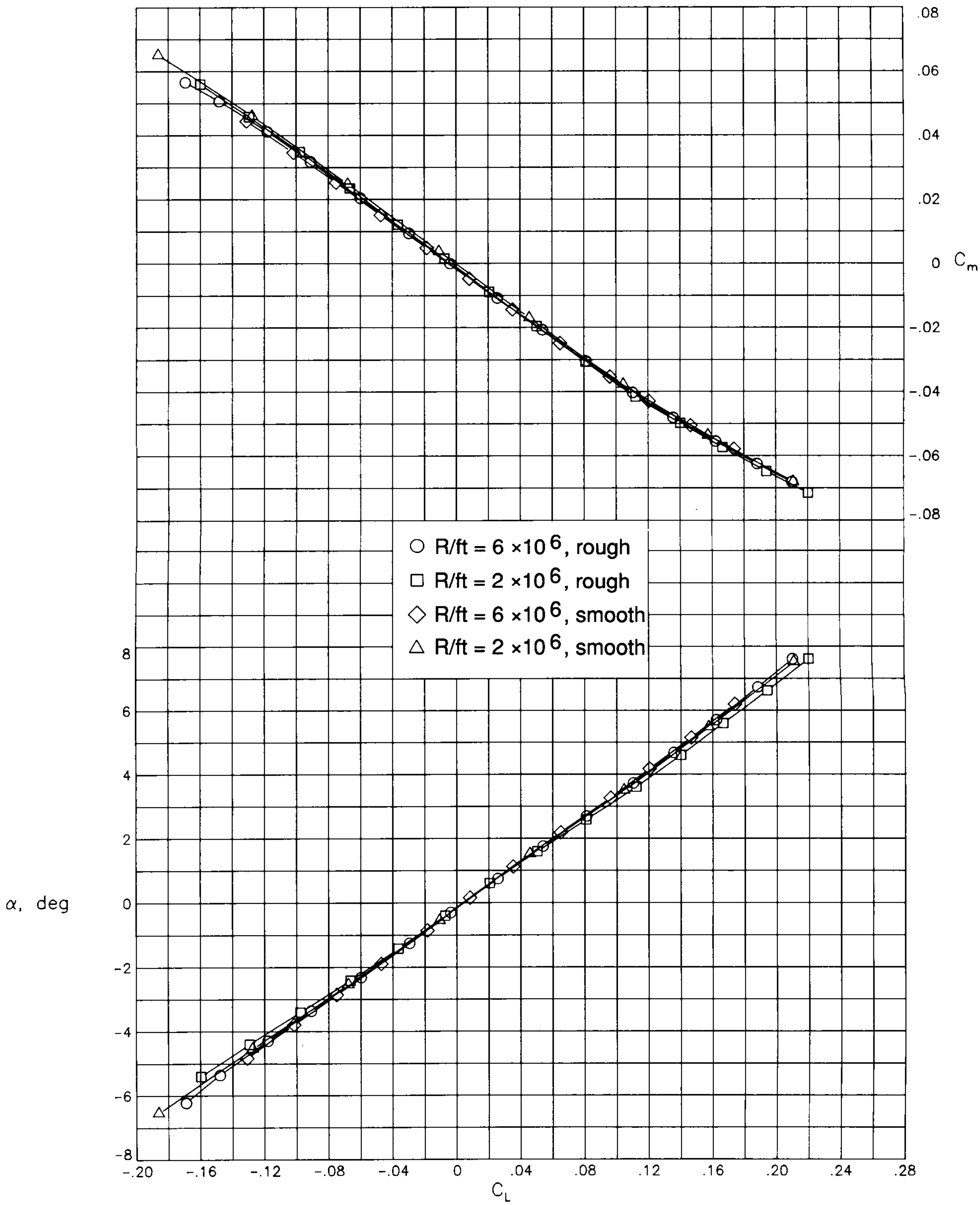

(b) Angle of attack and pitching moment as a function of lift.

Figure 5. Concluded.

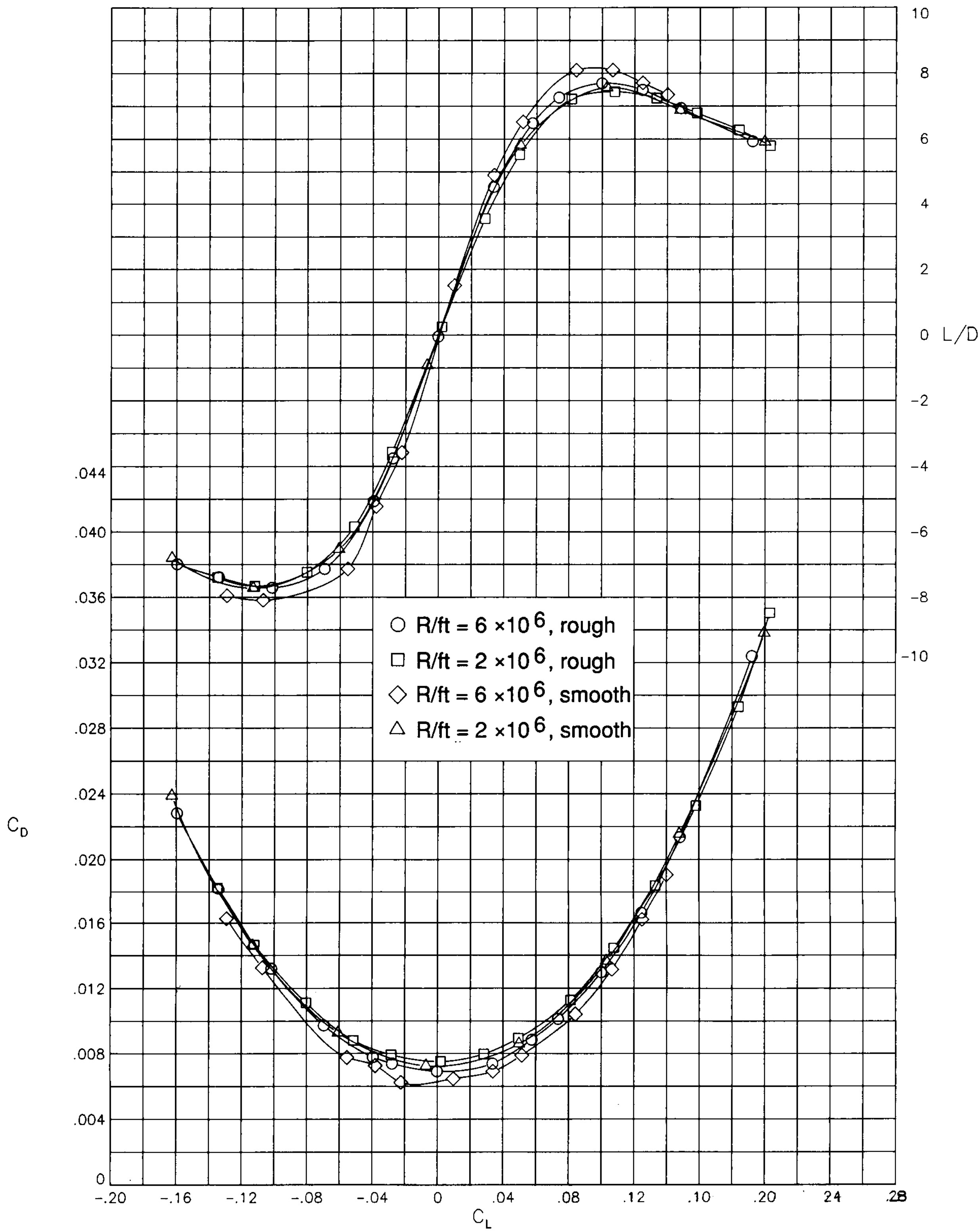

(a) Drag and performance as a function of lift.

Figure 6. Reynolds number effect on rough and smooth models; $M = 2.4$.

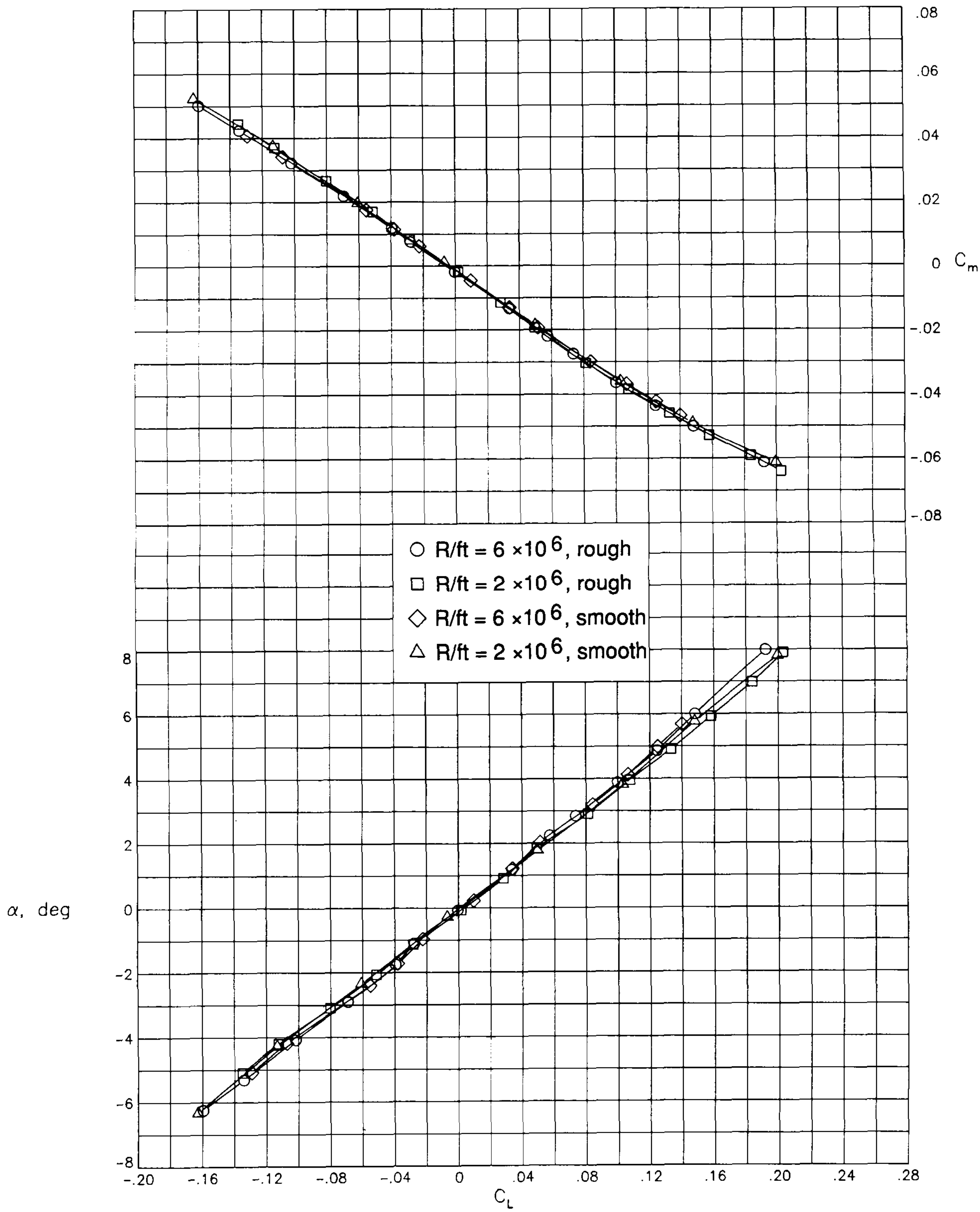

(b) Angle of attack and pitching moment as a function of lift.

Figure 6. Concluded.

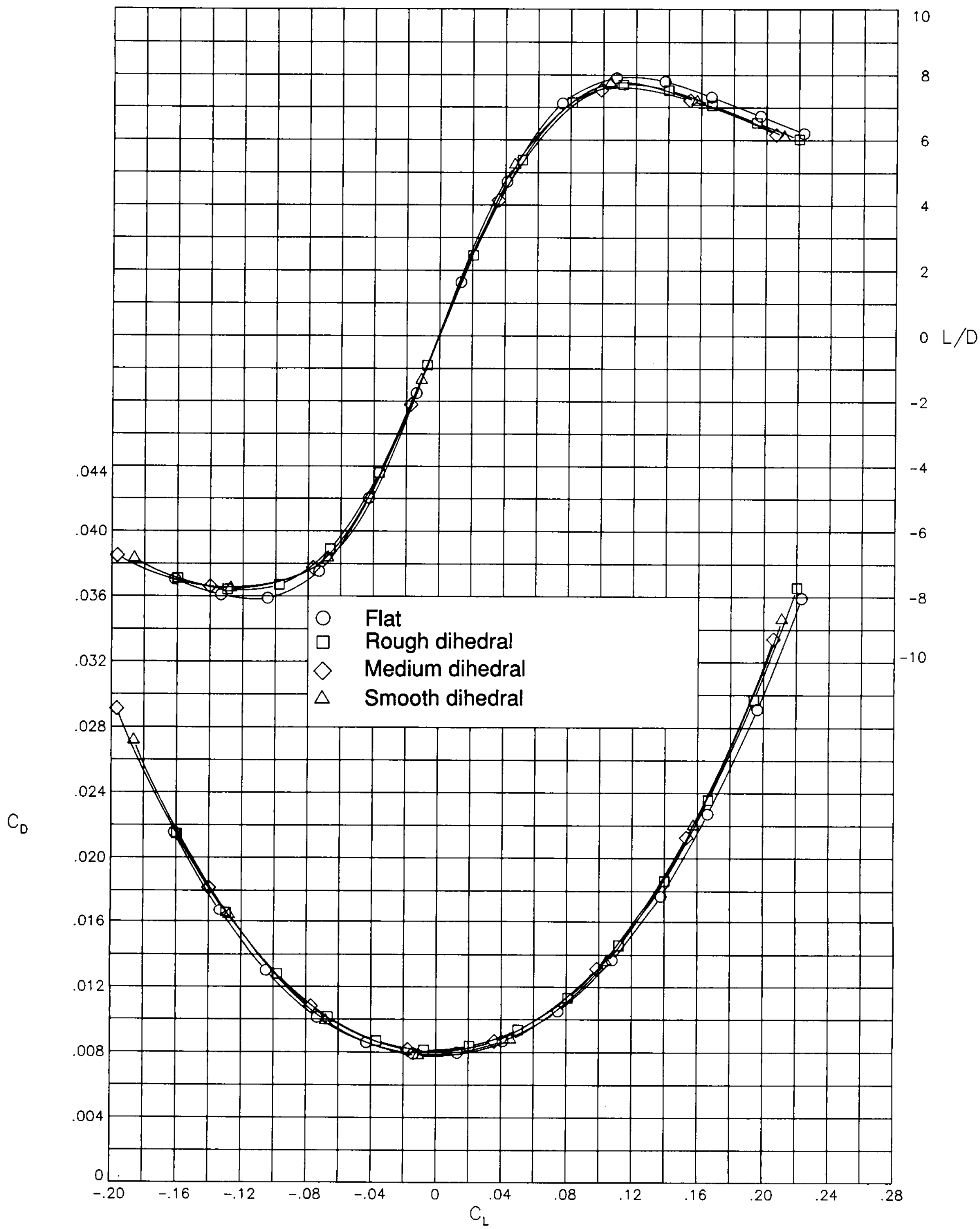

(a) Drag and performance as a function of lift.

Figure 7. Effect of scallop height on experimental results; $R/\mathrm{ft} = 2 \times 10^6$; $M = 2.0$.

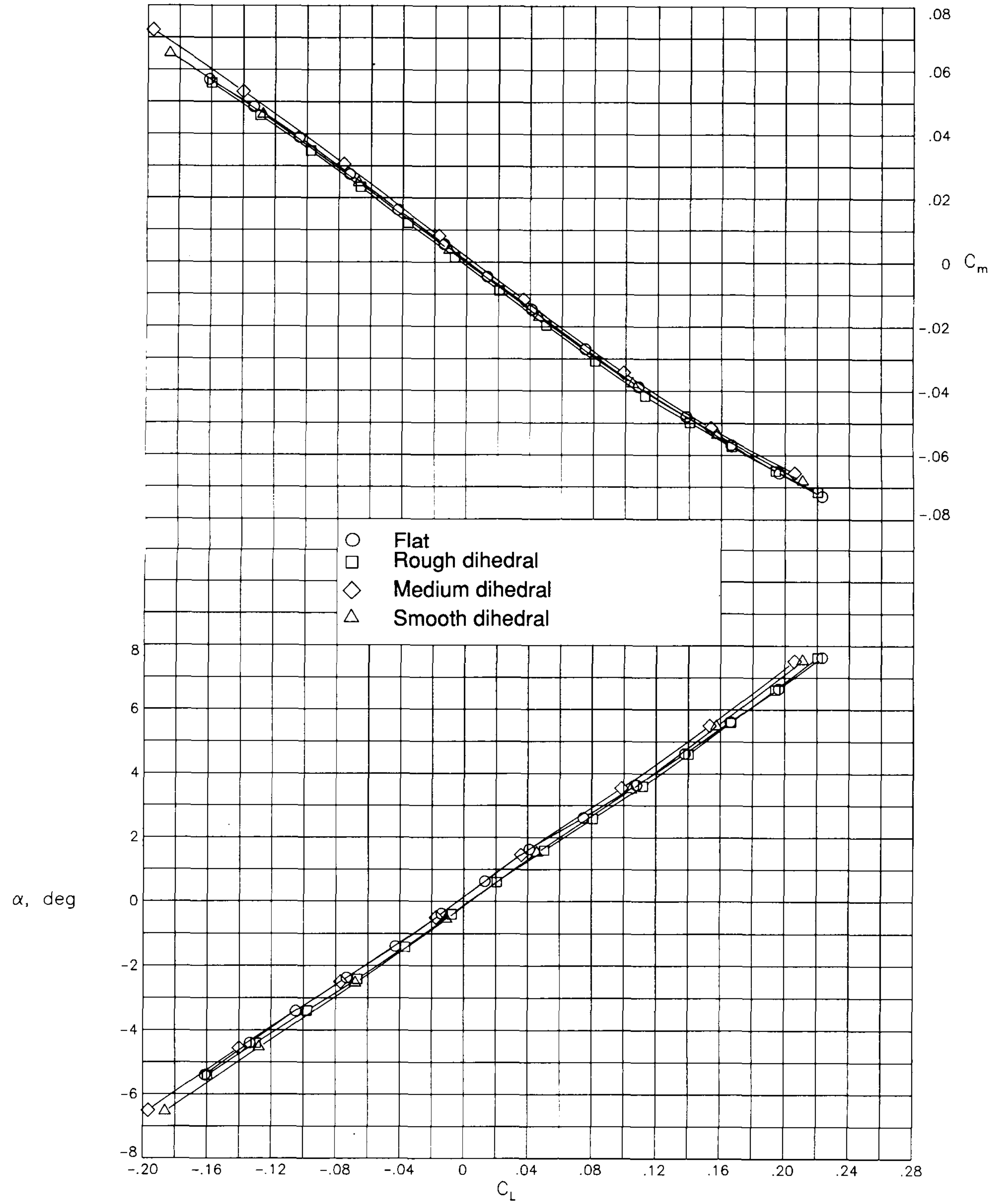

(b) Angle of attack and pitching moment as a function of lift.

Figure 7. Concluded.

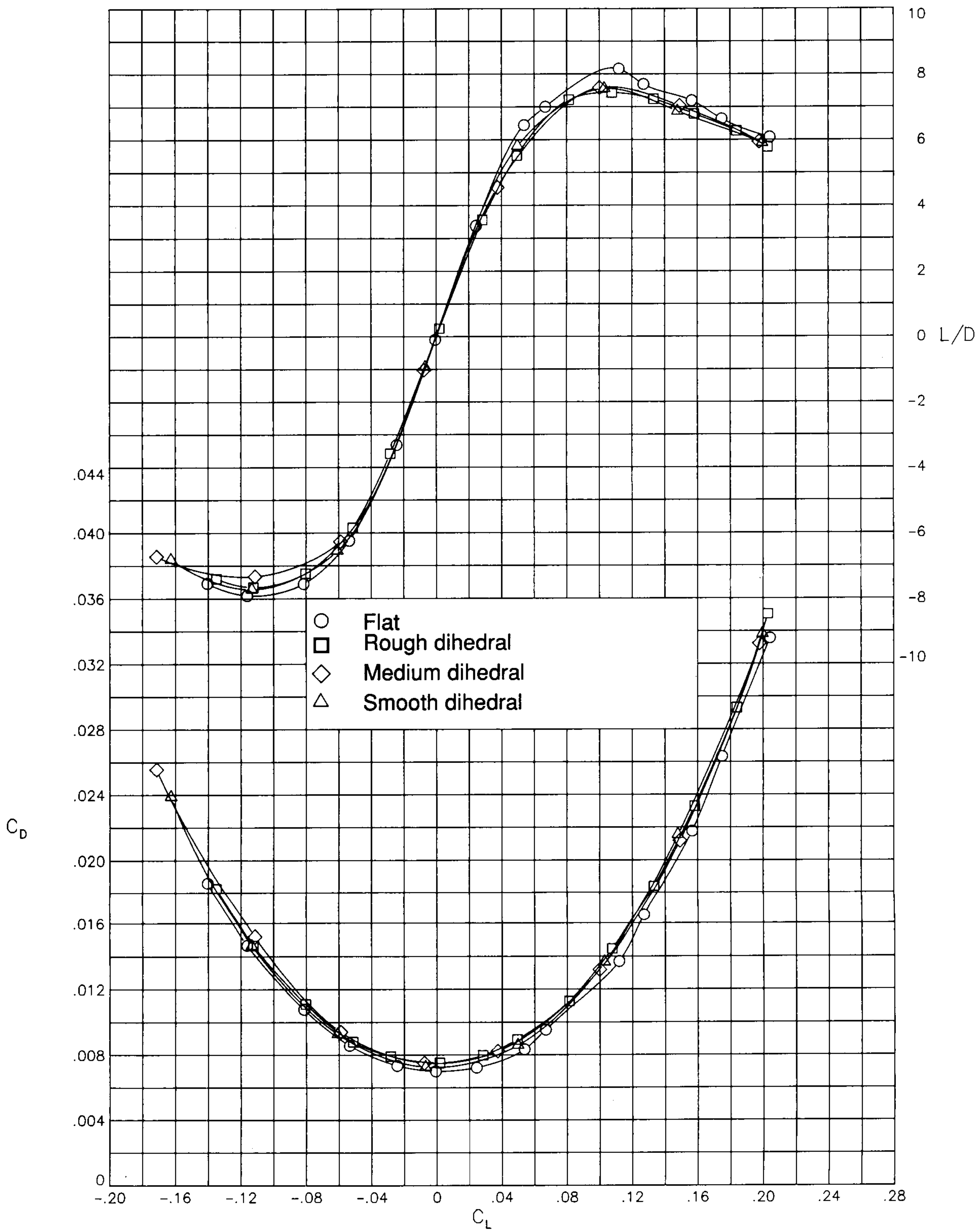

(a) Drag and performance as a function of lift.

Figure 8. Effect of scallop height on experimental results; $R/\text{ft} = 2 \times 10^6$; $M = 2.4$.

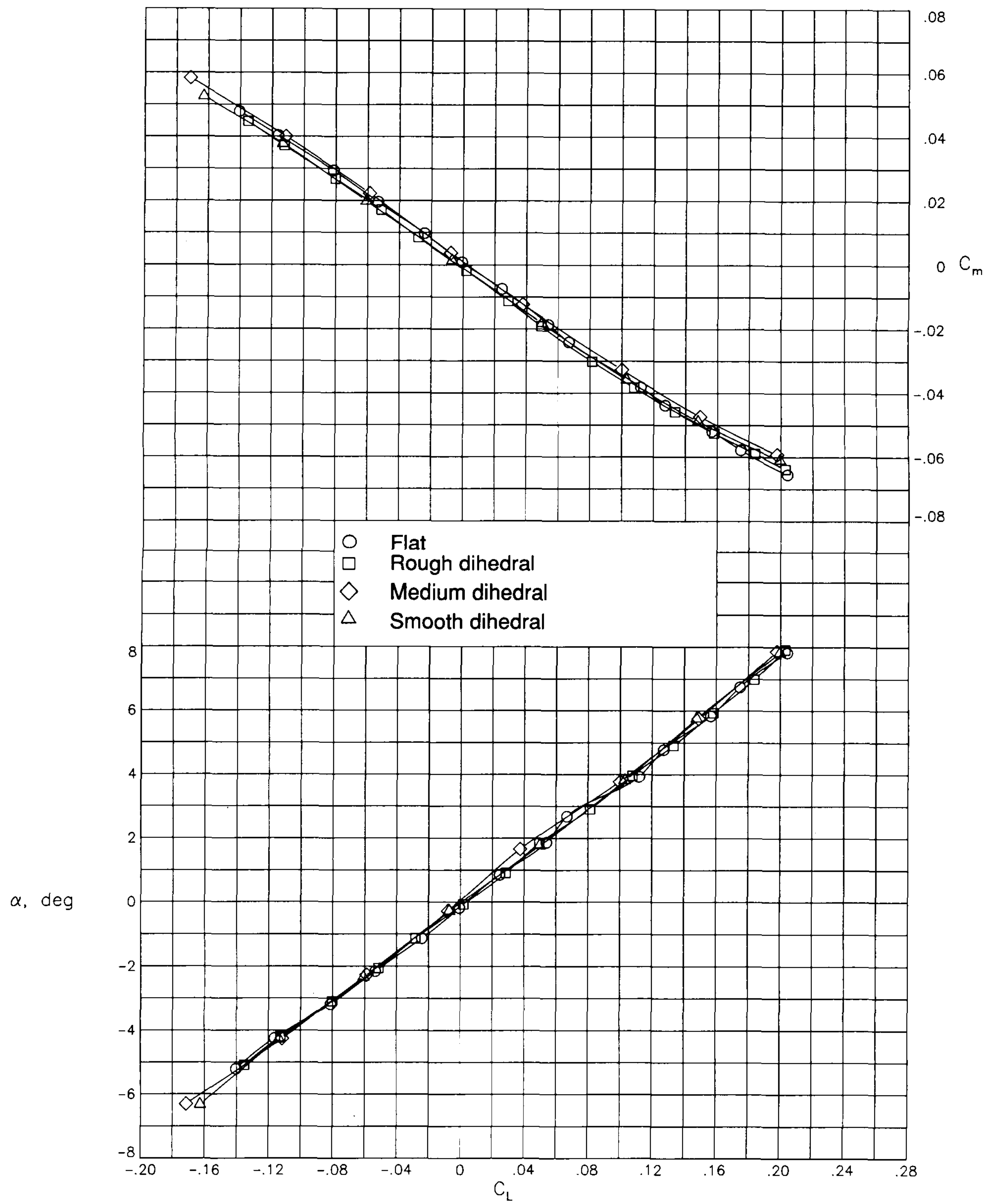

(b) Angle of attack and pitching moment as a function of lift.

Figure 8. Concluded.

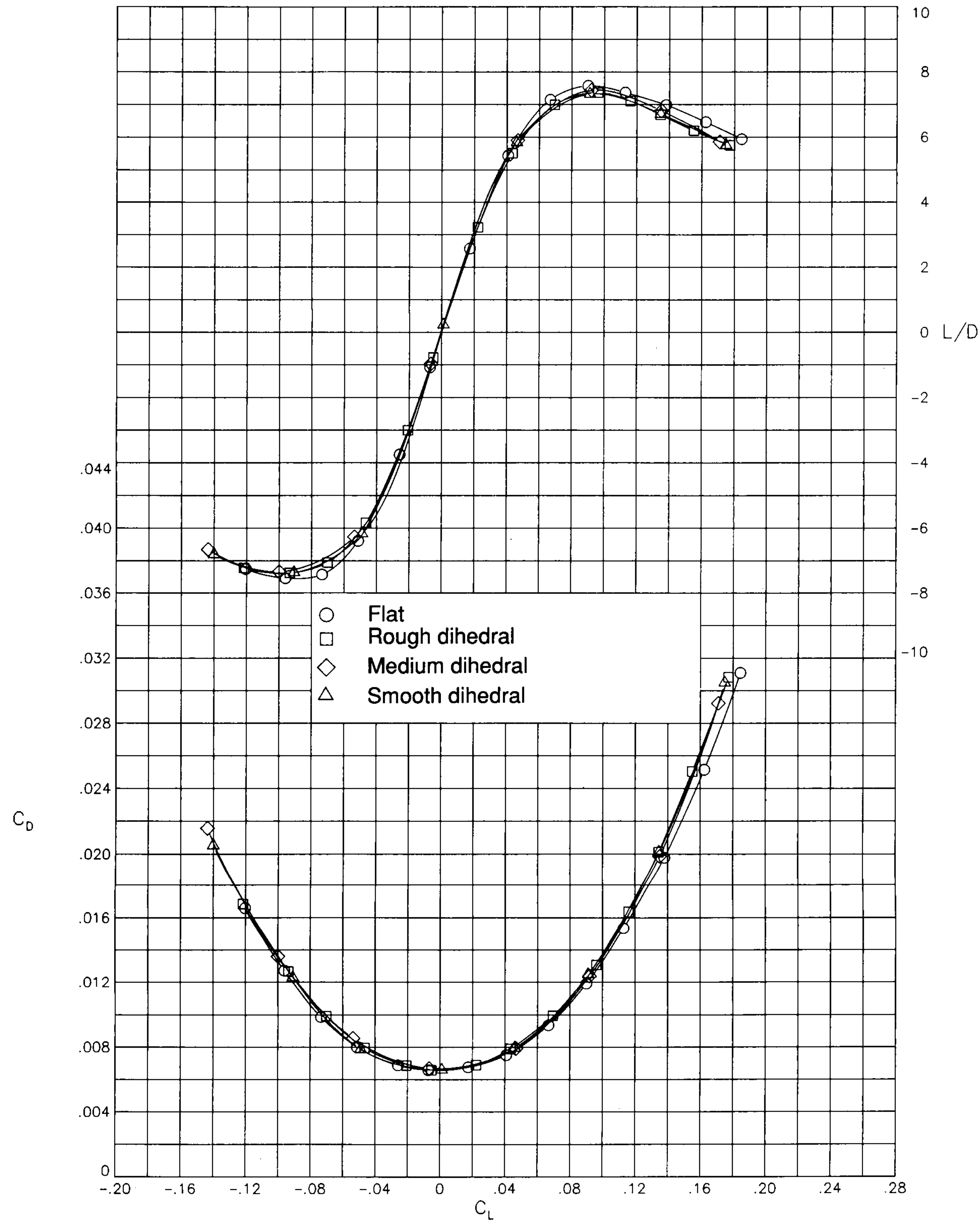

(a) Drag and performance as a function of lift.

Figure 9. Effect of scallop height on experimental results; $R/\text{ft} = 2 \times 10^6$; $M = 2.8$.

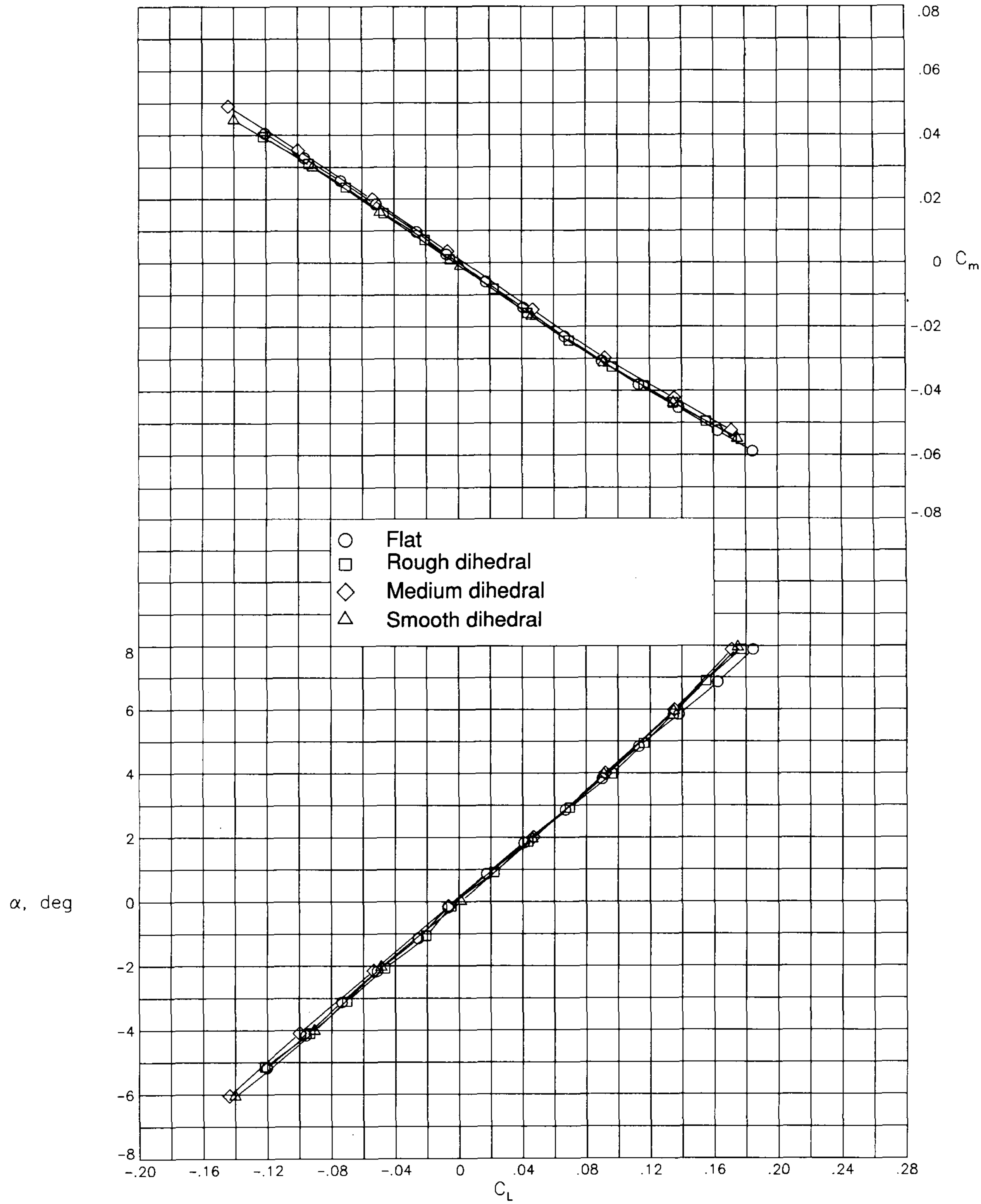

(b) Angle of attack and pitching moment as a function of lift.

Figure 9. Concluded.

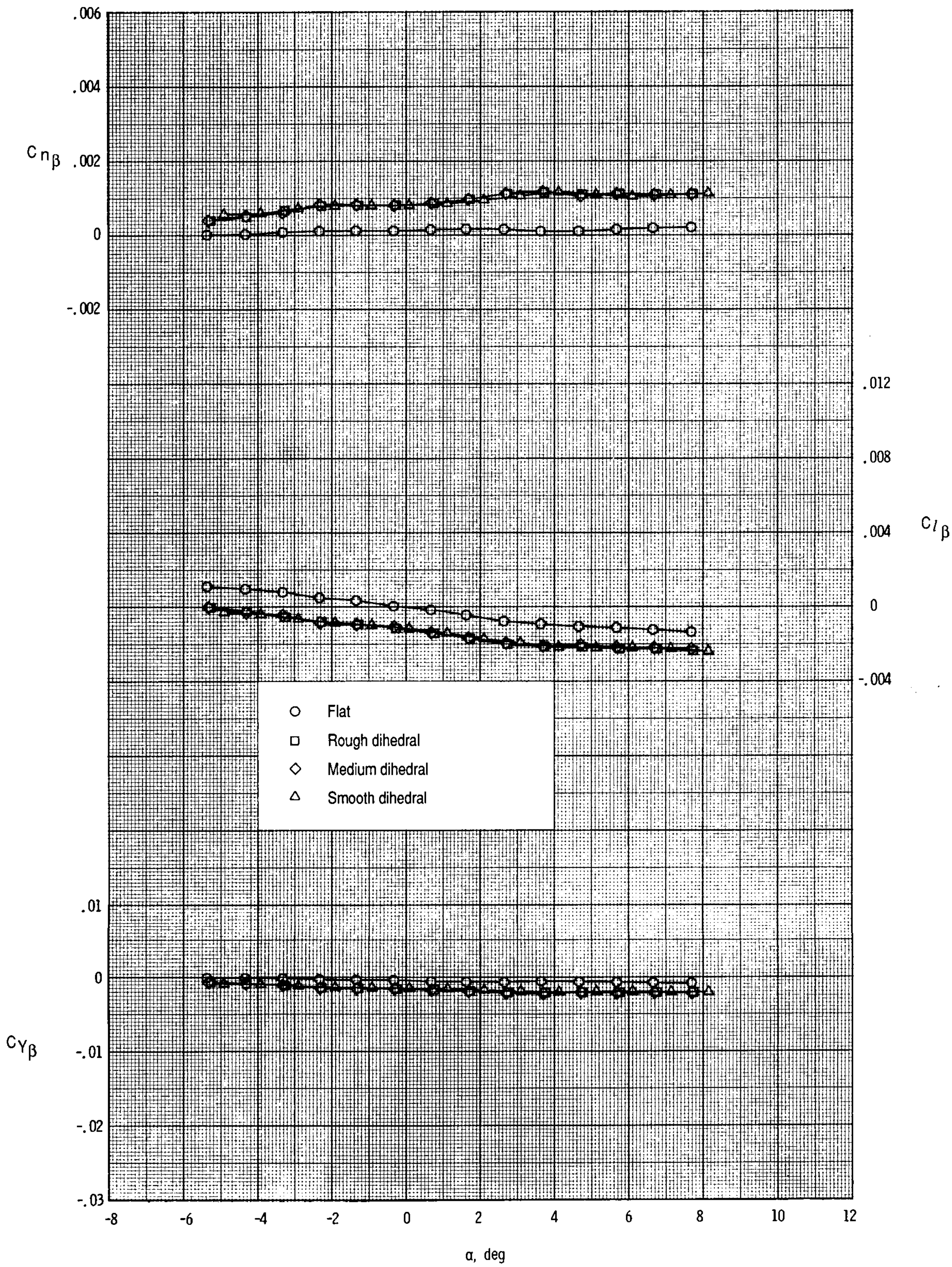

(a) $M = 1.8$.

Figure 10. Effect of scallop height on stability parameters as a function of α; $R/\text{ft} = 2 \times 10^6$.

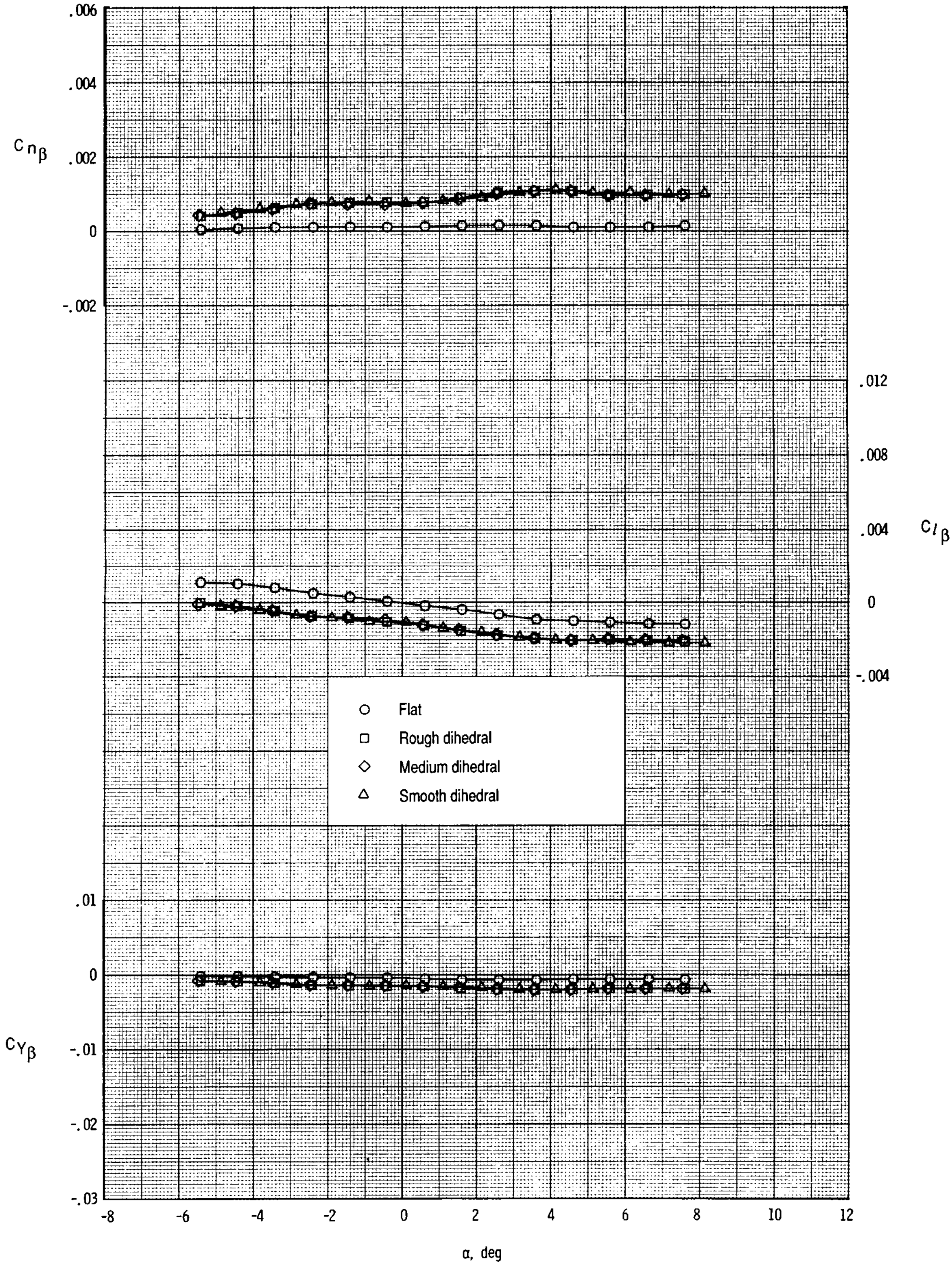

(b) $M = 2.0$.

Figure 10. Continued.

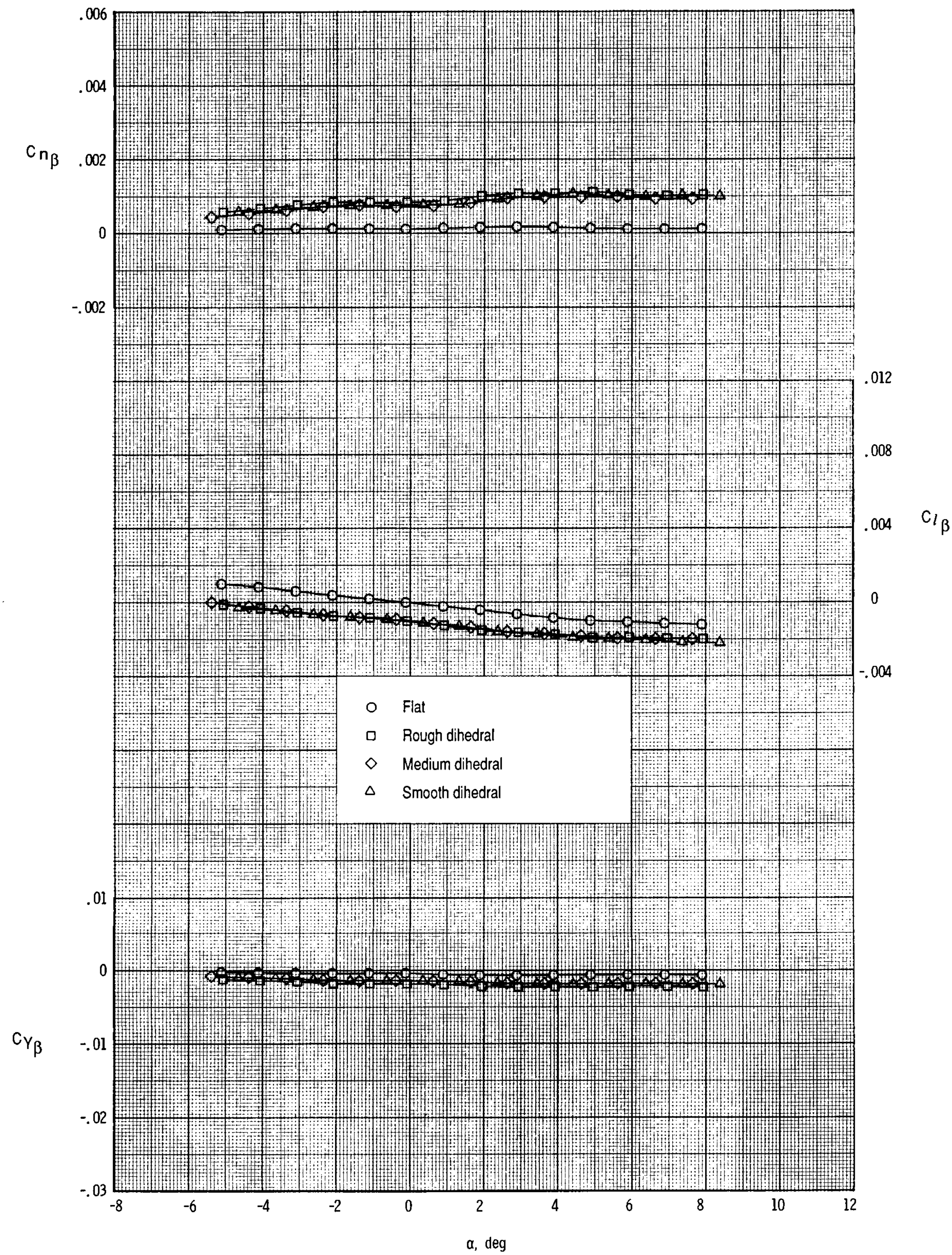

(c) $M = 2.16$.

Figure 10. Continued.

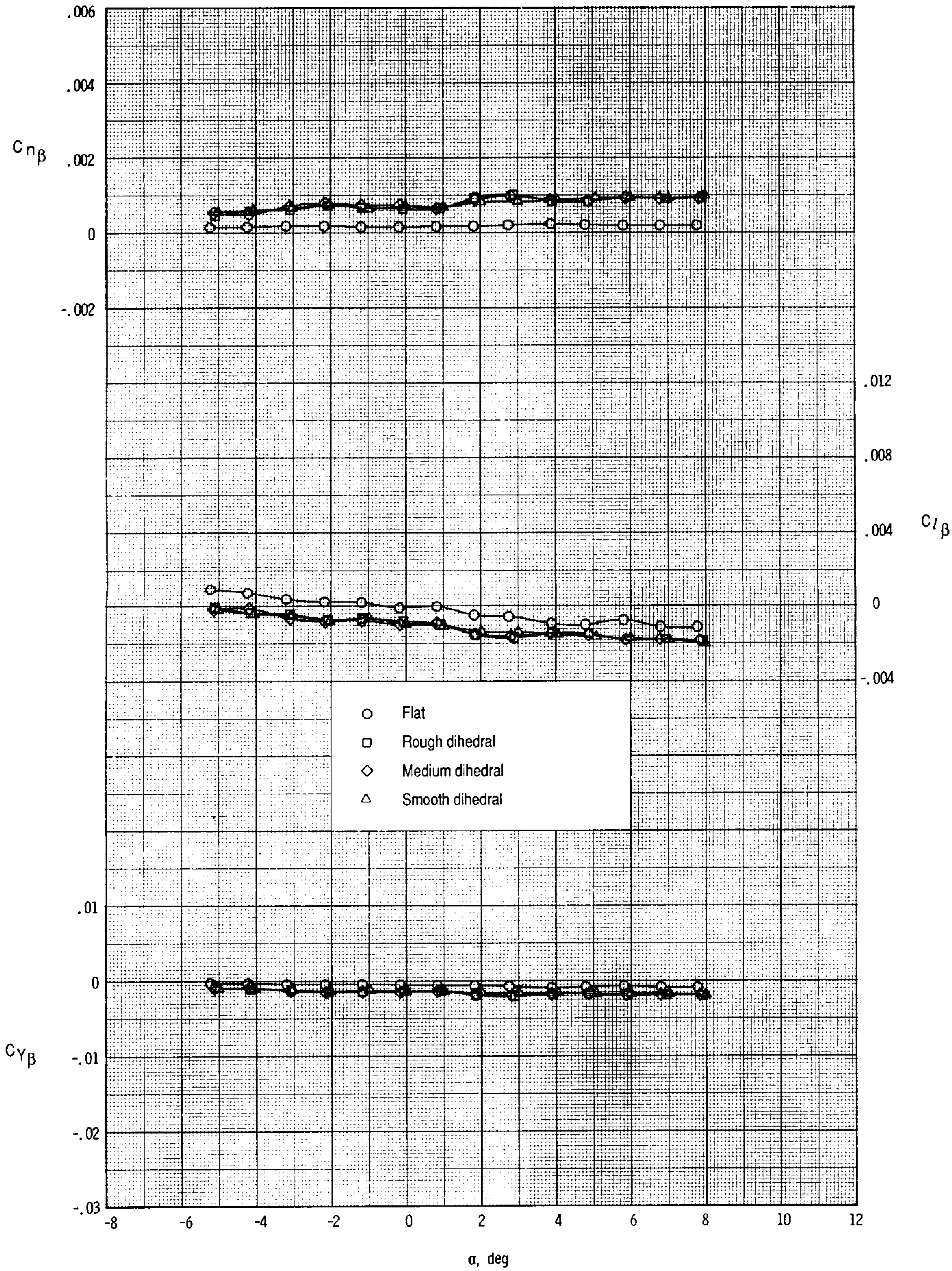

(d) $M = 2.4$.

Figure 10. Continued.

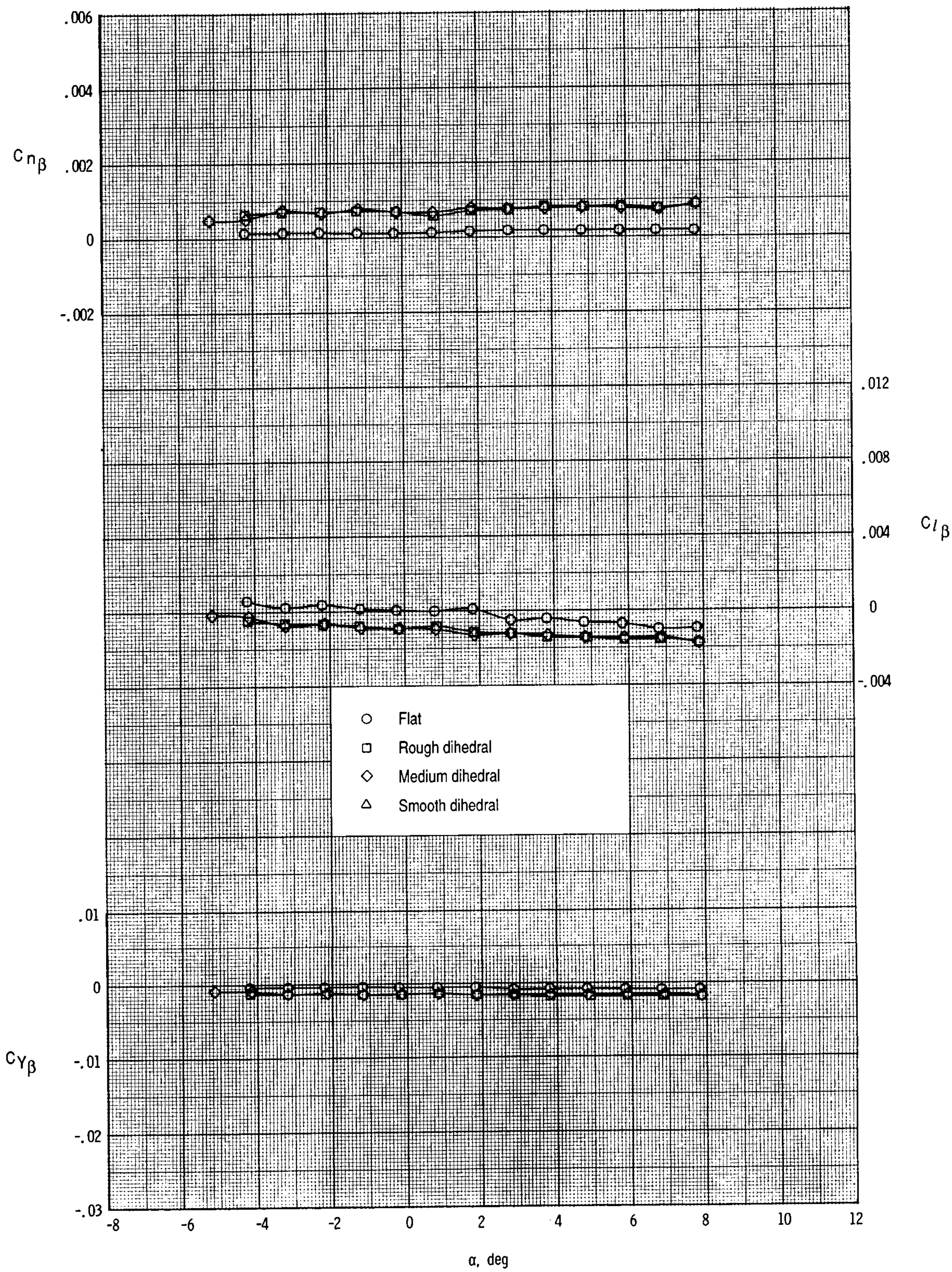

(e) $M = 2.6$.

Figure 10. Continued.

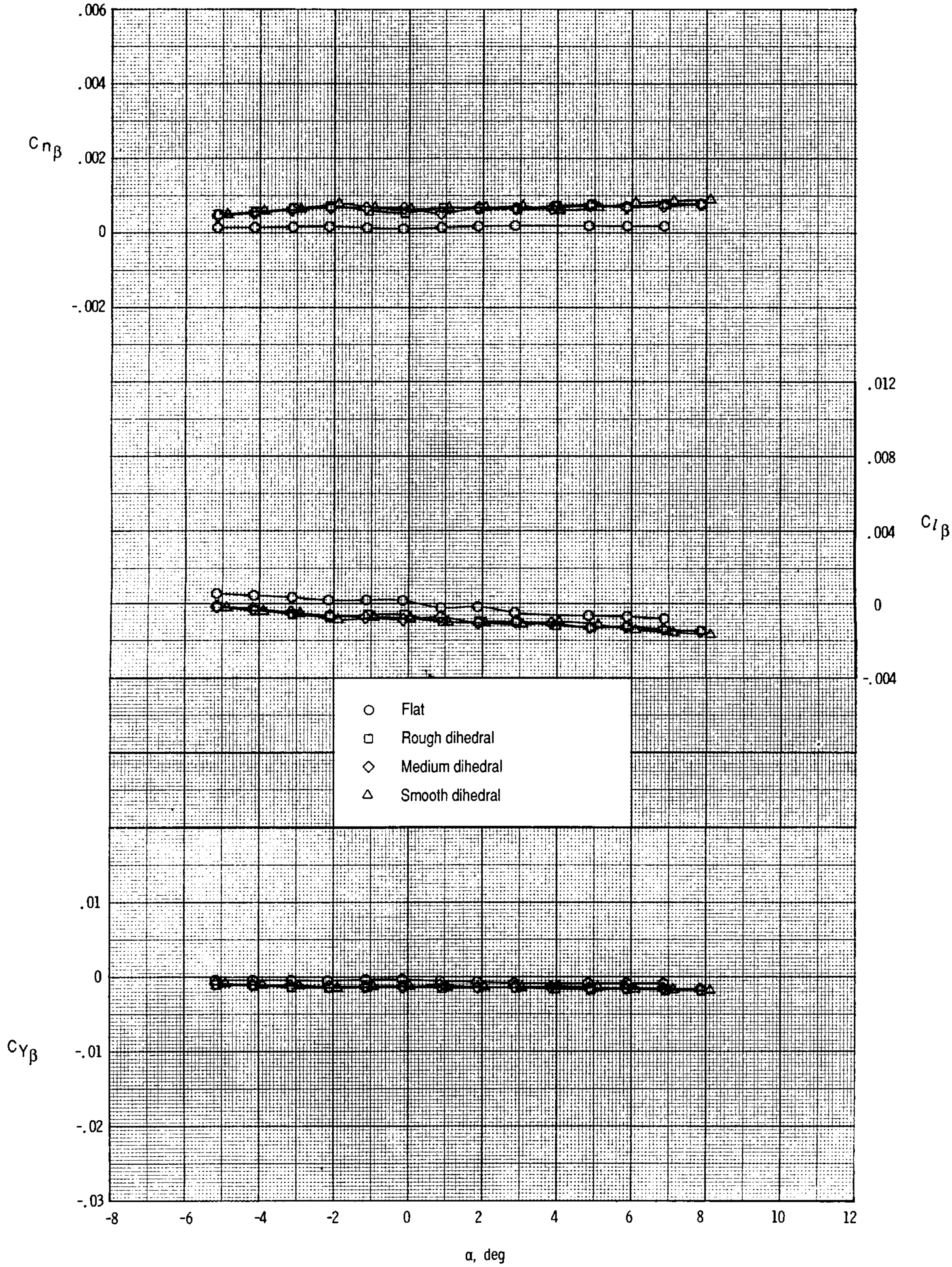

(f) $M = 2.8$.

Figure 10. Concluded.

ORIGINAL PAGE
BLACK AND WHITE PHOTOGRAPH

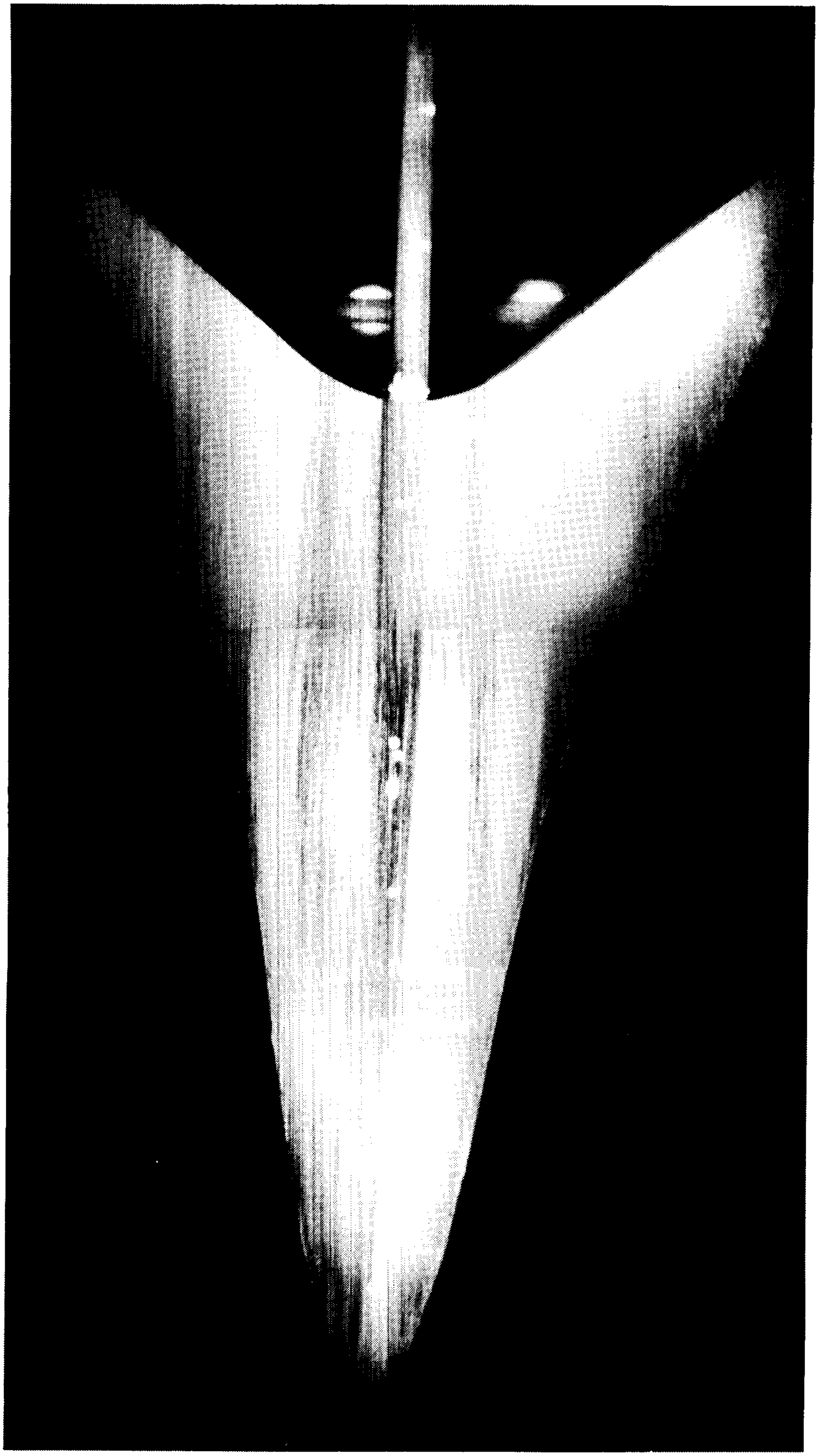

(a) $\alpha = 0°$.

Figure 11. Oil flow photograph of flat wing; $M = 2.4$.

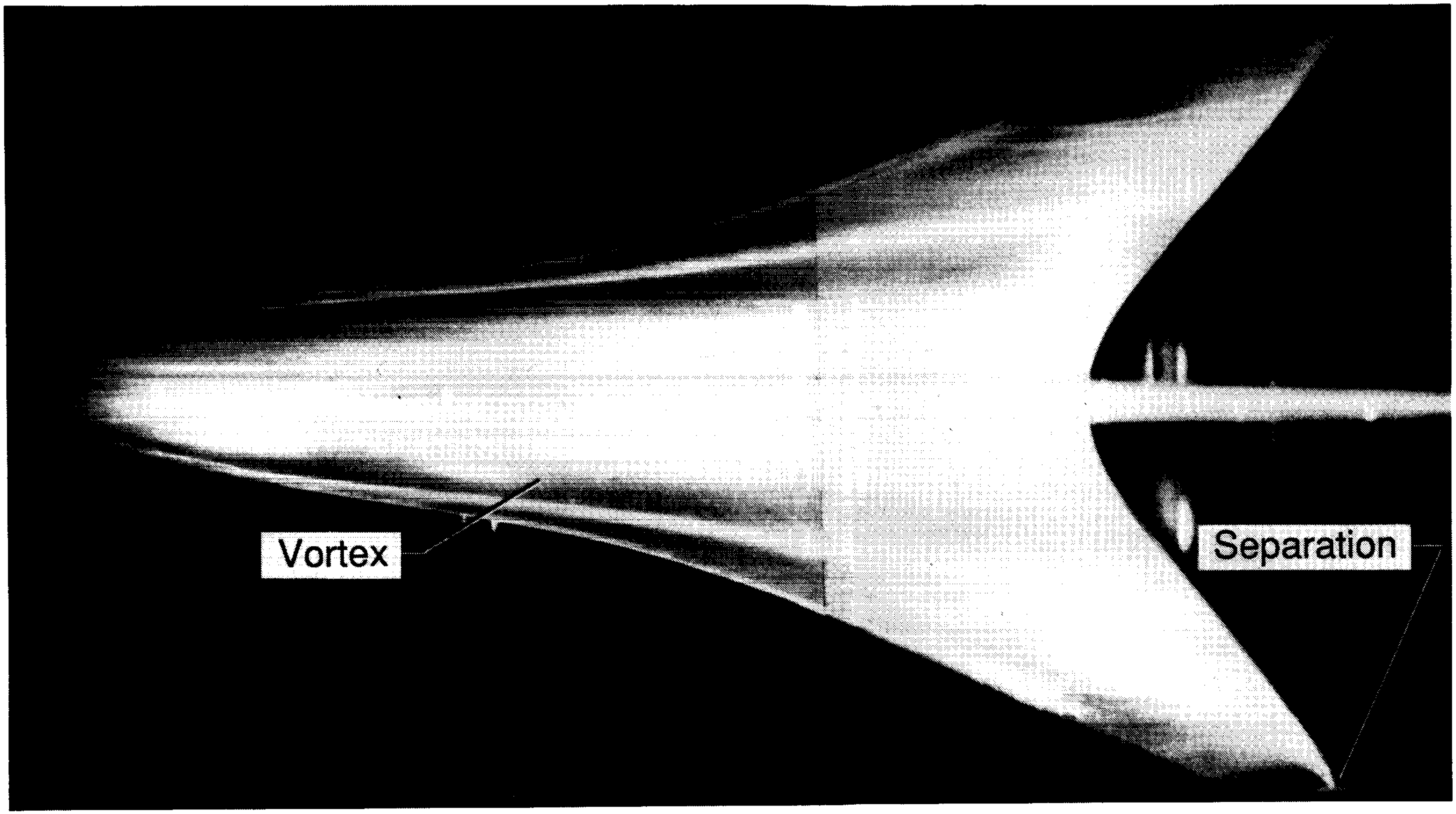

(b) $\alpha = 5°$.

Figure 11. Concluded.

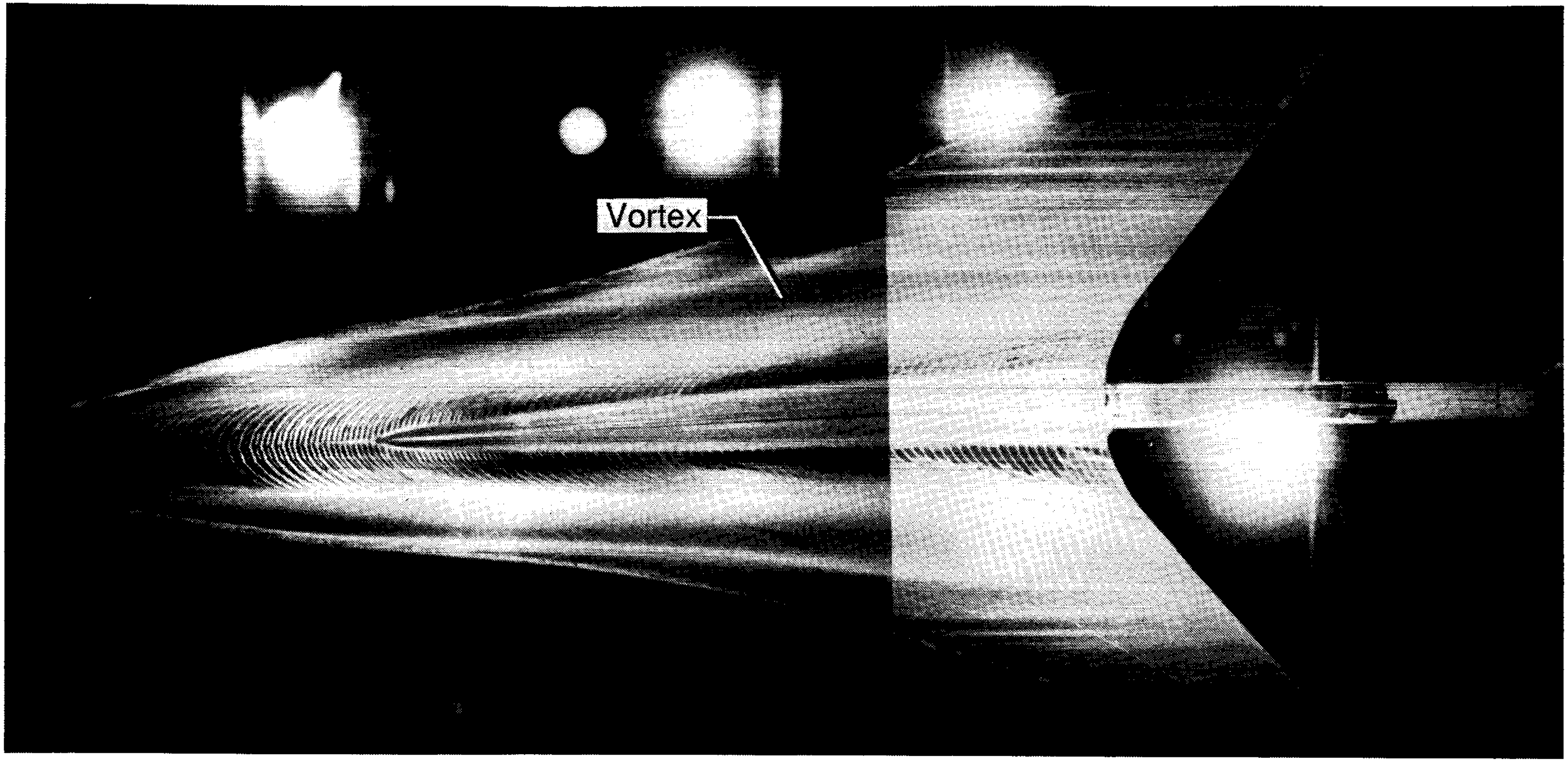

(a) $\alpha = -5°$.

Figure 12. Oil flow photograph of rough dihedral model; $M = 2.4$; $R/\mathrm{ft} = 2 \times 10^6$; bottom.

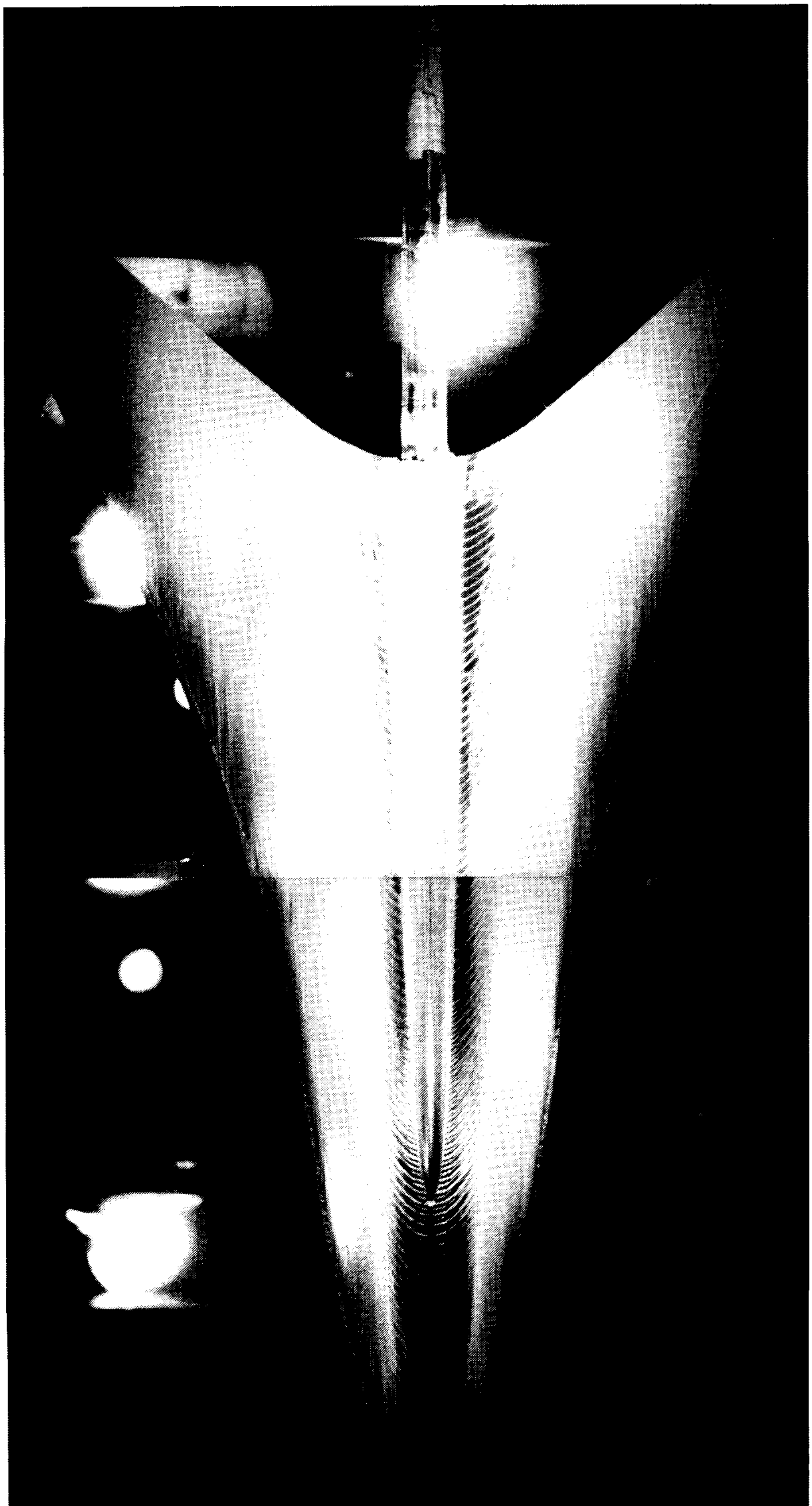

(b) $\alpha = 0°$.

Figure 12. Continued.

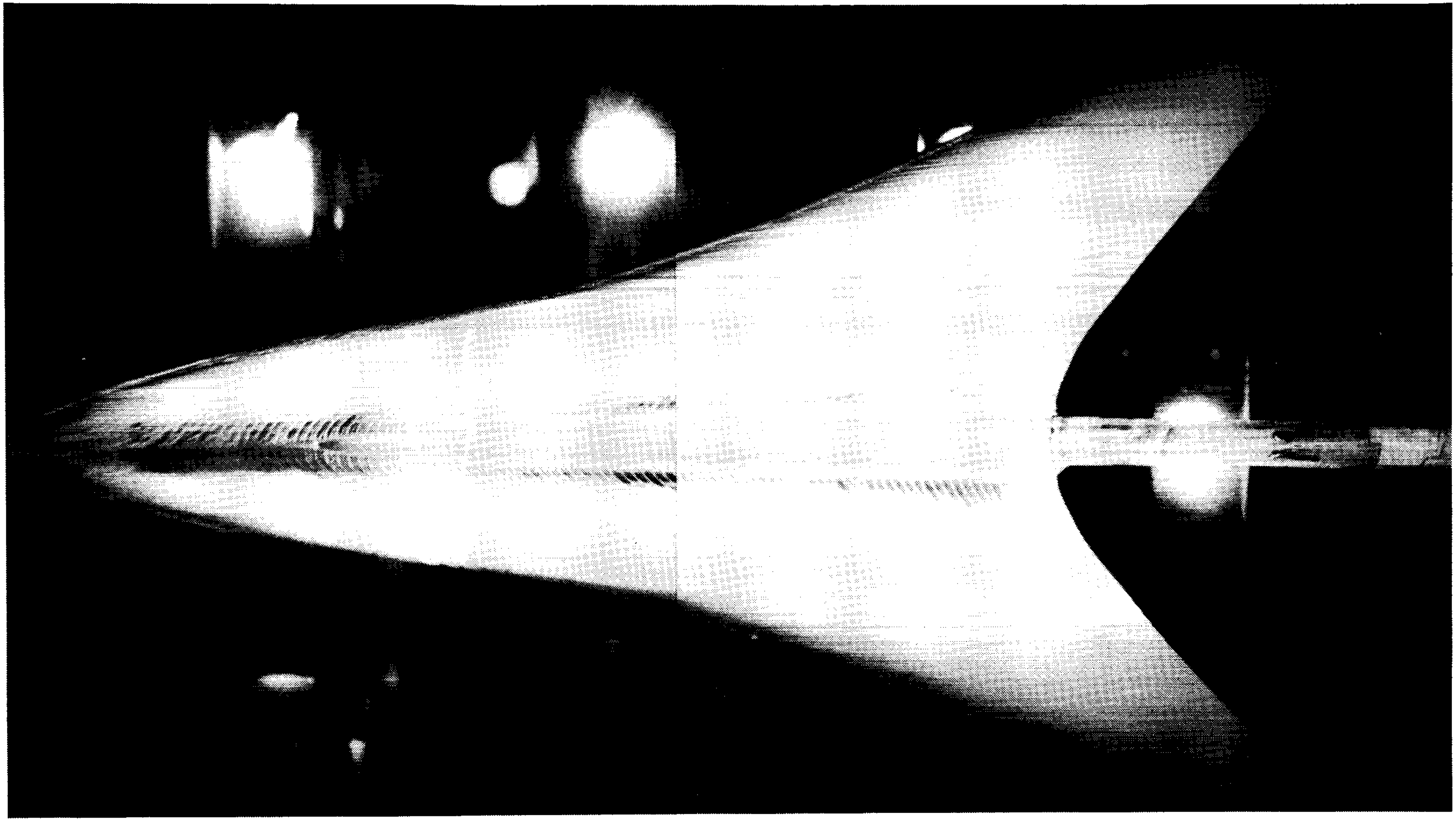

(c) $\alpha = 5°$.

Figure 12. Concluded.

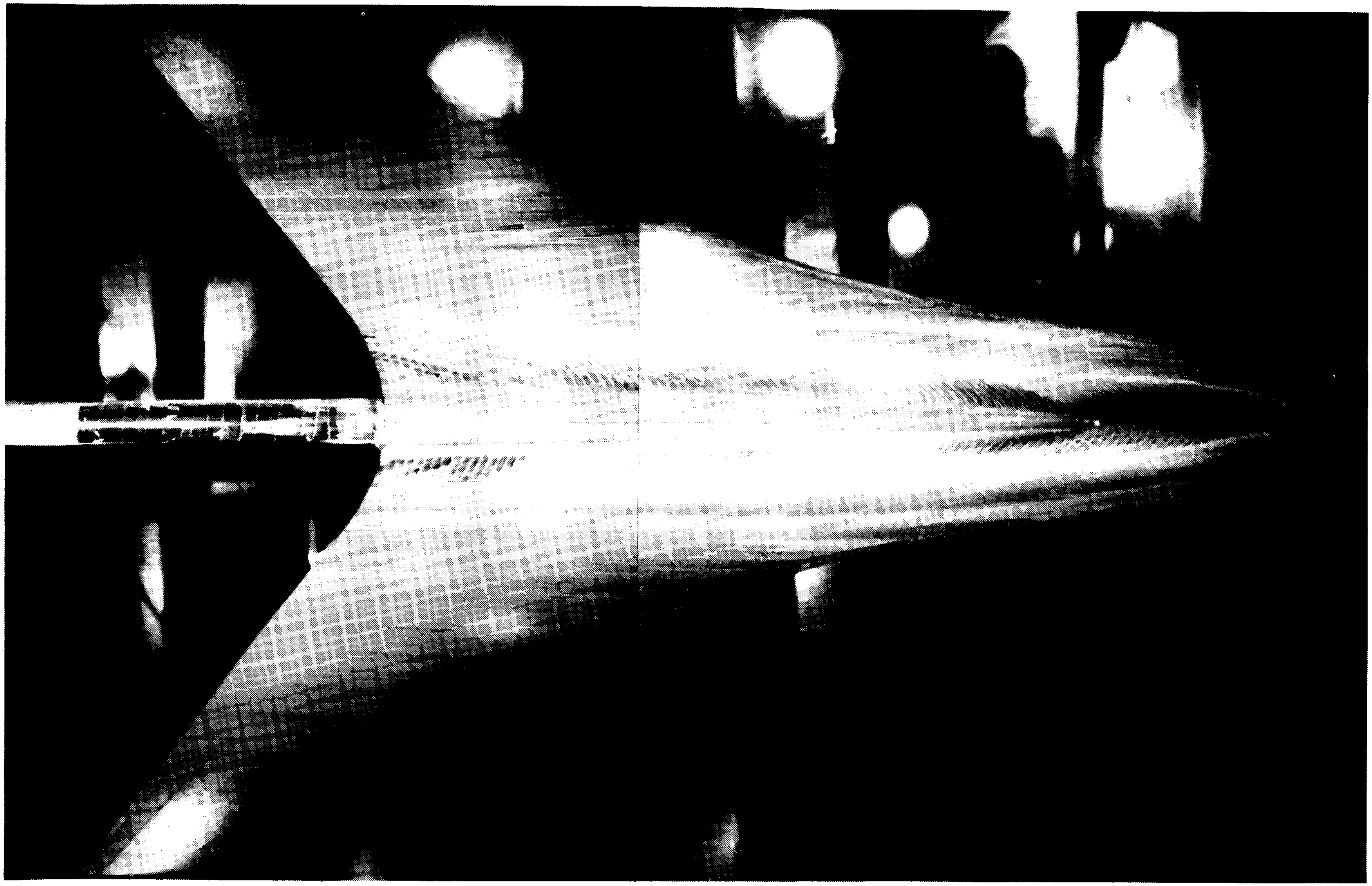

(a) $\alpha = -5°$.

Figure 13. Oil flow photograph of rough dihedral; $M = 2.4$; $R/\mathrm{ft} = 2 \times 10^6$; top.

ORIGINAL PAGE
BLACK AND WHITE PHOTOGRAPH

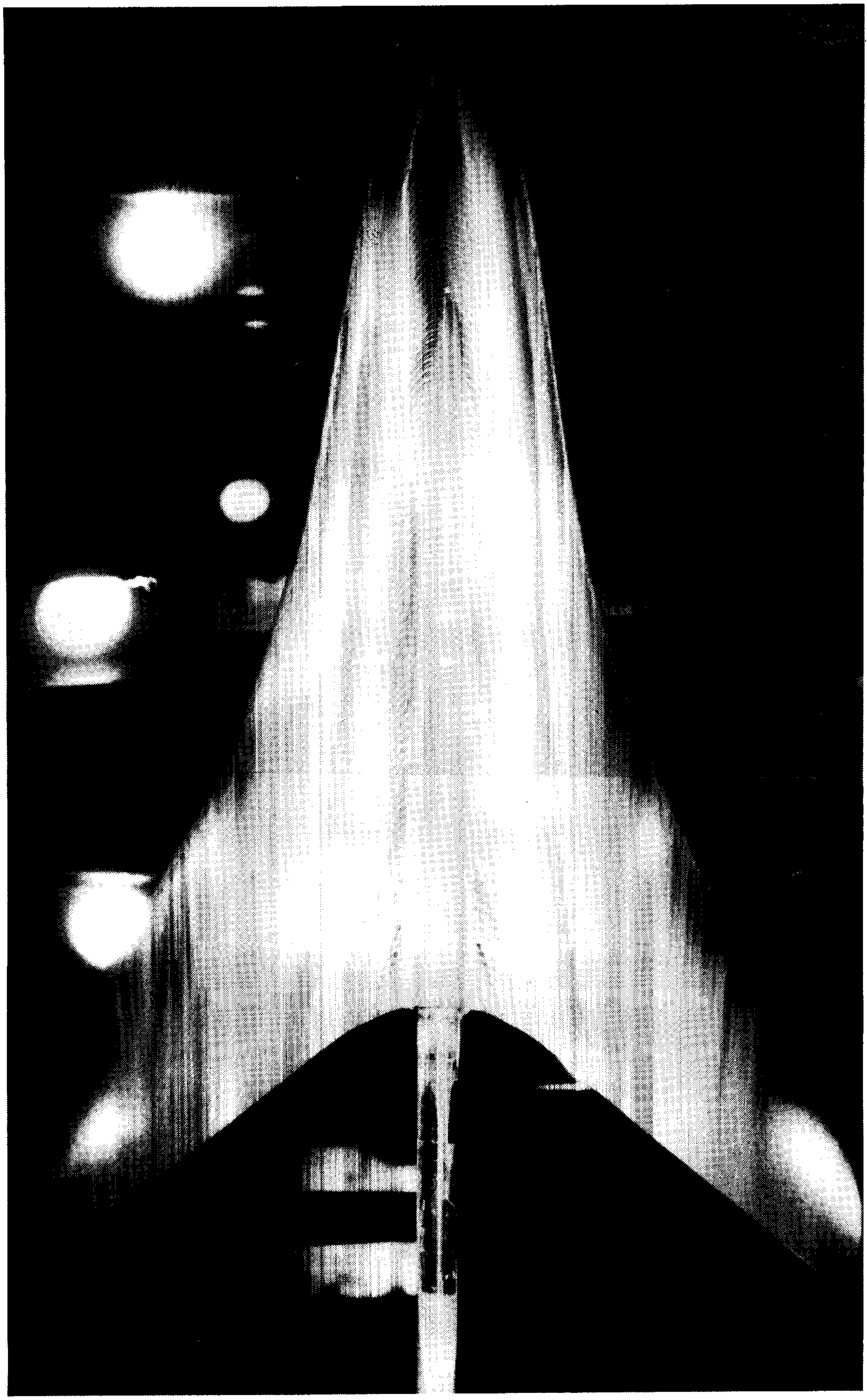

(b) $\alpha = 0°$.

Figure 13. Continued.

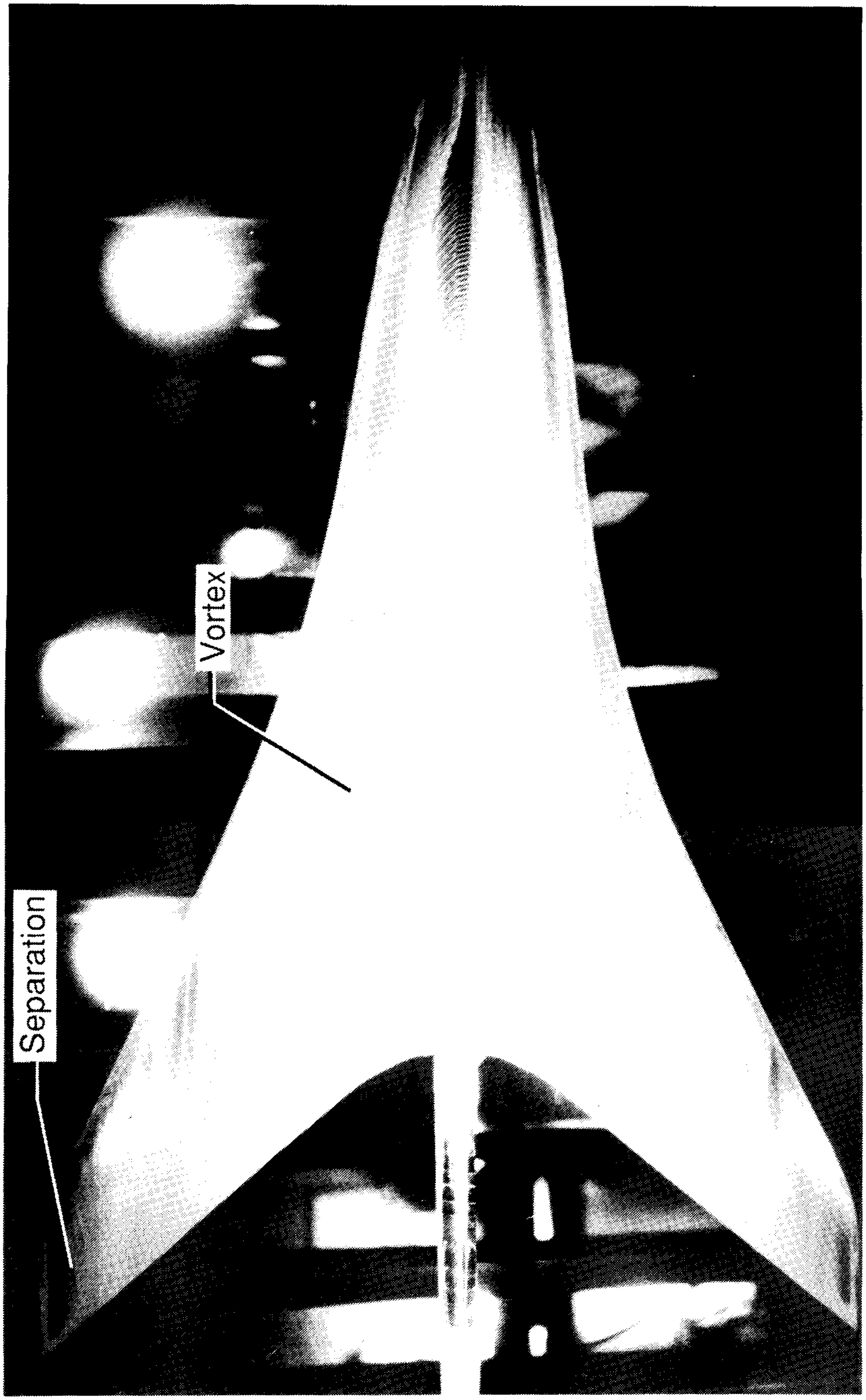

(c) $\alpha = 5°$.

Figure 13. Concluded.

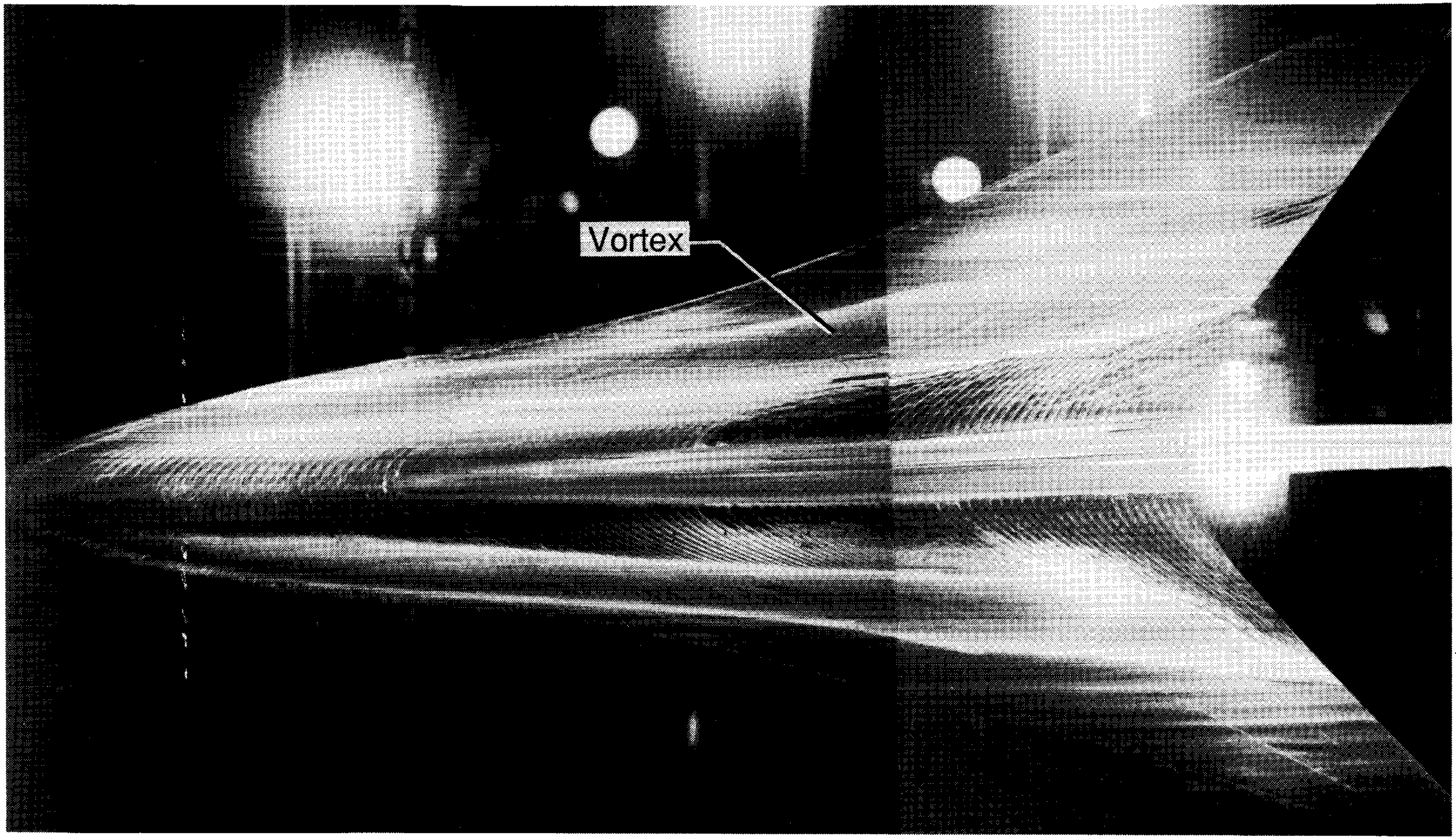

(a) $\alpha = -5°$.

Figure 14. Oil flow photograph of rough dihedral; $R/\text{ft} = 6 \times 10^6$; $M = 2.0$; bottom.

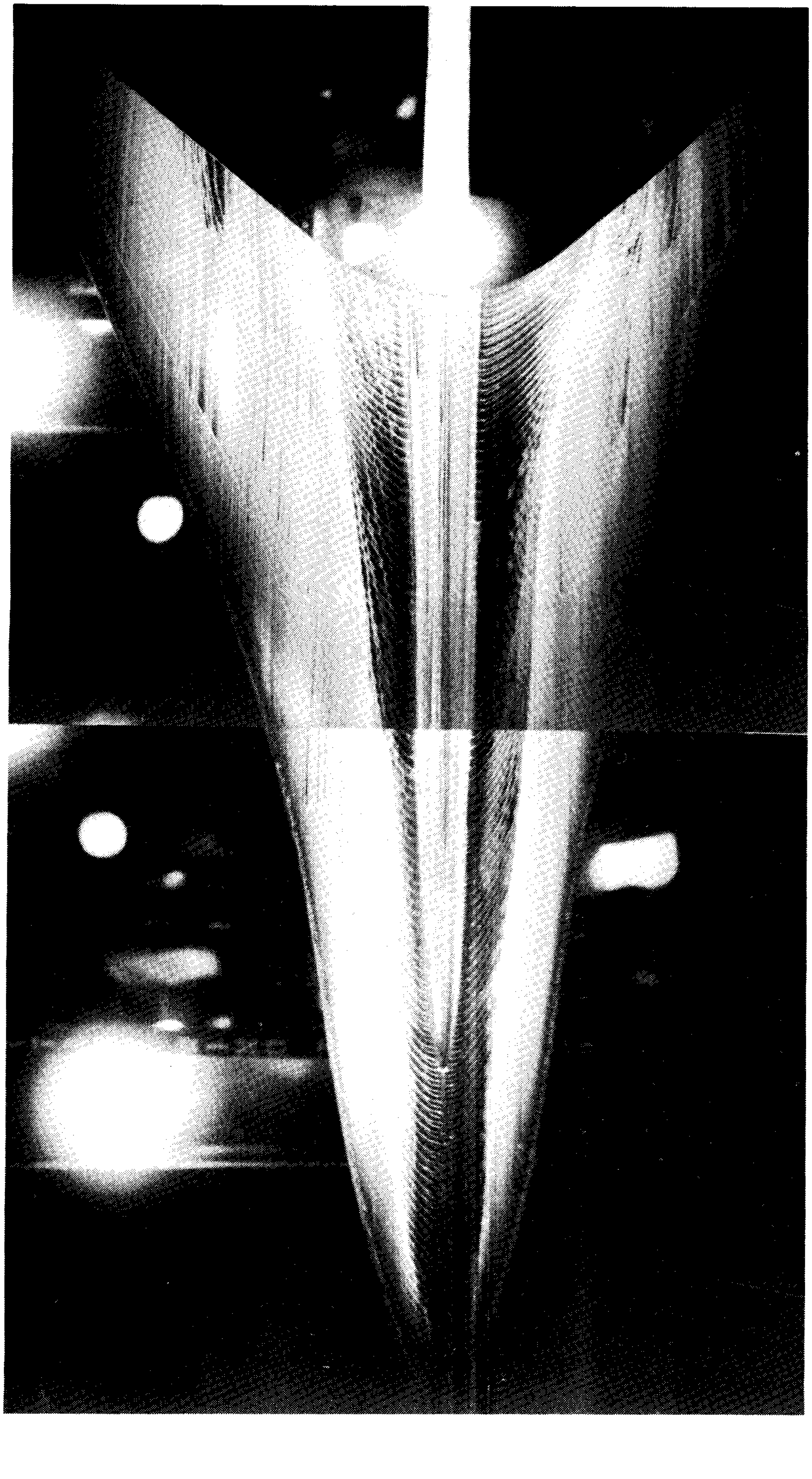

(b) $\alpha = 0°$.

Figure 14. Continued.

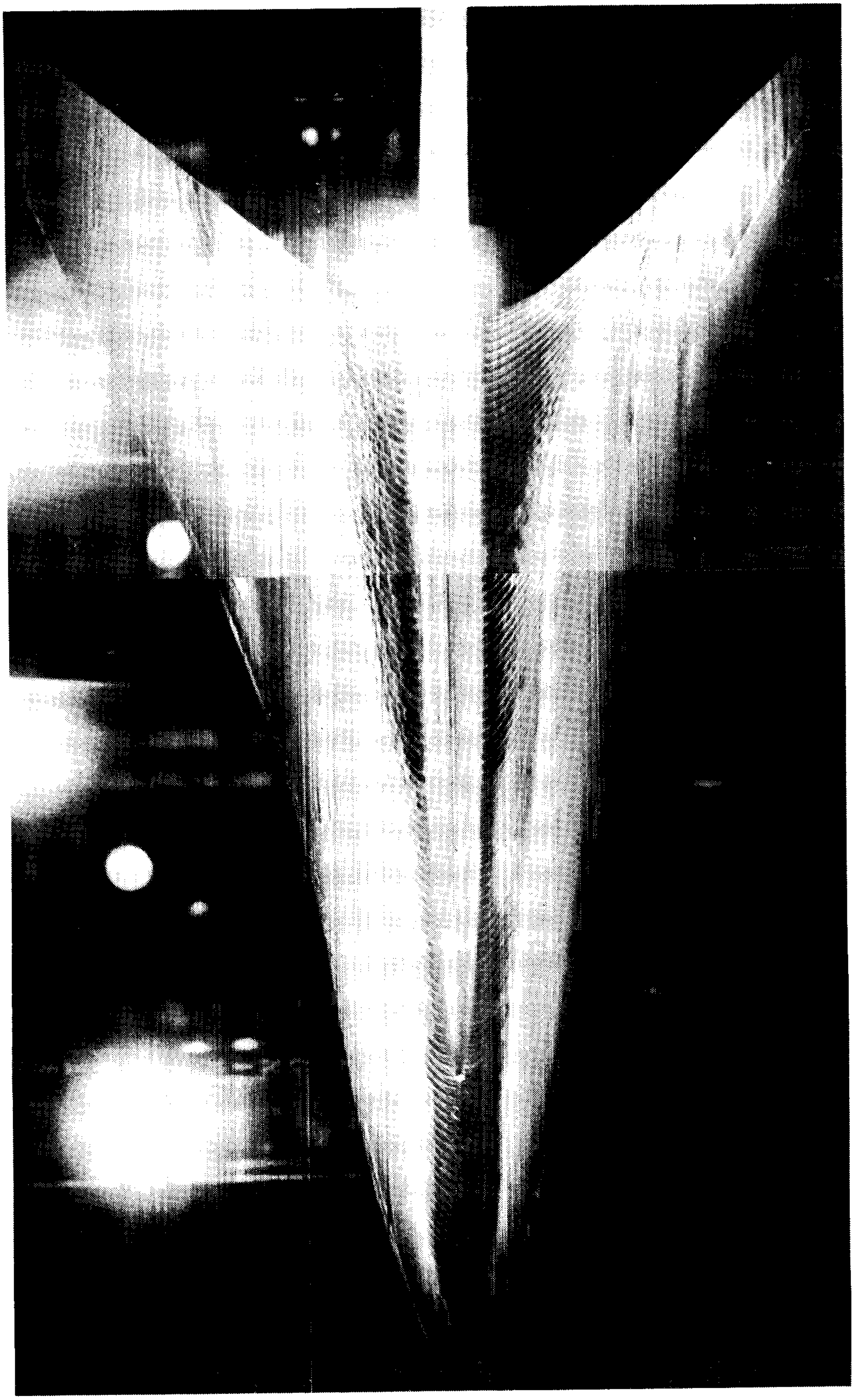

(c) $\alpha = 5^\circ$.

Figure 14. Concluded.

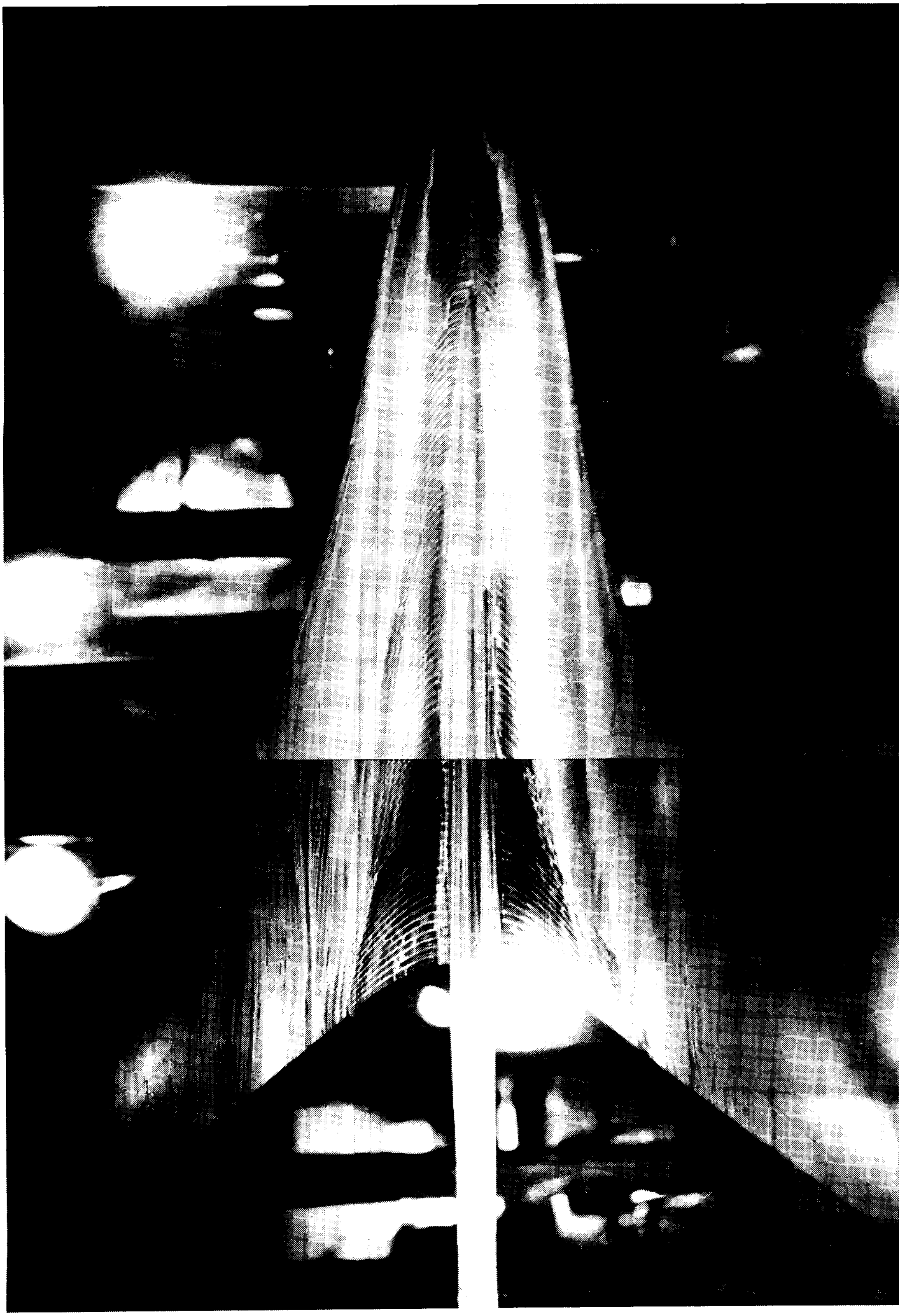

(a) $\alpha = -5^\circ$.

Figure 15. Oil flow photograph of rough dihedral model; $R/\mathrm{ft} = 6 \times 10^6$; $M = 2.0$; top.

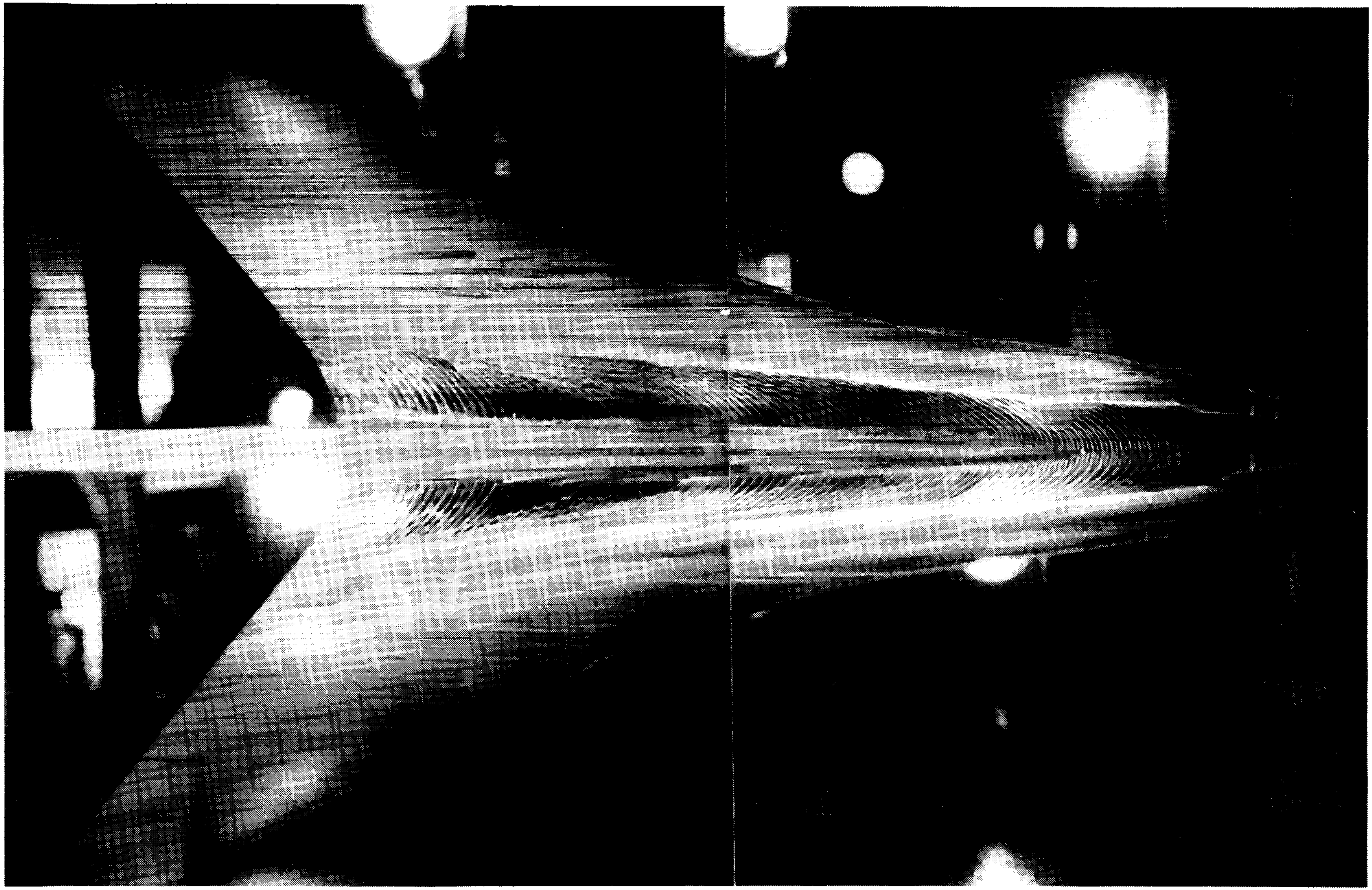

(b) $\alpha = 0°$.

Figure 15. Continued.

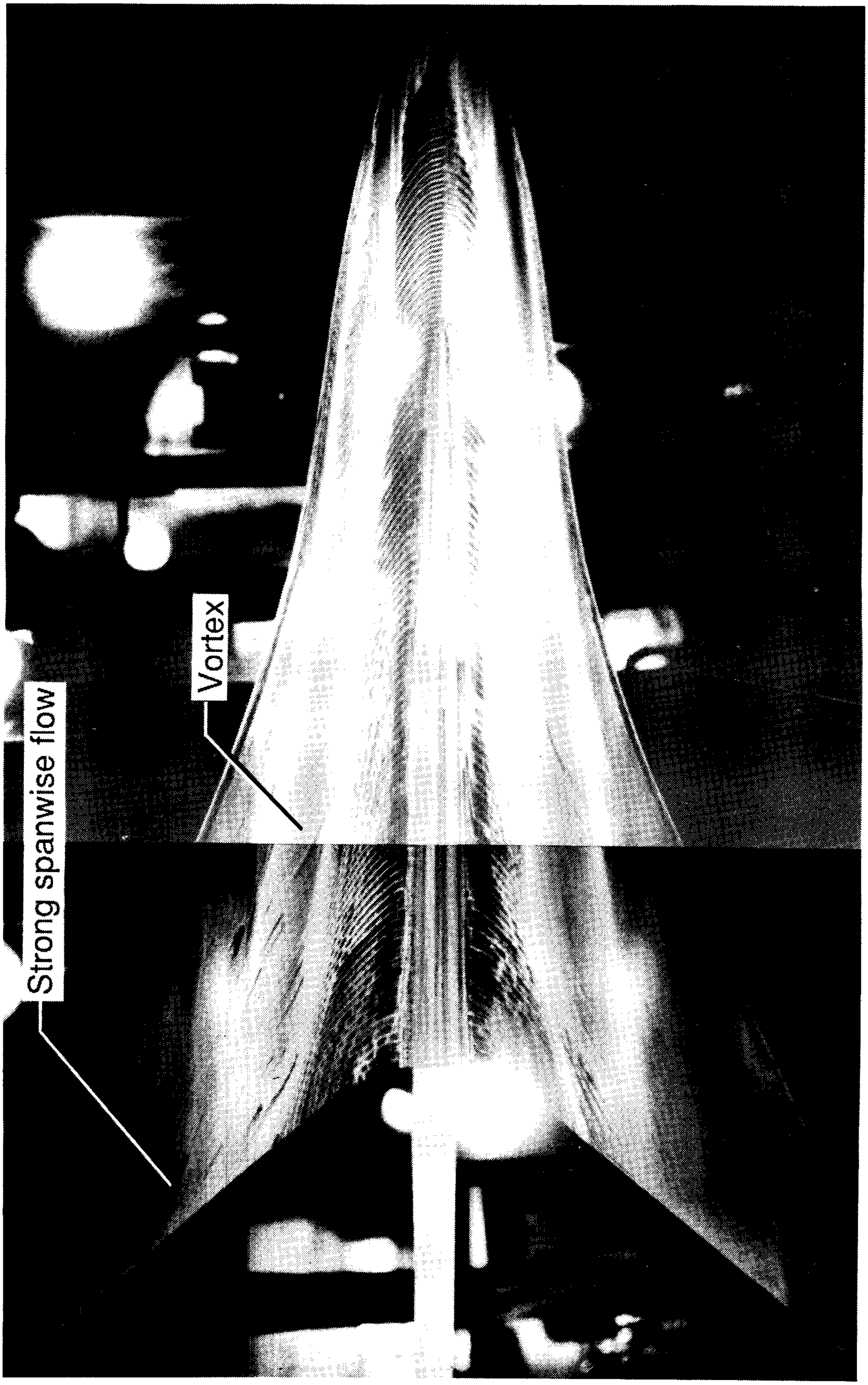

(c) $\alpha = 5°$.

Figure 15. Concluded.

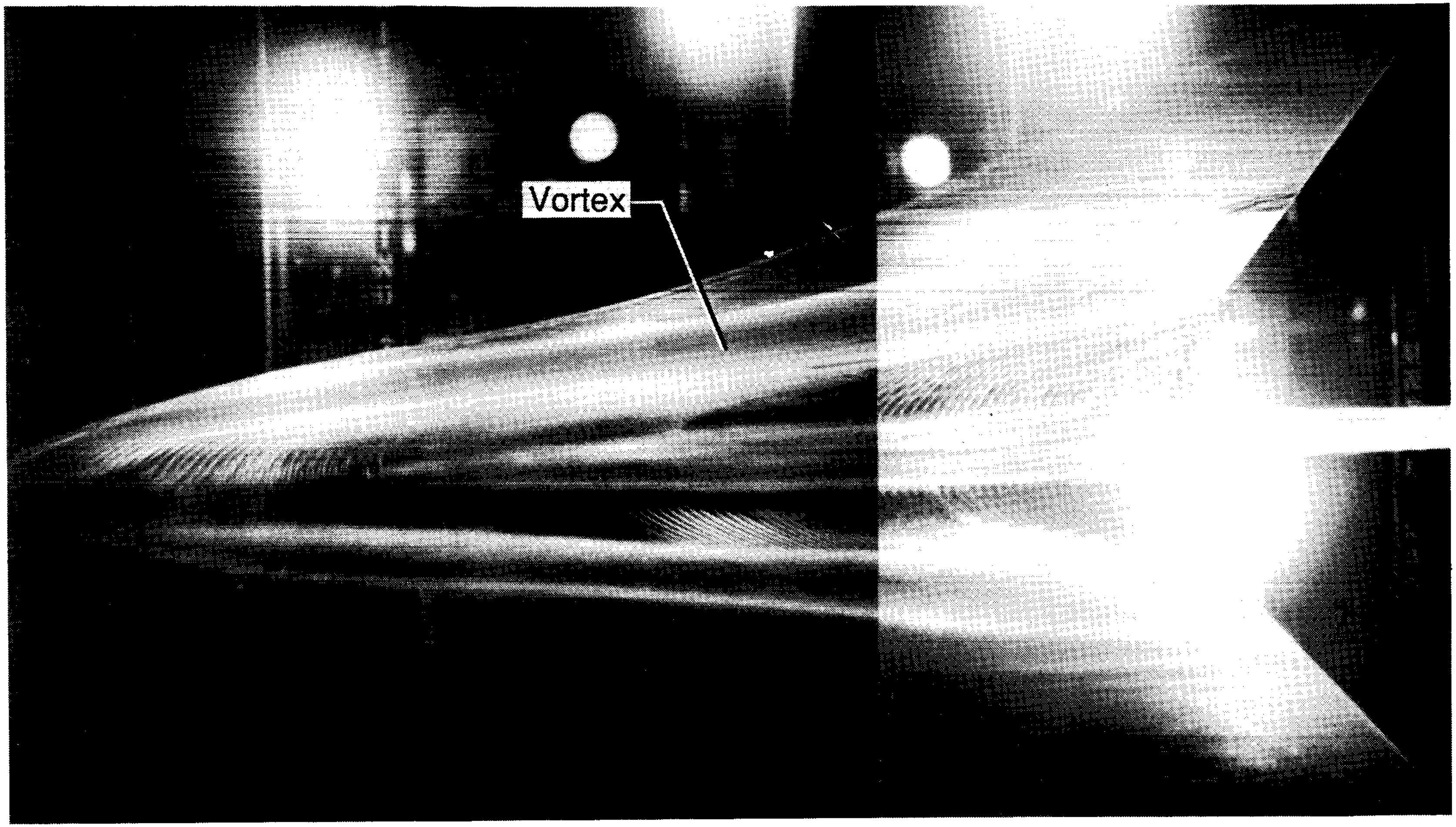

(a) $\alpha = -5°$.

Figure 16. Oil flow photograph of rough dihedral; $M = 2.4$; $R/\text{ft} = 6 \times 10^6$; bottom.

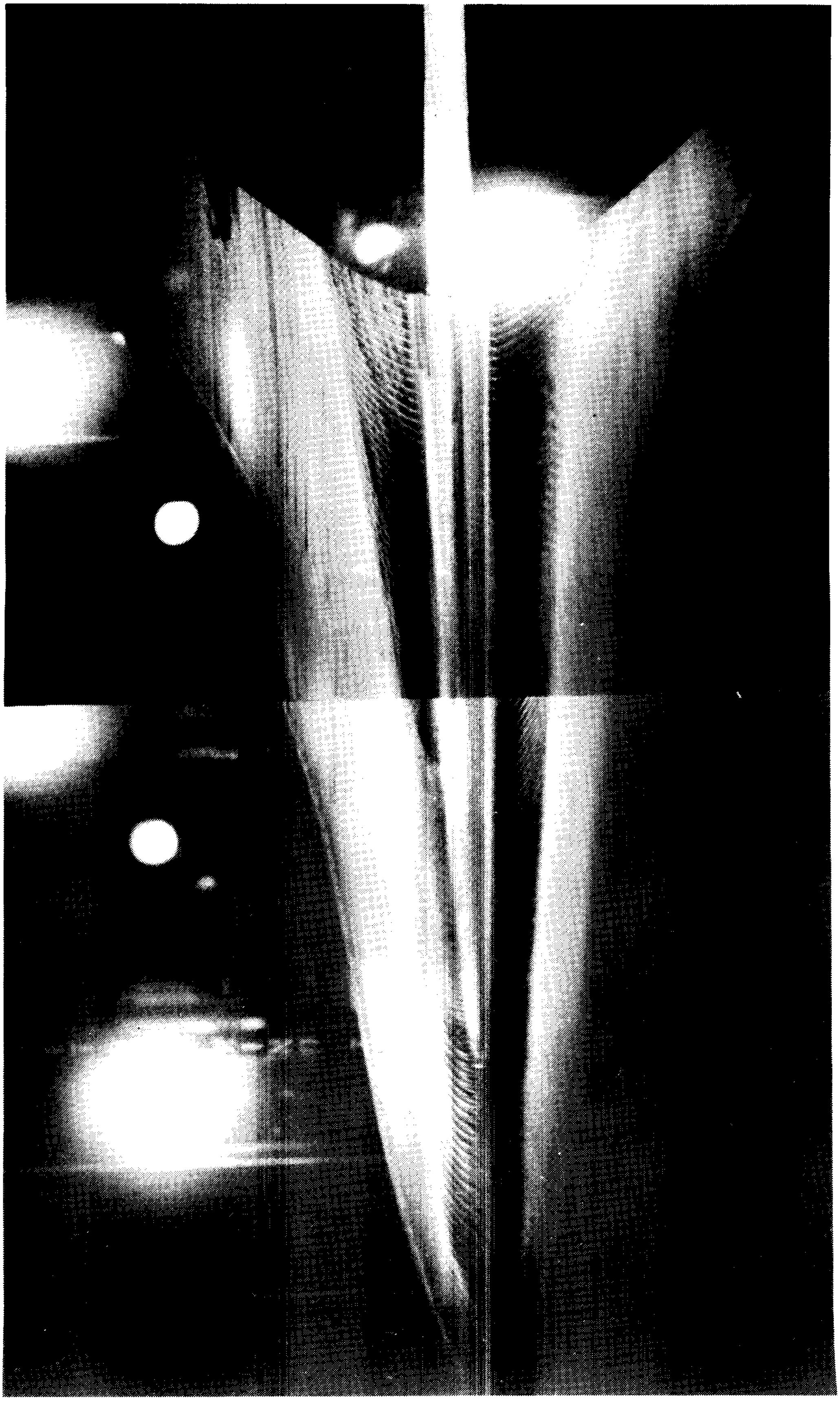

(b) $\alpha = 0°$.

Figure 16. Continued.

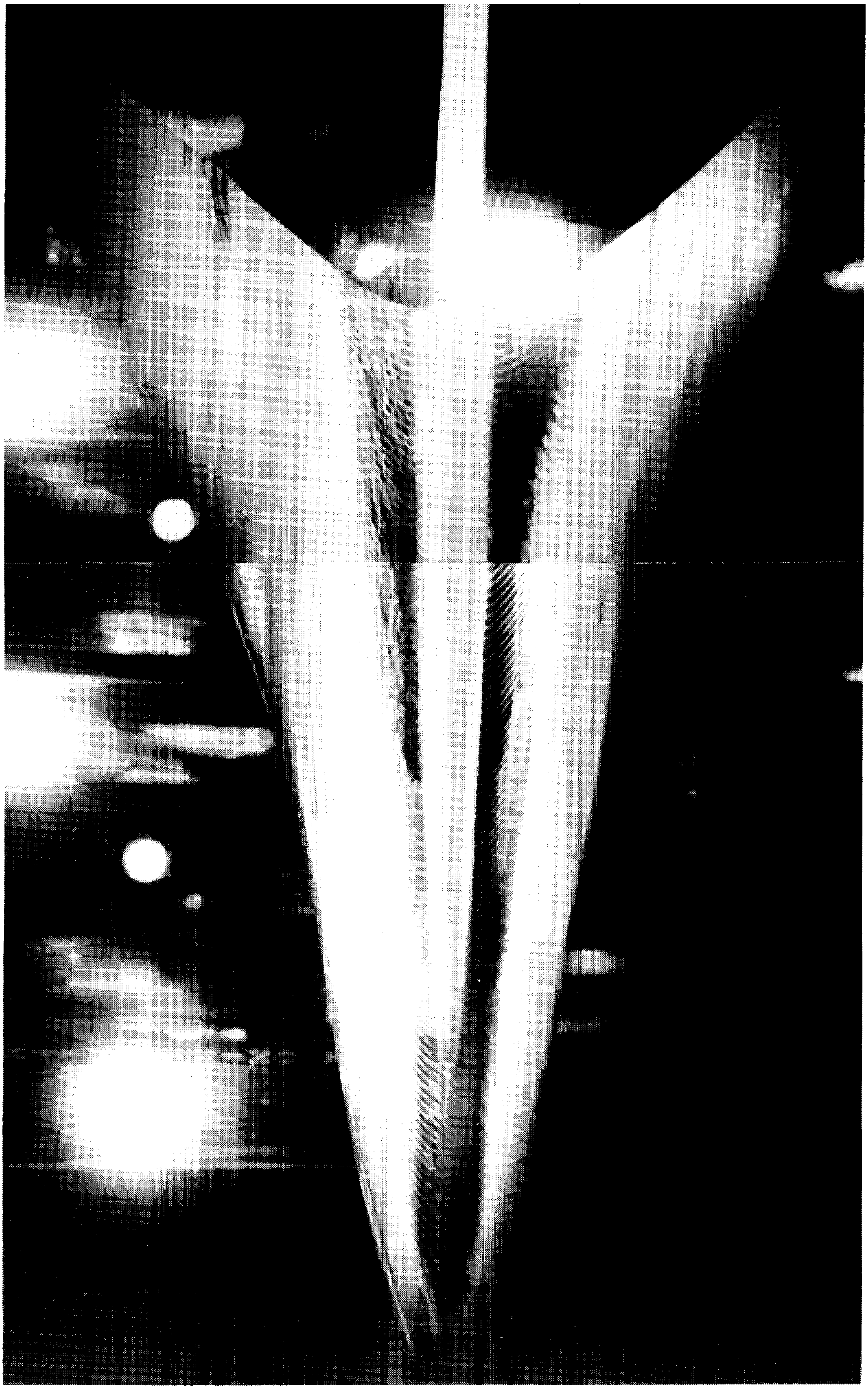

(c) $\alpha = 5^{\circ}$.

Figure 16. Concluded.

(a) $\alpha = 0°$.

Figure 17. Oil flow photograph of rough dihedral; $M = 2.4$; $R/\text{ft} = 6 \times 10^6$; top.

ORIGINAL PAGE
BLACK AND WHITE PHOTOGRAPH

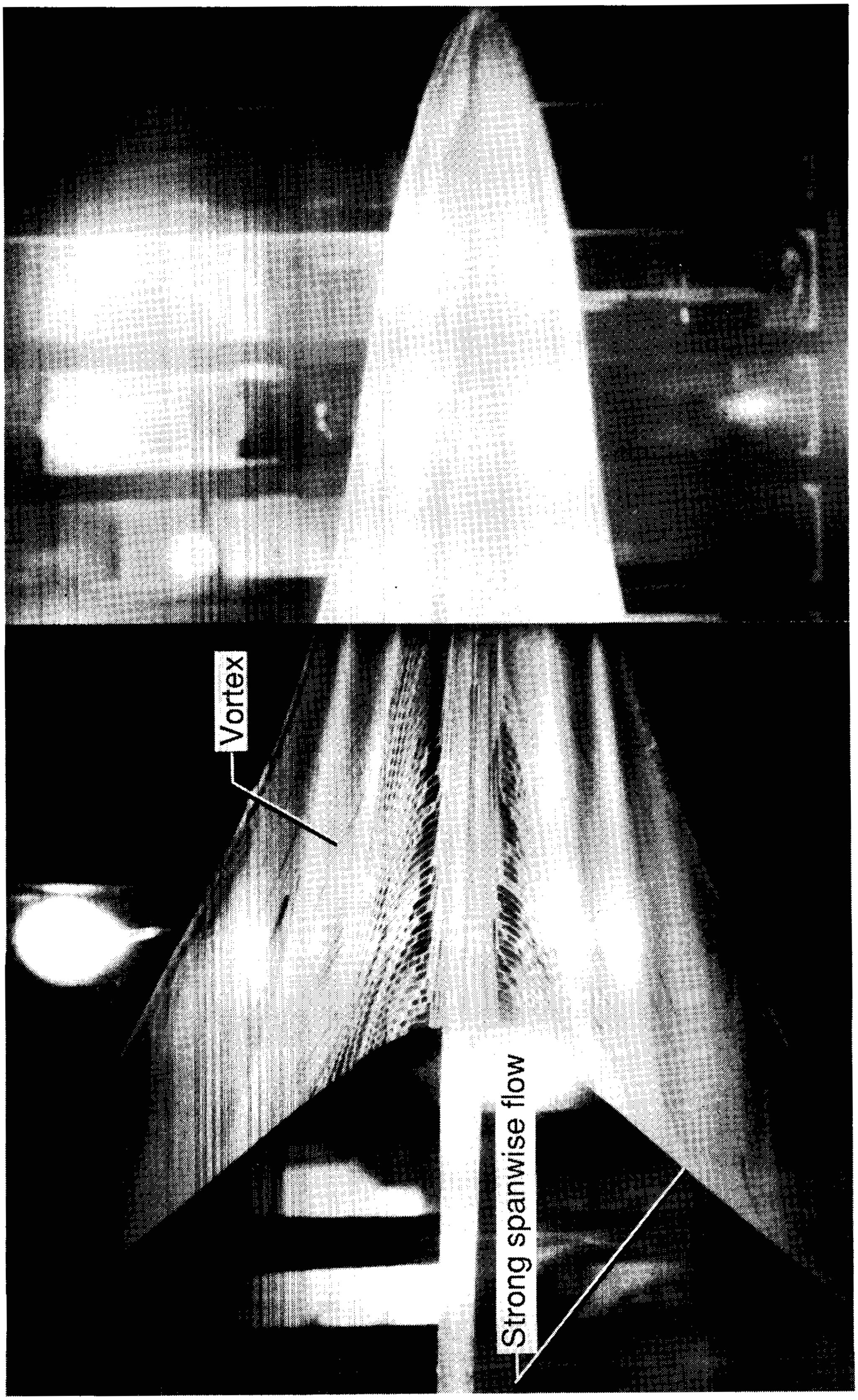

(b) $\alpha = 5$.

Figure 17. Concluded.

ORIGINAL PAGE
BLACK AND WHITE PHOTOGRAPH

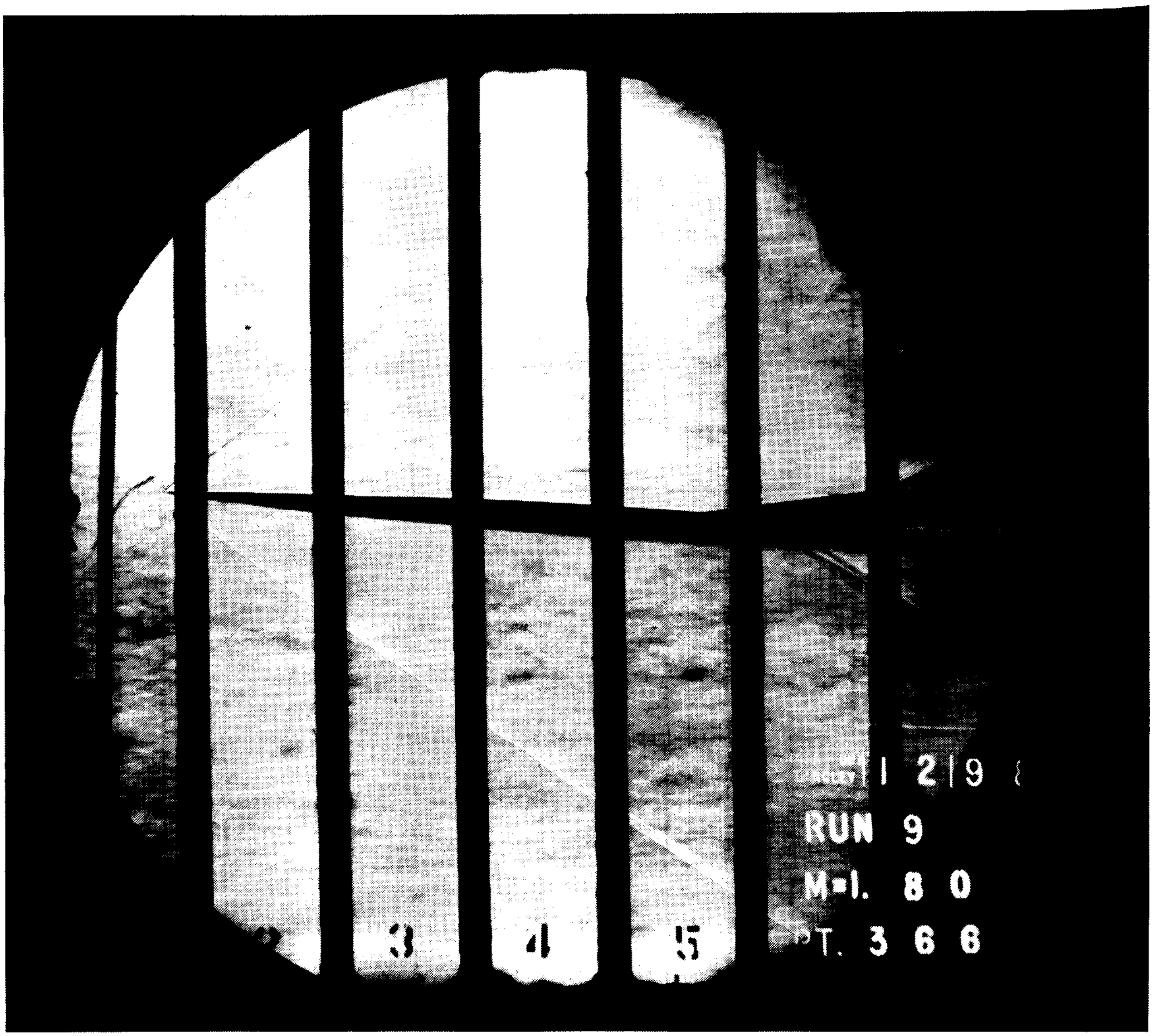

(a) $M = 1.8$.

Figure 18. Schlieren photograph of rough dihedral; $R/\text{ft} = 2 \times 10^6$; $\alpha = 5°$.

ORIGINAL PAGE
BLACK AND WHITE PHOTOGRAPH

(b) $M = 2.4$.

Figure 18. Continued.

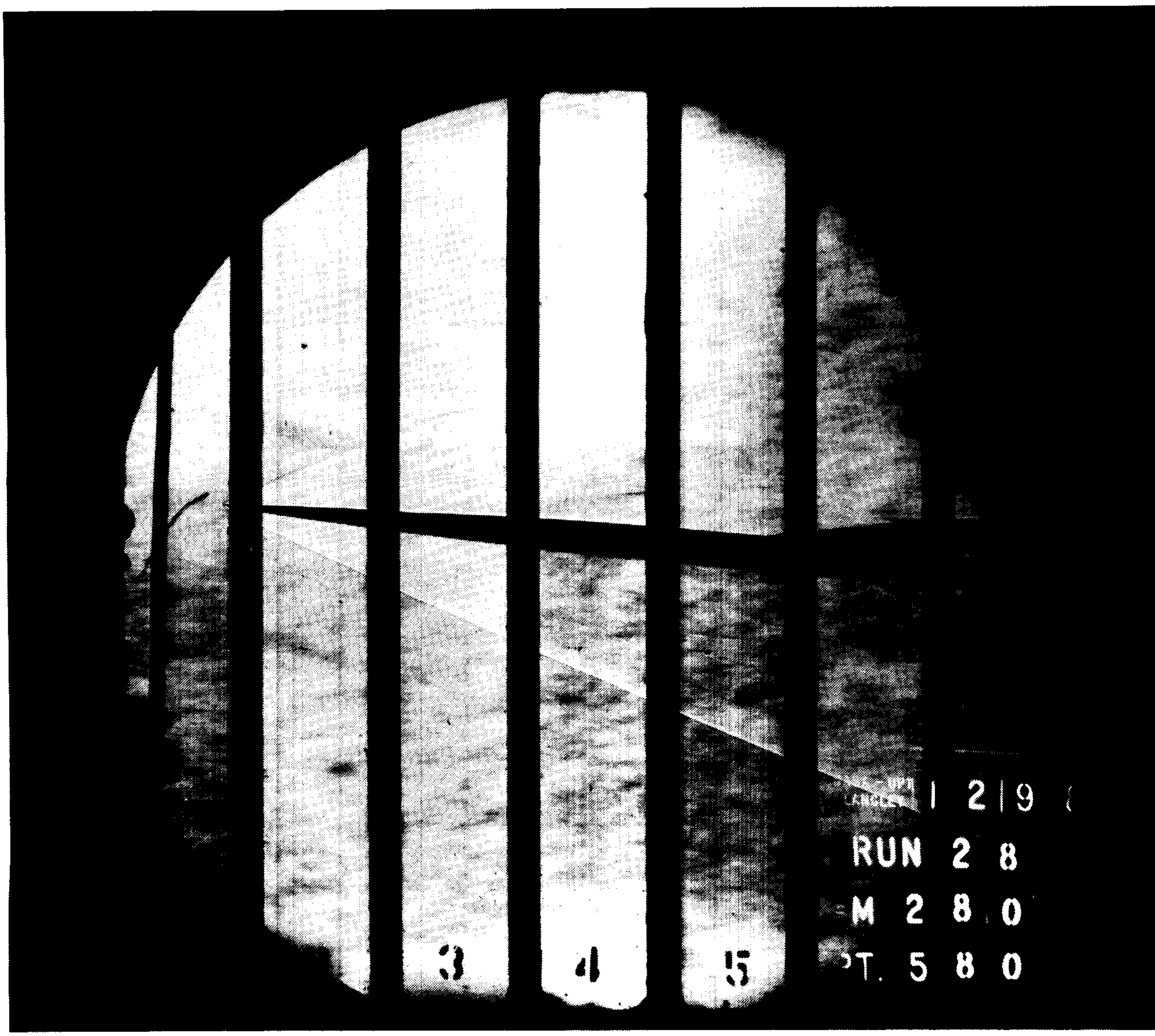

(c) $M = 2.8$.

Figure 18. Concluded.

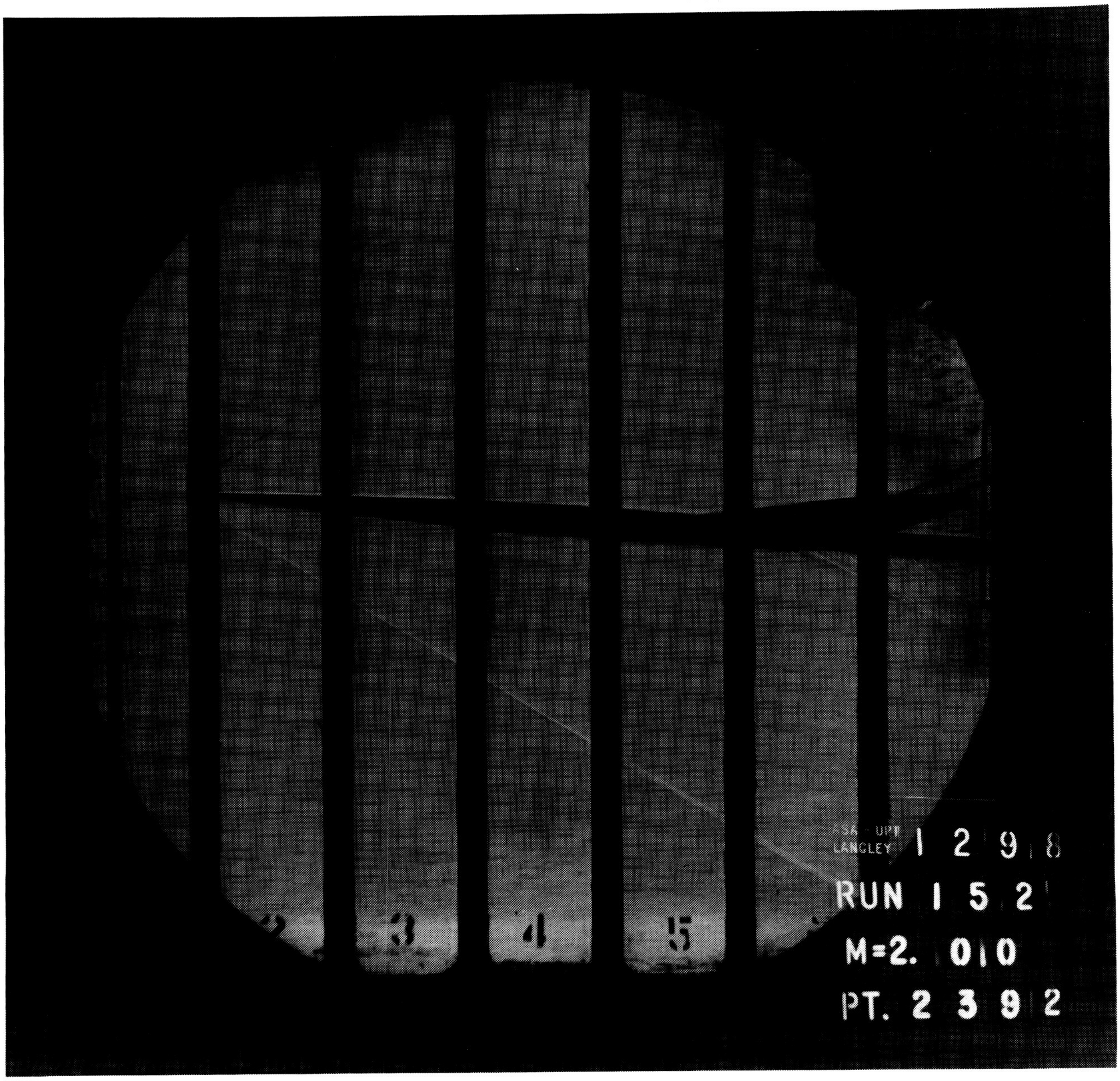

(a) $M = 2.0$.

Figure 19. Schlieren photograph of smooth dihedral; $R/\text{ft} = 2 \times 10^6$; $\alpha = 5°$.

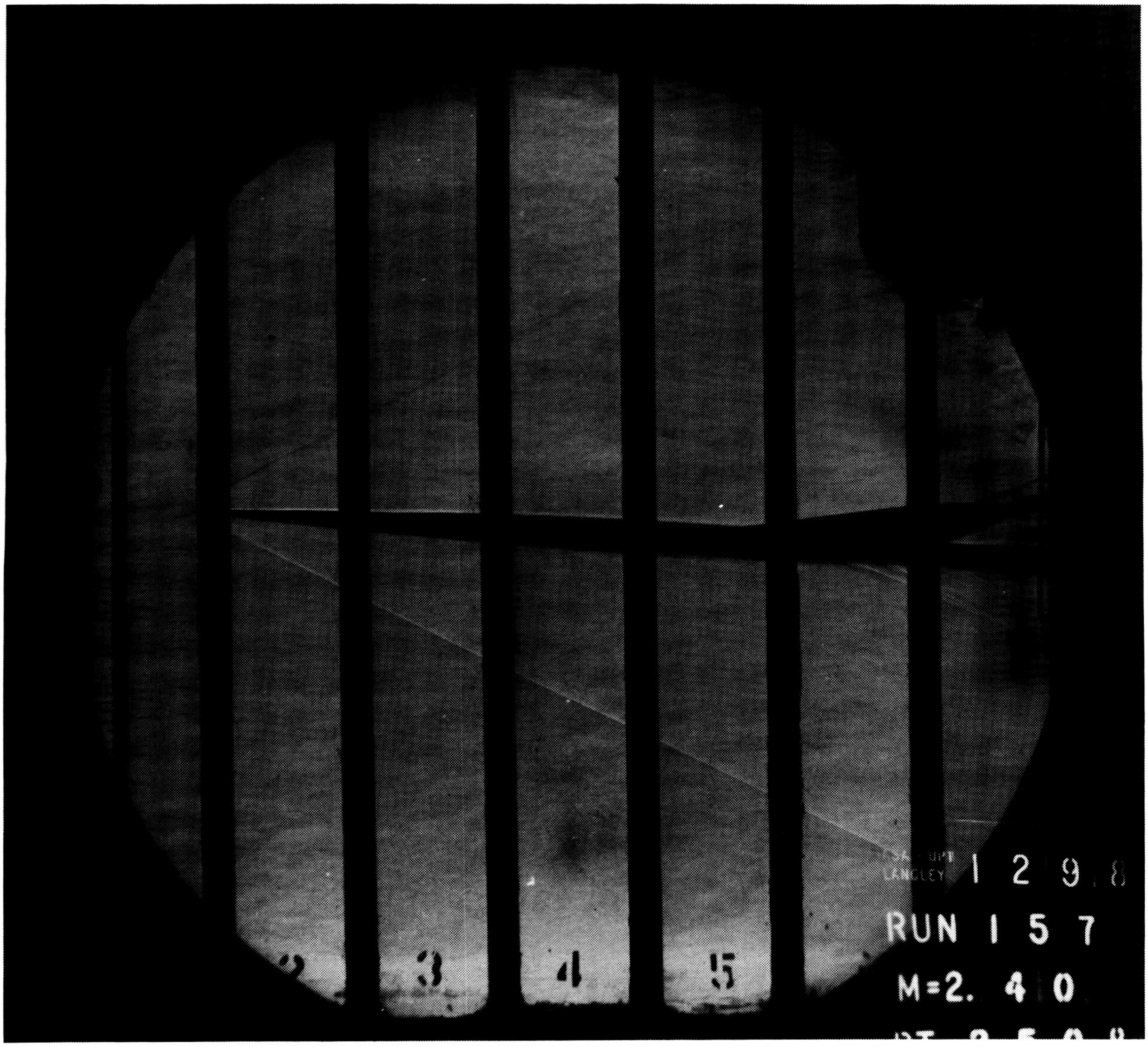

(b) $M = 2.4$.

Figure 19. Continued.

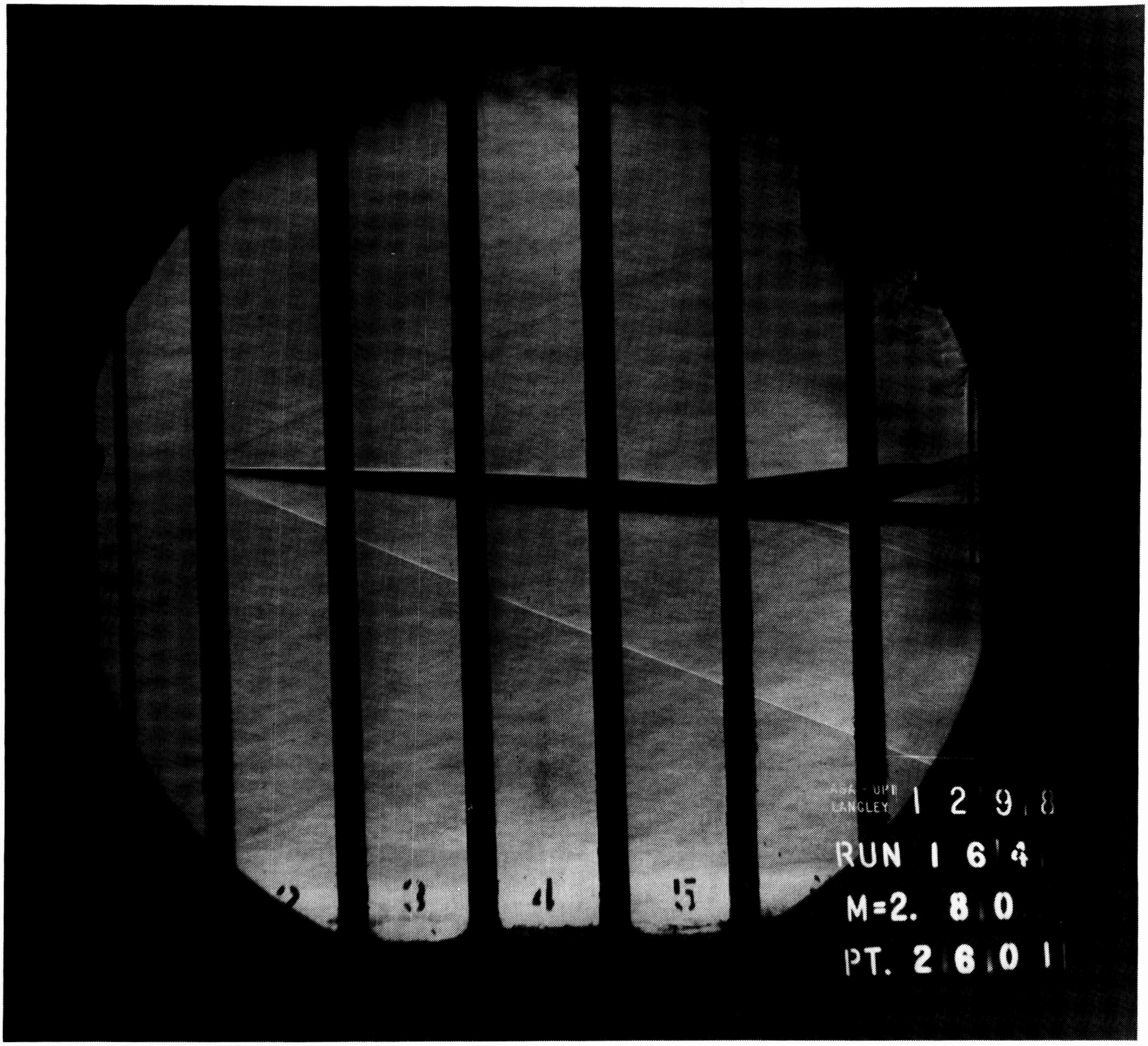

(c) $M = 2.8$.

Figure 19. Concluded.

ORIGINAL PAGE
BLACK AND WHITE PHOTOGRAPH

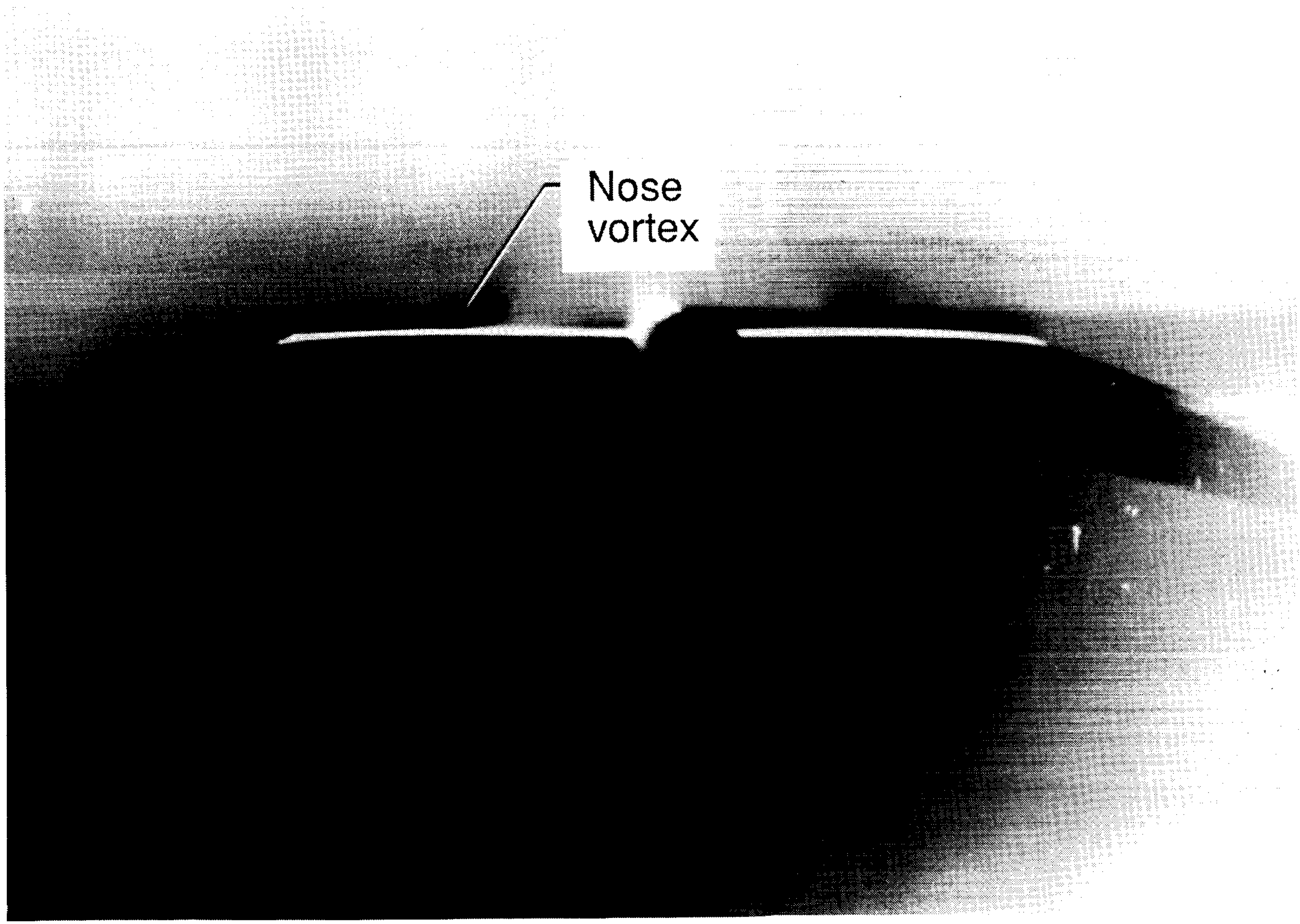

Figure 20. Vapor-screen photograph of flat wing; $M = 2.4°$; $R/\mathrm{ft} = 2 \times 10^6$; $\alpha = 5°$.

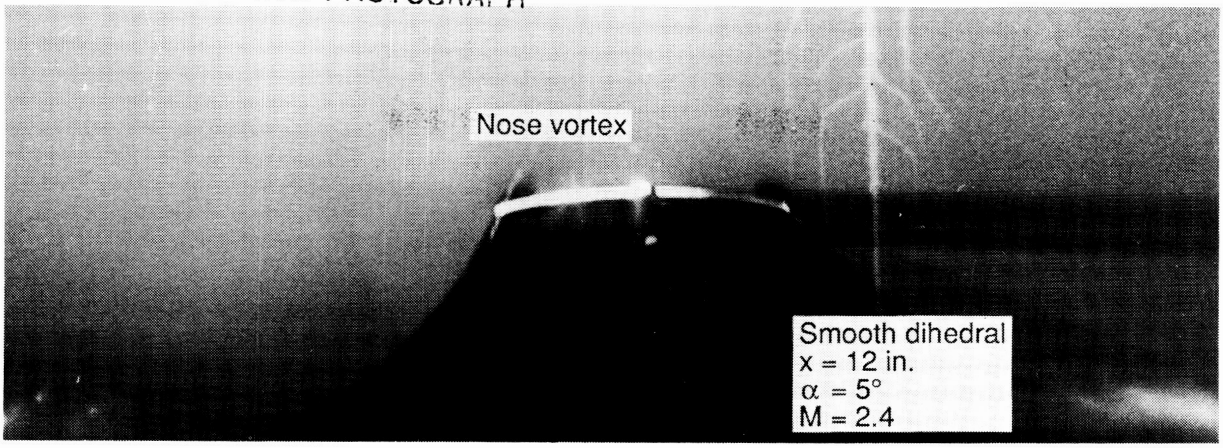

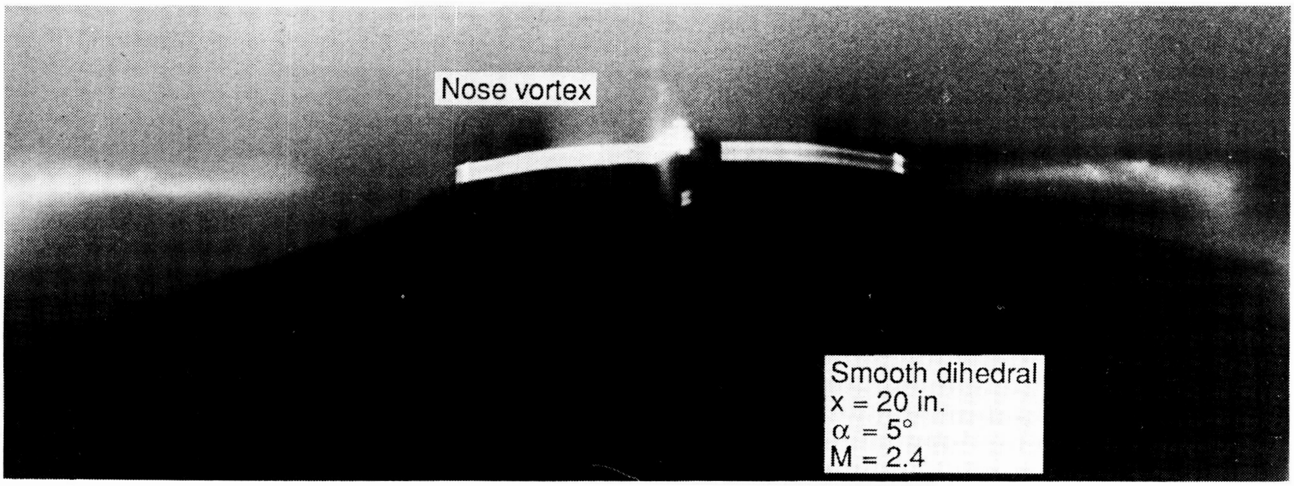

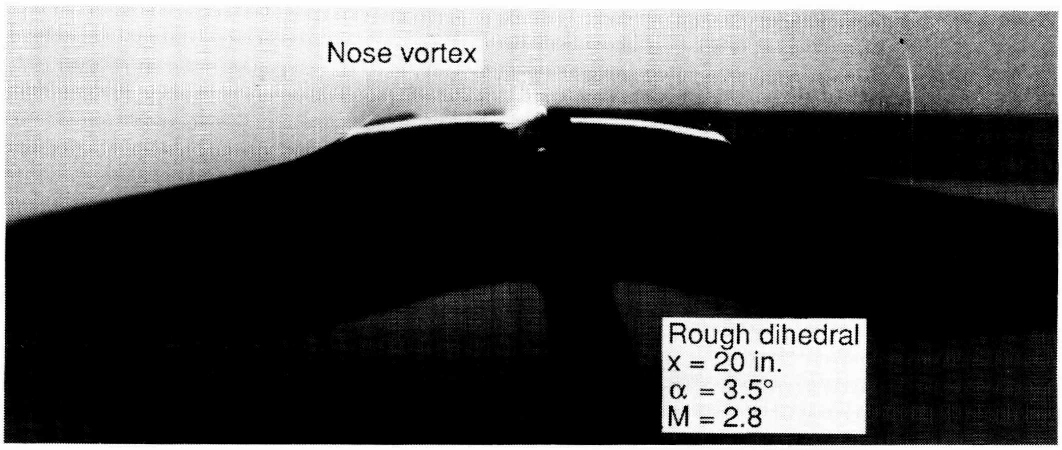

(a) $x = 12$ in. and 20 in.

Figure 21. Vapor-screen photographs of rough and smooth dihedral models.

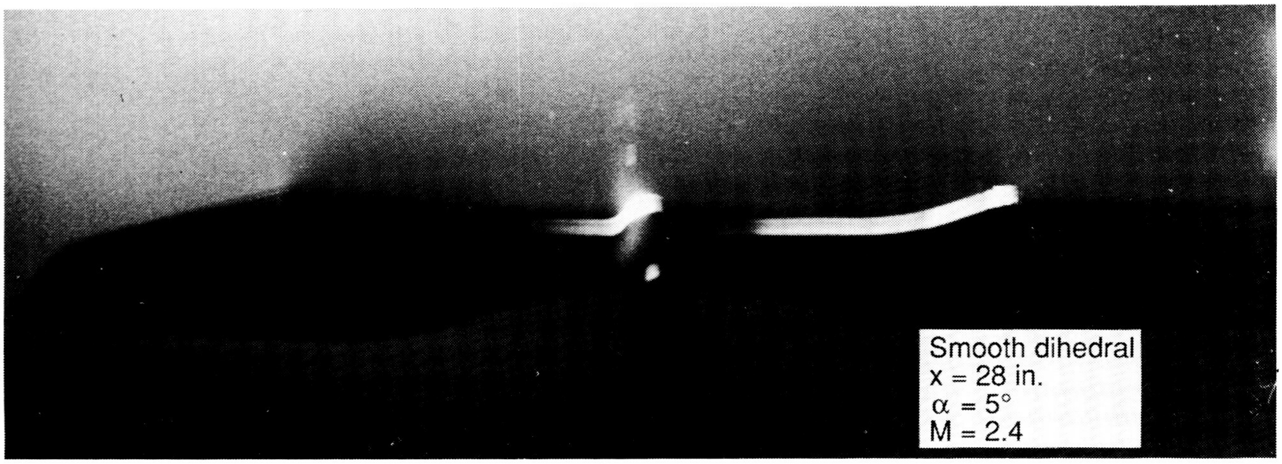

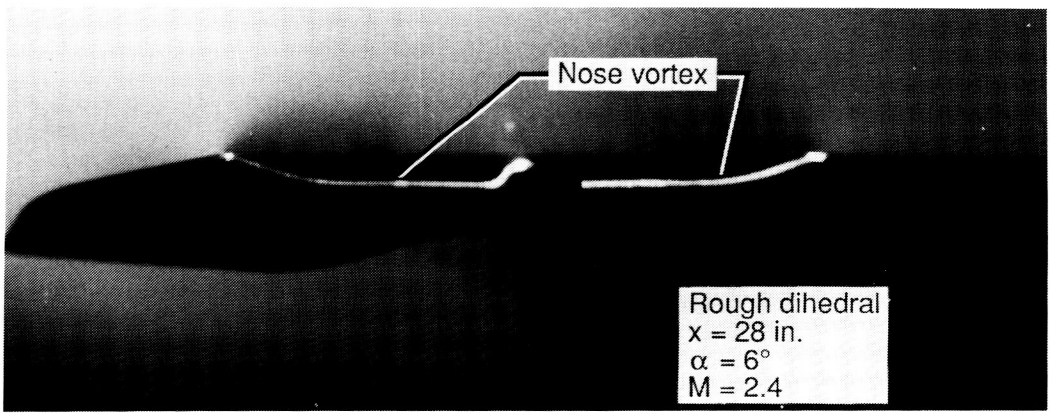

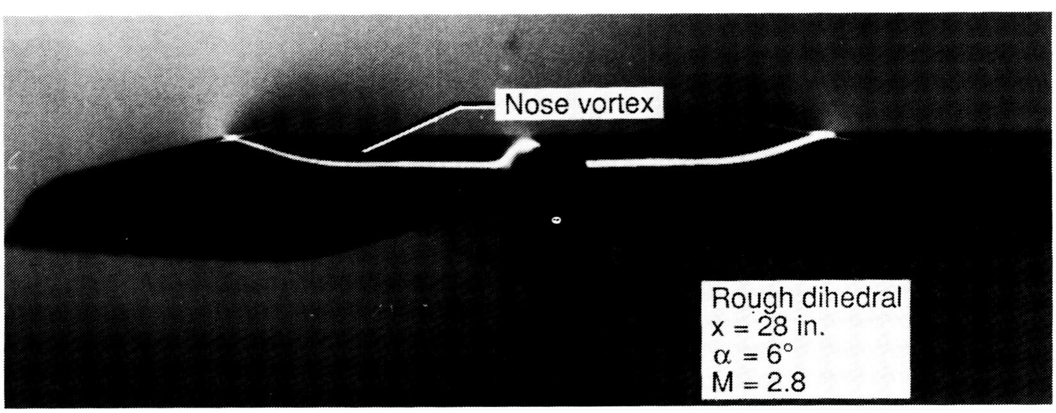

(b) $x = 28$ in.

Figure 21. Continued.

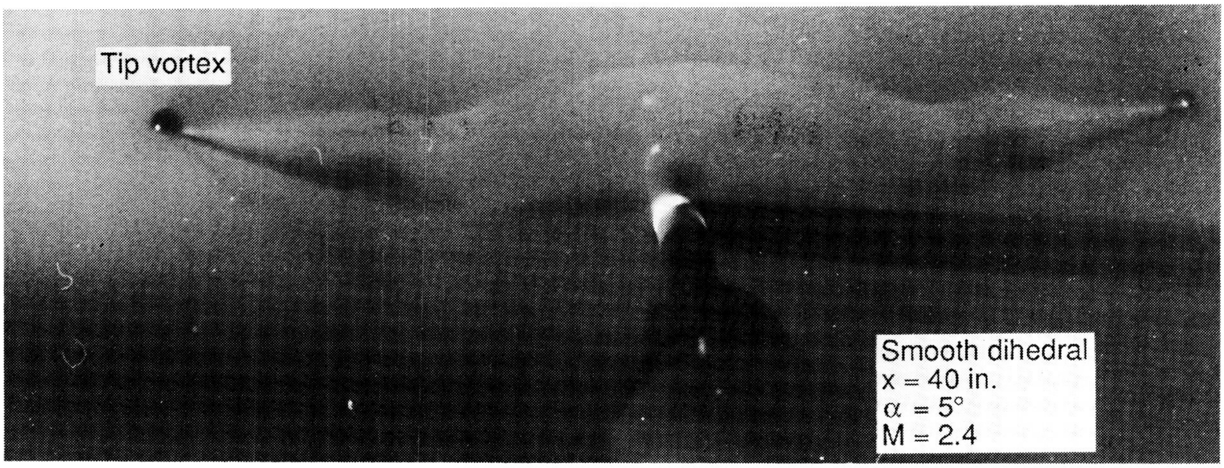

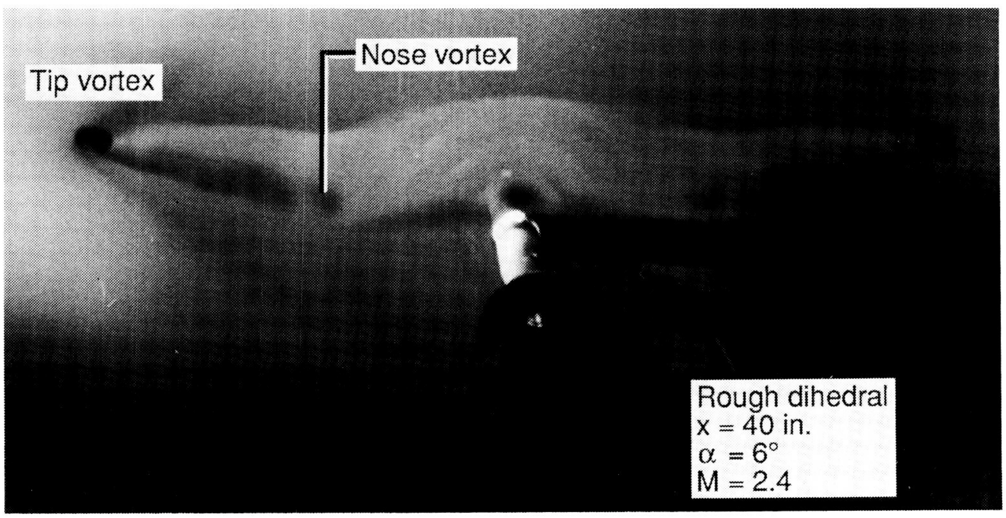

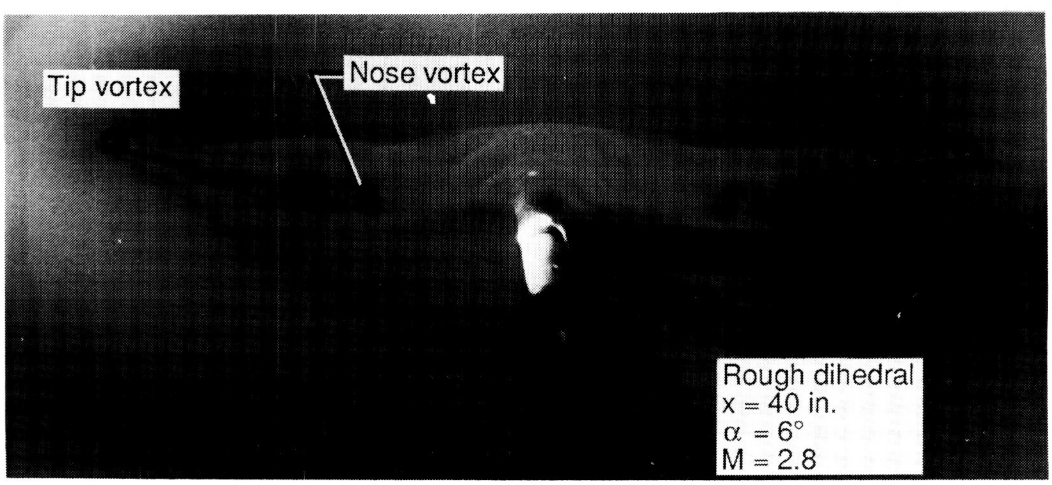

(c) $x = 40$ in.

Figure 21. Concluded.

Appendix A

Cutting Procedure for Models

The following sketch shows an example of how step size is determined. For a maximum scallop height of .005 in. the procedure is as follows:

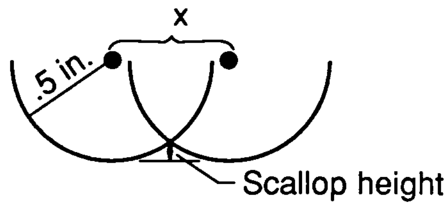

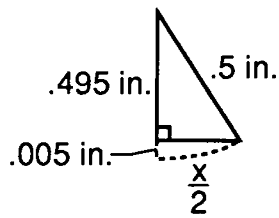

$$
\begin{aligned}
(.5)^2 &= (.495)^2 + (x/2)^2 \\
.25 &= .2450 + x^2/4 \\
\frac{x^2}{4} &= .005 \\
x^2 &= .020 \\
x &= .1414 \text{ in.}
\end{aligned}
$$

To determine number of passes, divide step size into maximum chord of 31.00 in.

Number of passes = 220

Each pass is made from the root chord to the tip, cutting along a constant percent chord pass. Thus, the maximum scallop height theoretically lies along the root chord with smaller and smaller scallop heights toward the tip. Following this procedure, the next sketch illustrates what the theoretical scallop heights would be for the rough model (shown on the right) and on the medium model (shown on the left).

Measurements that were actually made on the medium model are shown by the black dots on the left portion of the sketch. Though the measurements do not match exactly the predicted values, they do fall within the acceptable scallop heights for the medium model.

Maximum scallop height, in.	Maximum step size, in.	Number of passes
0.002	0.089	347
.005	.141	220

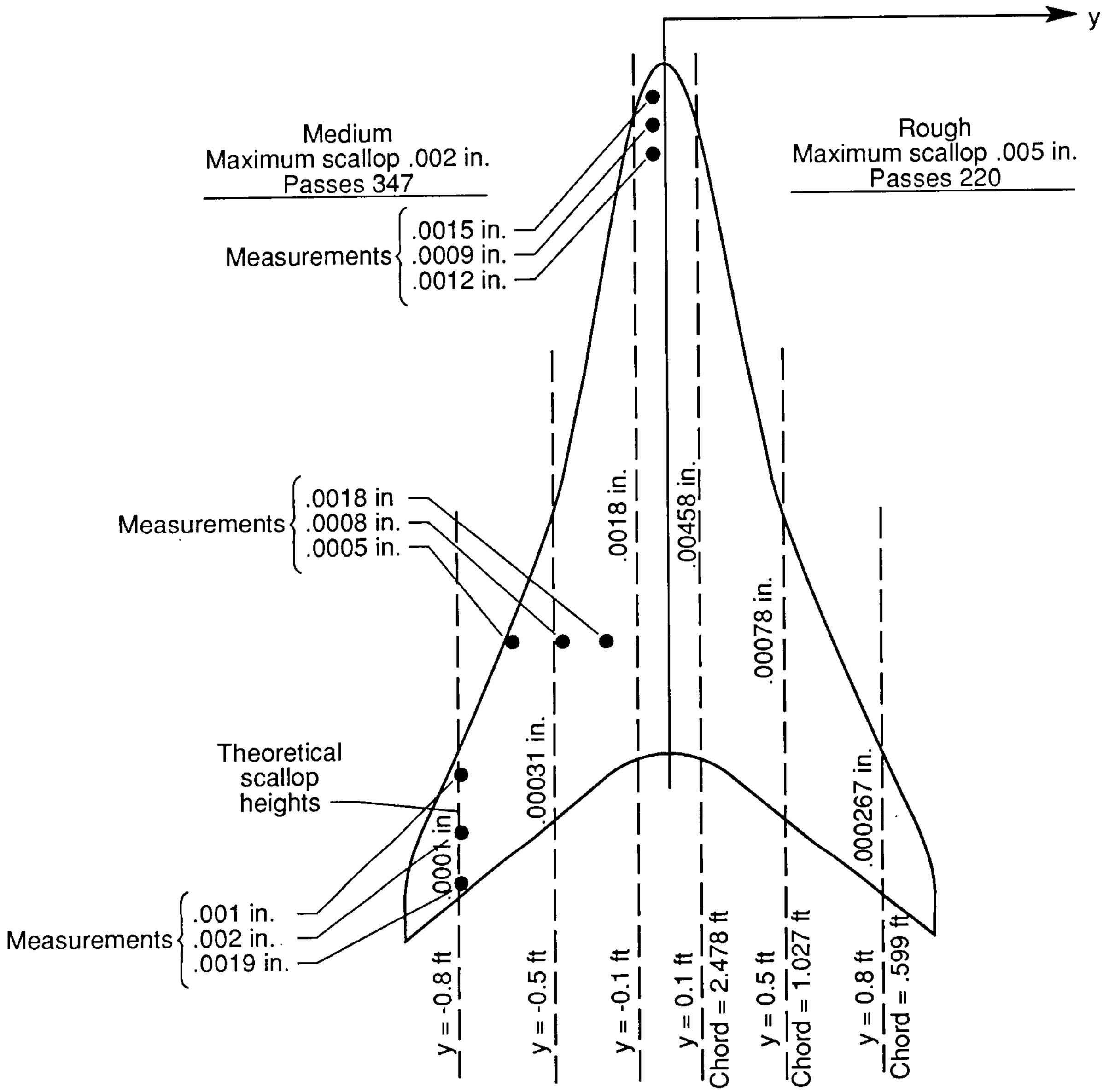

Appendix B

Schedule of Tabulated Data and Tunnel Conditions

Table B1. Schedule of Tabulated Data and Tunnel Conditions

ID	Test	Run no.	Model	Mach	R/ft	Balance	T_o, °F	q, psf	H_o, psf
1	1298	1	Rough	2.0	6×10^6	845A	100	1266	3539
2		2		2.0	2			423	1180
3		6		2.4	6			1181	4283
4	↓	4	↓	2.4	2	↓	↓	394	1428
5	1298	35	Rough	1.8	2×10^6	740	125	456	1154
6		42		2.0				448	1253
7		44		2.16				438	1349
8		47		2.4				419	1520
9		53		2.6				400	1686
10	↓	55	↓	2.8	↓	↓	↓	378	1873
11	1298	66	Flat	1.8	2×10^6	740	125	456	1154
12		77		2.0				448	1253
13		69		2.16				438	1349
14		61		2.4				419	1520
15		79		2.6				400	1686
16	↓	81	↓	2.8	↓	↓	↓	378	1873
17	1298	145	Smooth	1.8	2×10^6	740	125	456	1154
18		152		2.0				448	1253
19		154		2.16				438	1349
20		157		2.4				418	1520
21		162		2.6				399	1686
22	↓	164	↓	2.8	↓	↓	↓	379	1873
23	1482	1	Smooth	2.0	6×10^6	845A	125	1347	3760
24	1482	4	Smooth	2.4	6×10^6	845A	150	1333	4838
25	1482	17	Medium	1.8	2×10^6	845B	125	457	1154
26		24		2.0				448	1253
27		26		2.16				439	1349
28		6		2.4				418	1520
29		10		2.6				399	1686
30	↓	11	↓	2.8	↓	↓	↓	379	1873
31	1570	3	Medium	2.0	2×10^6	740	125	448	1253
32		4		2.4				418	1520
33		7	↓	2.8				379	1873
34		10	Smooth	2.0				448	1253
35		8		2.4				418	1520
36	↓	9	↓	2.8	↓	↓	↓	379	1873

Appendix C

Balance Accuracy Values

Table C1. Coefficient Accuracy

M	Bal	T_o, °F	q, psf	R/ft	C_N	C_A	C_m	C_l	C_n	C_Y
2.0	845A	100	1266	6×10^6	0.00093	0.00009	0.00138	0.00031	0.00078	0.00047
2.0			423	2	.00279	.00028	.00414	.00093	.00233	.00140
2.4			1181	6	.00100	.00010	.00148	.00033	.00083	.00050
2.4			394	2	.00300	.00030	.00445	.00100	.00250	.00150
2.0		125	1347	6	.00088	.00009	.00130	.00029	.00073	.00044
2.4		150	1333	6	.00089	.00009	.00132	.00029	.00074	.00044
1.8	845B	125	457	2×10^6	0.00258	0.00026	0.00384	0.00086	0.00216	0.00129
2.0			448		.00264	.00026	.00391	.00088	.00220	.00132
2.16			439		.00269	.00027	.00399	.00090	.00224	.00135
2.4			418		.00283	.00028	.00419	.00094	.00236	.00141
2.6			399		.00296	.00029	.00439	.00099	.00247	.00148
2.8			379		.00312	.00031	.00463	.00104	.00260	.00156
1.8	740	125	457	2×10^6	0.00172	0.00013	0.00256	0.00065	0.00216	0.00129
2.0			448		.00176	.00013	.00261	.00066	.00220	.00132
2.16			439		.00179	.00013	.00266	.00067	.00224	.00135
2.4			418		.00188	.00014	.00279	.00071	.00236	.00141
2.6			399		.00197	.00015	.00293	.00074	.00247	.00148
2.8			379		.00208	.00016	.00308	.00078	.00260	.00156

Appendix D

Tabulated Data

ROUGH DIHEDRAL

PROJECT 1298 RUN 1 MACH 2.00

ALPHA	CN	CA	CL	CD	L/D	CM	CAC	CDC	R/FT	DYN PRS
-6.22	-.1707	.0051	-.1691	.0235	-7.1844	.0565	.0009	.0009	5.998	1266.01
-5.37	-.1491	.0056	-.1480	.0195	-7.5883	.0506	.0009	.0009	5.998	1266.01
-4.30	-.1188	.0059	-.1180	.0148	-7.9725	.0412	.0009	.0009	6.004	1267.19
-3.36	-.0916	.0063	-.0910	.0117	-7.8034	.0318	.0009	.0009	6.007	1267.80
-2.32	-.0603	.0068	-.0600	.0092	-6.5271	.0204	.0009	.0009	6.012	1268.98
-1.26	-.0298	.0074	-.0297	.0080	-3.6996	.0094	.0009	.0009	6.019	1270.41
-.31	-.0039	.0076	-.0039	.0076	-.5095	-.0001	.0009	.0009	5.994	1265.04
.74	.0258	.0075	.0257	.0079	3.2625	-.0108	.0008	.0008	5.998	1265.94
1.75	.0542	.0072	.0539	.0089	6.0870	-.0207	.0008	.0008	6.001	1266.69
2.69	.0816	.0068	.0811	.0106	7.6263	-.0305	.0008	.0008	6.003	1267.08
3.72	.1110	.0065	.1103	.0137	8.0679	-.0403	.0008	.0008	6.016	1269.84
4.67	.1366	.0062	.1356	.0173	7.8282	-.0481	.0008	.0008	5.992	1264.76
5.70	.1637	.0060	.1623	.0222	7.3011	-.0555	.0008	.0008	6.001	1266.58
6.72	.1902	.0058	.1882	.0280	6.7190	-.0625	.0008	.0008	6.003	1267.05
7.61	.2128	.0056	.2101	.0338	6.2207	-.0681	.0008	.0008	6.004	1267.23
-.35	-.0049	.0076	-.0049	.0076	-.6427	.0003	.0009	.0009	6.002	1266.91

ROUGH DIHEDRAL

PROJECT 1298 RUN 2 MACH 2.00

ALPHA	CN	CA	CL	CD	L/D	CM	CAC	CDC	R/FT	DYN PRS
-6.31	-.1826	.0060	-.1808	.0260	-6.9477	.0621	.0010	.0010	2.007	423.59
-5.33	-.1536	.0062	-.1523	.0204	-7.4487	.0531	.0010	.0010	2.006	423.41
-4.31	-.1237	.0066	-.1229	.0159	-7.7394	.0433	.0010	.0010	2.006	423.48
-3.29	-.0926	.0069	-.0921	.0122	-7.5539	.0325	.0010	.0010	2.007	423.63
-2.30	-.0629	.0073	-.0625	.0098	-6.3910	.0214	.0010	.0010	2.008	423.77
-1.29	-.0333	.0078	-.0332	.0085	-3.8997	.0106	.0010	.0010	2.008	423.80
-.30	-.0057	.0080	-.0056	.0081	-.6981	.0005	.0010	.0010	2.008	423.91
.69	.0214	.0080	.0213	.0083	2.5706	-.0094	.0010	.0010	2.008	423.77
1.70	.0495	.0078	.0492	.0092	5.3256	-.0197	.0010	.0010	2.002	422.66
2.71	.0807	.0075	.0803	.0113	7.1261	-.0308	.0010	.0010	2.002	422.55
3.68	.1085	.0073	.1078	.0142	7.5815	-.0407	.0010	.0010	2.003	422.87
4.71	.1367	.0071	.1357	.0183	7.4256	-.0493	.0010	.0010	2.005	423.09
5.70	.1638	.0069	.1623	.0232	7.0068	-.0568	.0010	.0010	2.004	423.02
7.70	.2167	.0067	.2138	.0357	5.9889	-.0708	.0010	.0010	2.004	423.05
9.70	.2683	.0066	.2633	.0517	5.0982	-.0828	.0010	.0010	2.004	423.05
11.70	.3184	.0064	.3105	.0708	4.3836	-.0942	.0010	.0010	2.005	423.09
13.70	.3679	.0063	.3560	.0933	3.8149	-.1046	.0011	.0010	2.005	423.12
15.70	.4170	.0061	.3998	.1187	3.3674	-.1153	.0011	.0010	2.005	423.23
-.30	-.0048	.0081	-.0048	.0081	-.5905	.0001	.0010	.0010	2.005	423.20

ROUGH DIHEDRAL

PROJECT 1298 RUN 6 MACH 2.40

ALPHA	CN	CA	CL	CD	L/D	CM	CAC	CDC	R/FT	DYN PRS
-6.24	-.1612	.0053	-.1596	.0228	-6.9886	.0503	.0007	.0007	5.984	1178.02
-5.31	-.1355	.0057	-.1344	.0182	-7.3853	.0425	.0007	.0007	6.004	1181.96
-4.08	-.1025	.0059	-.1018	.0132	-7.7017	.0323	.0007	.0007	6.001	1181.33
-2.90	-.0699	.0062	-.0695	.0097	-7.1353	.0219	.0008	.0008	5.995	1180.03
-1.75	-.0397	.0066	-.0394	.0078	-5.0636	.0119	.0007	.0007	6.003	1181.74
-1.10	-.0279	.0069	-.0278	.0074	-3.7582	.0076	.0007	.0007	6.004	1181.96
-.07	-.0003	.0069	-.0003	.0069	-.0457	-.0017	.0007	.0007	6.003	1181.69
1.18	.0337	.0067	.0335	.0074	4.5319	-.0132	.0007	.0007	6.003	1181.69
.96	.0256	.0071	.0255	.0075	3.4077	-.0110	.0007	.0007	6.005	1182.02
2.24	.0578	.0066	.0575	.0089	6.4859	-.0219	.0007	.0007	6.002	1181.44
2.84	.0740	.0065	.0736	.0101	7.2601	-.0274	.0007	.0007	6.002	1181.58
3.88	.1005	.0062	.0999	.0130	7.6939	-.0364	.0007	.0007	6.002	1181.58
4.87	.1256	.0060	.1246	.0166	7.4907	-.0435	.0007	.0007	6.002	1181.58
6.00	.1497	.0058	.1483	.0214	6.9401	-.0500	.0007	.0007	6.002	1181.52
7.99	.1947	.0054	.1921	.0324	5.9290	-.0612	.0007	.0007	6.005	1182.13
-.05	.0009	.0069	.0009	.0069	.1293	-.0022	.0007	.0007	5.997	1180.45

ROUGH DIHEDRAL

PROJECT 1298 RUN 4 MACH 2.40

ALPHA	CN	CA	CL	CD	L/D	CM	CAC	CDC	R/FT	DYN PRS
-6.10	-.1557	.0060	-.1542	.0226	-6.8348	.0504	.0009	.0009	2.007	395.15
-5.17	-.1382	.0063	-.1371	.0187	-7.3226	.0441	.0009	.0009	2.009	395.45
-4.13	-.1068	.0065	-.1061	.0141	-7.5101	.0349	.0009	.0009	2.004	394.46
-3.17	-.0858	.0066	-.0853	.0114	-7.5142	.0277	.0009	.0009	2.004	394.57
-2.20	-.0611	.0070	-.0608	.0094	-6.5029	.0191	.0009	.0009	2.005	394.59
-1.09	-.0237	.0074	-.0236	.0078	-3.0142	.0066	.0009	.0009	2.005	394.59
-.10	.0011	.0075	.0011	.0075	.1485	-.0019	.0009	.0009	2.006	394.93
.90	.0258	.0075	.0257	.0079	3.2679	-.0103	.0009	.0009	2.005	394.68
1.87	.0517	.0073	.0514	.0089	5.7464	-.0197	.0009	.0009	2.005	394.71
2.86	.0737	.0071	.0733	.0107	6.8235	-.0277	.0009	.0009	2.006	394.82
3.89	.1025	.0069	.1018	.0138	7.3563	-.0366	.0009	.0009	2.005	394.76
4.93	.1324	.0067	.1313	.0181	7.2711	-.0451	.0009	.0009	2.006	394.79
5.82	.1476	.0066	.1462	.0216	6.7755	-.0500	.0009	.0009	2.006	394.95
7.92	.2002	.0064	.1974	.0339	5.8155	-.0626	.0009	.0009	2.006	394.87
9.83	.2416	.0063	.2370	.0475	4.9897	-.0725	.0009	.0009	2.007	394.98
11.97	.2920	.0063	.2844	.0667	4.2634	-.0833	.0009	.0009	2.004	394.40
13.88	.3283	.0063	.3172	.0848	3.7387	-.0913	.0009	.0009	2.002	394.07
15.86	.3718	.0062	.3559	.1076	3.3091	-.1005	.0010	.0009	2.004	394.40
-.11	.0004	.0075	.0004	.0075	.0516	-.0020	.0009	.0009	2.003	394.32

ROUGH DIHEDRAL

UPWT PROJECT 1298 RUN 35 MACH 1.80

ALPHA	CN	CA	CL	CD	L/D	CM	CAC	CDC	R/FT	DYN PRS
-5.25	-.1660	.0062	-.1648	.0214	-7.7088	.0596	.0009	.0009	2.000	455.35
-4.27	-.1350	.0066	-.1341	.0166	-8.0649	.0495	.0009	.0009	1.999	455.27
-3.24	-.0985	.0070	-.0979	.0126	-7.7768	.0361	.0009	.0009	1.999	455.23
-2.26	-.0656	.0075	-.0653	.0101	-6.4504	.0235	.0010	.0010	1.999	455.19
-1.26	-.0337	.0081	-.0336	.0088	-3.8121	.0117	.0010	.0010	1.999	455.19
-.26	-.0030	.0084	-.0030	.0084	-.3561	-.0000	.0010	.0010	1.999	455.23
.78	.0284	.0084	.0282	.0088	3.2242	-.0118	.0010	.0010	2.000	455.39
1.75	.0595	.0081	.0592	.0099	5.9652	-.0232	.0010	.0010	2.000	455.39
2.77	.0930	.0078	.0925	.0123	7.5299	-.0356	.0010	.0010	1.999	455.31
3.77	.1242	.0075	.1234	.0157	7.8672	-.0462	.0010	.0010	1.999	455.31
4.77	.1558	.0074	.1547	.0204	7.5958	-.0560	.0010	.0010	1.999	455.27
5.79	.1864	.0073	.1847	.0261	7.0697	-.0651	.0010	.0010	2.000	455.39
6.75	.2146	.0072	.2123	.0324	6.5481	-.0730	.0010	.0010	2.000	455.47
7.74	.2430	.0071	.2398	.0398	6.0250	-.0802	.0010	.0010	2.000	455.55
-.25	-.0032	.0084	-.0032	.0084	-.3767	.0001	.0010	.0010	2.001	455.67

ROUGH DIHEDRAL

UPWT PROJECT 1298 RUN 42 MACH 2.00

ALPHA	CN	CA	CL	CD	L/D	CM	CAC	CDC	R/FT	DYN PRS
-5.40	-.1611	.0063	-.1598	.0215	-7.4424	.0560	.0009	.0009	1.999	448.17
-4.40	-.1303	.0066	-.1294	.0166	-7.7928	.0458	.0009	.0009	1.999	448.17
-3.40	-.0983	.0070	-.0977	.0128	-7.6506	.0348	.0009	.0009	1.999	448.17
-2.41	-.0669	.0073	-.0665	.0102	-6.5533	.0234	.0009	.0009	1.999	448.28
-1.42	-.0368	.0078	-.0365	.0087	-4.2011	.0121	.0009	.0009	1.999	448.35
-.40	-.0074	.0081	-.0073	.0081	-.9027	.0016	.0009	.0009	1.999	448.32
.60	.0206	.0082	.0206	.0084	2.4535	-.0088	.0009	.0009	1.999	448.17
1.59	.0506	.0080	.0504	.0094	5.3780	-.0196	.0009	.0009	1.998	448.10
2.59	.0813	.0077	.0809	.0113	7.1428	-.0307	.0009	.0009	1.999	448.21
3.61	.1128	.0075	.1121	.0146	7.6979	-.0416	.0009	.0009	1.999	448.28
4.60	.1411	.0073	.1401	.0186	7.5242	-.0498	.0009	.0009	1.999	448.28
5.60	.1681	.0072	.1666	.0236	7.0639	-.0573	.0009	.0009	1.999	448.25
6.62	.1962	.0071	.1941	.0297	6.5361	-.0649	.0009	.0009	1.999	448.21
7.62	.2231	.0070	.2202	.0366	6.0209	-.0715	.0009	.0009	1.999	448.17
-.41	-.0077	.0081	-.0077	.0082	-.9352	.0016	.0009	.0009	1.999	448.25

ROUGH DIHEDRAL

UPWT PROJECT 1298 RUN 44 MACH 2.16

ALPHA	CN	CA	CL	CD	L/D	CM	CAC	CDC	R/FT	DYN PRS
-5.06	-.1430	.0064	-.1419	.0190	-7.4779	.0487	.0008	.0008	2.000	438.71
-4.05	-.1138	.0067	-.1131	.0147	-7.7035	.0390	.0008	.0008	1.998	438.29
-3.03	-.0836	.0070	-.0831	.0114	-7.3112	.0287	.0008	.0008	1.998	438.16
-2.06	-.0555	.0073	-.0552	.0093	-5.9417	.0184	.0008	.0008	1.997	438.03
-1.06	-.0260	.0077	-.0258	.0082	-3.1654	.0079	.0008	.0008	1.997	438.09
-.06	.0010	.0079	.0010	.0079	.1282	-.0018	.0008	.0008	1.997	438.09
.96	.0291	.0078	.0290	.0083	3.4816	-.0118	.0008	.0008	1.997	438.12
1.95	.0576	.0076	.0573	.0096	5.9709	-.0220	.0008	.0008	1.997	438.06
2.96	.0877	.0074	.0872	.0119	7.3023	-.0326	.0008	.0008	1.997	438.06
3.96	.1161	.0073	.1153	.0153	7.5543	-.0420	.0008	.0008	1.997	438.06
4.96	.1434	.0071	.1422	.0195	7.3043	-.0498	.0008	.0008	1.997	438.09
5.96	.1685	.0070	.1669	.0245	6.8237	-.0565	.0008	.0008	1.997	438.09
6.98	.1955	.0069	.1932	.0307	6.3029	-.0634	.0008	.0008	1.997	438.09
7.97	.2202	.0069	.2172	.0373	5.8166	-.0695	.0008	.0008	1.997	438.06
-.06	.0018	.0079	.0018	.0079	.2309	-.0021	.0008	.0008	1.997	438.09

ROUGH DIHEDRAL

UPWT PROJECT 1298 RUN 47 MACH 2.40

ALPHA	CN	CA	CL	CD	L/D	CM	CAC	CDC	R/FT	DYN PRS
-5.09	-.1362	.0062	-.1351	.0183	-7.3910	.0446	.0008	.0007	2.006	420.30
-4.19	-.1132	.0064	-.1124	.0147	-7.6549	.0371	.0007	.0007	2.006	420.33
-3.10	-.0808	.0067	-.0803	.0111	-7.2370	.0267	.0007	.0007	2.007	420.41
-2.06	-.0517	.0069	-.0514	.0088	-5.8428	.0171	.0007	.0007	2.006	420.27
-1.14	-.0284	.0073	-.0283	.0079	-3.5725	.0084	.0007	.0007	2.005	420.19
-.08	.0019	.0075	.0019	.0075	.2529	-.0019	.0007	.0007	2.007	420.60
.91	.0285	.0075	.0283	.0080	3.5565	-.0114	.0007	.0007	2.006	420.33
1.84	.0497	.0074	.0494	.0089	5.5271	-.0193	.0008	.0008	2.005	420.19
2.91	.0818	.0071	.0813	.0113	7.2164	-.0302	.0007	.0007	2.005	420.08
3.96	.1084	.0070	.1076	.0145	7.4340	-.0384	.0007	.0007	2.005	420.11
4.91	.1344	.0069	.1333	.0184	7.2397	-.0459	.0007	.0007	2.006	420.33
5.93	.1597	.0068	.1581	.0233	6.7922	-.0527	.0007	.0007	2.006	420.33
6.99	.1861	.0067	.1839	.0293	6.2741	-.0590	.0007	.0007	2.006	420.35
7.91	.2058	.0068	.2029	.0350	5.7910	-.0639	.0007	.0007	2.006	420.24
-.10	.0001	.0075	.0001	.0075	.0186	-.0016	.0007	.0007	2.006	420.27

ROUGH DIHEDRAL

UPWT PROJECT 1298 RUN 53 MACH 2.60

ALPHA	CN	CA	CL	CD	L/D	CM	CAC	CDC	R/FT	DYN PRS
-5.11	-.1253	.0060	-.1243	.0171	-7.2539	.0464	.0007	.0007	1.998	399.21
-4.17	-.1016	.0062	-.1008	.0135	-7.4487	.0390	.0007	.0007	2.002	400.04
-3.24	-.0787	.0063	-.0782	.0107	-7.2766	.0311	.0007	.0007	2.000	399.73
-2.15	-.0529	.0066	-.0527	.0086	-6.1545	.0223	.0007	.0007	2.002	400.02
-1.15	-.0237	.0068	-.0236	.0073	-3.2229	.0126	.0007	.0007	2.002	400.09
-.16	-.0028	.0070	-.0027	.0070	-.3924	.0047	.0007	.0007	2.003	400.18
.89	.0237	.0069	.0236	.0073	3.2246	-.0043	.0007	.0007	2.003	400.23
1.87	.0498	.0068	.0495	.0085	5.8474	-.0135	.0007	.0007	2.002	400.09
2.89	.0785	.0067	.0780	.0106	7.3471	-.0229	.0007	.0007	2.002	400.11
3.84	.0987	.0067	.0980	.0133	7.3967	-.0296	.0007	.0007	2.002	400.02
4.97	.1300	.0066	.1289	.0178	7.2452	-.0384	.0007	.0007	2.004	400.42
5.88	.1487	.0065	.1473	.0217	6.7930	-.0438	.0007	.0007	2.003	400.21
6.86	.1684	.0065	.1664	.0265	6.2760	-.0489	.0007	.0007	2.001	399.97
7.88	.1930	.0064	.1903	.0328	5.7973	-.0549	.0007	.0006	2.000	399.64
-.18	-.0030	.0070	-.0030	.0070	-.4213	.0049	.0007	.0007	2.001	399.97

ROUGH DIHEDRAL

UPWT PROJECT 1298 RUN 55 MACH 2.80

ALPHA	CN	CA	CL	CD	L/D	CM	CAC	CDC	R/FT	DYN PRS
-5.13	-.1227	.0059	-.1216	.0168	-7.2283	.0396	.0006	.0006	1.999	378.50
-4.10	-.0941	.0060	-.0934	.0127	-7.3823	.0311	.0006	.0006	2.001	378.95
-3.10	-.0706	.0061	-.0701	.0099	-7.0624	.0237	.0006	.0006	1.998	378.34
-2.08	-.0467	.0063	-.0465	.0080	-5.8383	.0156	.0006	.0006	2.001	378.91
-1.06	-.0208	.0065	-.0207	.0069	-3.0106	.0072	.0006	.0006	2.000	378.80
-.14	-.0051	.0066	-.0051	.0066	-.7780	.0012	.0006	.0006	2.000	378.72
.91	.0224	.0066	.0223	.0069	3.2270	-.0081	.0006	.0006	2.000	378.83
1.86	.0437	.0065	.0435	.0079	5.5047	-.0157	.0006	.0006	1.999	378.64
2.92	.0700	.0064	.0696	.0100	6.9890	-.0243	.0006	.0006	2.001	378.87
3.98	.0970	.0064	.0963	.0131	7.3606	-.0325	.0006	.0006	2.000	378.74
4.93	.1171	.0063	.1161	.0163	7.1040	-.0384	.0006	.0006	1.999	378.54
5.85	.1359	.0063	.1346	.0201	6.6869	-.0437	.0006	.0006	2.000	378.78
6.89	.1570	.0062	.1552	.0250	6.1969	-.0495	.0006	.0006	2.000	378.80
7.89	.1797	.0062	.1772	.0308	5.7484	-.0551	.0006	.0006	2.000	378.85
-.09	-.0008	.0066	-.0008	.0066	-.1273	-.0001	.0006	.0006	2.001	378.91

FLAT WING

UPWT PROJECT 1298 RUN 66 MACH 1.80

ALPHA	CN	CA	CL	CD	L/D	CM	CAC	CDC	R/FT	DYN PRS
-5.37	-.1731	.0061	-.1718	.0222	-7.7260	.0632	.0008	.0008	2.006	456.81
-4.32	-.1396	.0062	-.1387	.0167	-8.2931	.0524	.0008	.0008	2.005	456.62
-3.34	-.1082	.0065	-.1077	.0128	-8.3809	.0413	.0008	.0008	2.005	456.58
-2.33	-.0741	.0070	-.0738	.0100	-7.3695	.0286	.0008	.0008	2.005	456.66
-1.34	-.0428	.0075	-.0426	.0085	-5.0143	.0169	.0008	.0008	2.006	456.77
-.33	-.0122	.0078	-.0121	.0078	-1.5450	.0054	.0008	.0008	2.006	456.81
.67	.0165	.0078	.0164	.0080	2.0551	-.0056	.0008	.0008	2.005	456.66
1.63	.0467	.0074	.0465	.0087	5.3142	-.0168	.0008	.0008	2.006	456.77
2.66	.0856	.0069	.0852	.0109	7.8060	-.0313	.0008	.0008	2.007	456.93
3.66	.1205	.0066	.1199	.0142	8.4125	-.0434	.0008	.0008	2.004	456.46
4.69	.1549	.0064	.1539	.0190	8.0890	-.0548	.0008	.0008	2.001	455.75
5.67	.1867	.0062	.1851	.0246	7.5230	-.0647	.0008	.0008	2.000	455.47
6.69	.2183	.0060	.2161	.0314	6.8902	-.0740	.0008	.0008	2.000	455.55
7.67	.2497	.0058	.2467	.0391	6.3098	-.0831	.0008	.0008	2.001	455.71
-.34	-.0098	.0079	-.0097	.0079	-1.2287	.0044	.0008	.0008	2.002	455.87

FLAT WING

UPWT PROJECT 1298 RUN 77 MACH 2.00

ALPHA	CN	CA	CL	CD	L/D	CM	CAC	CDC	R/FT	DYN PRS
-5.40	-.1627	.0063	-.1614	.0216	-7.4818	.0571	.0008	.0008	2.005	449.53
-4.40	-.1342	.0065	-.1333	.0168	-7.9579	.0485	.0008	.0008	2.005	449.50
-3.41	-.1054	.0067	-.1048	.0130	-8.0592	.0389	.0008	.0008	2.005	449.68
-2.37	-.0736	.0071	-.0733	.0101	-7.2332	.0274	.0008	.0008	2.005	449.57
-1.40	-.0430	.0076	-.0428	.0086	-4.9823	.0163	.0008	.0008	2.005	449.57
-.38	-.0140	.0078	-.0139	.0079	-1.7554	.0056	.0008	.0008	2.005	449.64
.63	.0132	.0078	.0131	.0080	1.6393	-.0045	.0008	.0008	2.005	449.64
1.63	.0412	.0075	.0410	.0087	4.7161	-.0146	.0008	.0008	2.005	449.64
2.61	.0752	.0071	.0748	.0105	7.1175	-.0270	.0008	.0008	2.005	449.61
3.64	.1087	.0068	.1080	.0137	7.9030	-.0386	.0008	.0008	2.005	449.57
4.62	.1388	.0065	.1378	.0177	7.7953	-.0479	.0008	.0008	2.005	449.53
5.61	.1677	.0064	.1662	.0227	7.3155	-.0568	.0008	.0008	2.005	449.50
6.65	.1983	.0062	.1963	.0291	6.7404	-.0655	.0008	.0008	2.005	449.53
7.62	.2258	.0060	.2230	.0359	6.2066	-.0728	.0008	.0008	2.005	449.64
-.40	-.0135	.0078	-.0135	.0079	-1.7013	.0055	.0008	.0008	2.005	449.68

FLAT WING

UPWT PROJECT 1298 RUN 69 MACH 2.16

ALPHA	CN	CA	CL	CD	L/D	CM	CAC	CDC	R/FT	DYN PRS
-5.12	-.1469	.0061	-.1457	.0191	-7.6206	.0514	.0007	.0007	2.006	439.94
-4.11	-.1183	.0063	-.1175	.0147	-7.9702	.0427	.0007	.0007	2.001	438.84
-3.09	-.0885	.0065	-.0880	.0113	-7.7853	.0328	.0007	.0007	2.000	438.71
-2.09	-.0593	.0069	-.0591	.0090	-6.5407	.0222	.0007	.0007	2.002	439.23
-1.10	-.0311	.0073	-.0309	.0079	-3.9236	.0119	.0007	.0007	2.002	439.10
-.11	-.0048	.0074	-.0048	.0075	-.6415	.0023	.0007	.0007	2.002	439.10
.90	.0213	.0074	.0212	.0077	2.7543	-.0072	.0007	.0007	2.002	439.07
1.91	.0505	.0070	.0502	.0087	5.7981	-.0176	.0007	.0007	2.002	439.10
2.90	.0823	.0067	.0818	.0108	7.5656	-.0292	.0007	.0007	2.002	439.20
3.89	.1136	.0064	.1129	.0141	8.0071	-.0398	.0007	.0007	2.002	439.20
4.90	.1430	.0062	.1419	.0184	7.7286	-.0487	.0007	.0007	2.002	439.10
5.92	.1705	.0060	.1690	.0236	7.1751	-.0566	.0007	.0007	2.002	439.16
6.91	.1977	.0059	.1955	.0296	6.6062	-.0642	.0007	.0007	2.001	439.00
7.93	.2252	.0057	.2223	.0368	6.0449	-.0717	.0007	.0007	2.002	439.20
-.09	-.0035	.0075	-.0035	.0075	-.4630	.0019	.0007	.0007	2.004	439.59

UPWT PROJECT 1298 RUN 61 MACH 2.40

ALPHA	CN	CA	CL	CD	L/D	CM	CAC	CDC	R/FT	DYN PRS
-5.21	-.1416	.0058	-.1404	.0186	-7.5388	.0478	.0006	.0006	2.001	419.20
-4.25	-.1170	.0061	-.1162	.0147	-7.9050	.0403	.0006	.0006	2.001	419.25
-3.19	-.0820	.0062	-.0815	.0108	-7.5561	.0293	.0006	.0006	2.003	419.69
-2.16	-.0538	.0066	-.0535	.0086	-6.2353	.0195	.0006	.0006	2.002	419.44
-1.14	-.0245	.0069	-.0243	.0074	-3.3097	.0097	.0006	.0006	2.000	419.03
-.18	-.0007	.0070	-.0007	.0070	-.0957	.0008	.0006	.0006	2.002	419.47
.85	.0245	.0069	.0244	.0072	3.3744	-.0075	.0006	.0006	2.000	419.03
1.86	.0541	.0066	.0538	.0083	6.4480	-.0187	.0006	.0006	2.000	419.03
2.68	.0671	.0064	.0668	.0095	7.0037	-.0241	.0006	.0006	2.001	419.28
3.93	.1126	.0060	.1119	.0137	8.1637	-.0382	.0006	.0006	2.002	419.53
4.78	.1280	.0059	.1271	.0165	7.6938	-.0438	.0006	.0006	1.999	418.92
5.84	.1580	.0057	.1566	.0218	7.1927	-.0520	.0006	.0006	2.000	419.06
6.75	.1767	.0056	.1749	.0263	6.6402	-.0579	.0006	.0006	2.001	419.28
7.82	.2068	.0055	.2042	.0336	6.0817	-.0656	.0006	.0006	2.001	419.28
3.86	.1082	.0060	.1076	.0133	8.0811	-.0369	.0006	.0006	2.001	419.17
2.78	.0746	.0063	.0742	.0099	7.4924	-.0263	.0006	.0006	2.003	419.58
-.19	-.0044	.0069	-.0044	.0069	-.6338	.0019	.0006	.0006	2.001	419.31

FLAT WING

UPWT PROJECT 1298 RUN 79 MACH 2.60

ALPHA	CN	CA	CL	CD	L/D	CM	CAC	CDC	R/FT	DYN PRS
-5.22	-.1339	.0057	-.1328	.0179	-7.4326	.0453	.0006	.0006	2.003	400.32
-4.18	-.1049	.0060	-.1042	.0136	-7.6483	.0368	.0006	.0006	2.000	399.76
-3.15	-.0799	.0061	-.0794	.0105	-7.5787	.0284	.0006	.0006	1.998	399.35
-2.22	-.0595	.0063	-.0592	.0086	-6.8663	.0214	.0006	.0006	2.003	400.28
-1.14	-.0247	.0067	-.0245	.0072	-3.4119	.0098	.0006	.0006	2.002	400.16
-.20	-.0062	.0069	-.0062	.0069	-.8982	.0029	.0006	.0006	2.003	400.21
.83	.0174	.0068	.0173	.0071	2.4470	-.0055	.0005	.0005	2.002	400.16
1.79	.0404	.0066	.0402	.0078	5.1302	-.0140	.0005	.0005	2.003	400.25
2.86	.0746	.0062	.0742	.0099	7.4724	-.0254	.0005	.0005	2.004	400.49
3.80	.0955	.0061	.0948	.0124	7.6348	-.0325	.0006	.0006	2.004	400.56
4.82	.1222	.0060	.1213	.0162	7.4775	-.0408	.0006	.0006	2.003	400.35
5.83	.1512	.0058	.1498	.0211	7.0918	-.0489	.0006	.0006	2.004	400.40
6.81	.1714	.0057	.1695	.0260	6.5151	-.0553	.0006	.0006	2.003	400.30
7.85	.1974	.0056	.1948	.0325	5.9918	-.0621	.0006	.0006	2.005	400.59
-.20	-.0058	.0069	-.0058	.0069	-.8354	.0024	.0006	.0006	2.003	400.30

FLAT WING

UPWT PROJECT 1298 RUN 81 MACH 2.80

ALPHA	CN	CA	CL	CD	L/D	CM	CAC	CDC	R/FT	DYN PRS
-5.16	-.1214	.0057	-.1204	.0166	-7.2602	.0406	.0005	.0005	2.002	379.13
-4.16	-.0967	.0057	-.0961	.0127	-7.5513	.0329	.0005	.0005	2.002	379.13
-3.12	-.0739	.0059	-.0734	.0099	-7.4353	.0258	.0005	.0005	2.004	379.61
-2.16	-.0516	.0061	-.0513	.0080	-6.3986	.0184	.0005	.0005	2.001	378.91
-1.14	-.0260	.0064	-.0258	.0069	-3.7495	.0097	.0005	.0005	2.003	379.29
-.17	-.0071	.0066	-.0071	.0066	-1.0766	.0027	.0005	.0005	2.004	379.61
.86	.0175	.0065	.0174	.0068	2.5668	-.0059	.0005	.0005	2.003	379.35
1.83	.0411	.0062	.0408	.0075	5.4332	-.0140	.0005	.0005	2.000	378.83
2.86	.0672	.0060	.0668	.0093	7.1464	-.0230	.0005	.0005	2.002	379.07
3.83	.0907	.0059	.0901	.0119	7.5693	-.0307	.0005	.0005	2.002	379.21
4.83	.1138	.0058	.1129	.0153	7.3623	-.0381	.0005	.0005	2.005	379.67
5.84	.1393	.0056	.1380	.0198	6.9815	-.0453	.0005	.0005	2.001	378.99
6.86	.1643	.0056	.1625	.0251	6.4611	-.0524	.0005	.0005	2.002	379.07
7.89	.1870	.0055	.1845	.0311	5.9338	-.0588	.0005	.0005	2.004	379.57
-.14	-.0025	.0066	-.0025	.0066	-.3770	.0016	.0005	.0005	2.003	379.41

SMOOTH DIHEDRAL

PROJECT 1298 RUN 145 MACH 1.80

ALPHA	CN	CA	CL	CD	L/D	CM	CAC	CDC	R/FT	DYN PRS
-5.32	-.1690	.0060	-.1678	.0217	-7.7372	.0592	.0008	.0008	1.996	454.60
-4.30	-.1346	.0064	-.1338	.0164	-8.1375	.0482	.0008	.0008	2.004	456.38
-3.31	-.1012	.0068	-.1006	.0126	-7.9657	.0361	.0008	.0008	2.009	457.56
-2.33	-.0678	.0073	-.0674	.0101	-6.6986	.0235	.0008	.0008	2.014	458.55
-1.33	-.0353	.0079	-.0351	.0087	-4.0458	.0115	.0008	.0008	2.013	458.39
-.29	-.0035	.0082	-.0034	.0082	-.4177	-.0003	.0009	.0009	2.013	458.43
.70	.0258	.0082	.0257	.0086	3.0093	-.0113	.0009	.0009	2.009	457.52
1.70	.0574	.0079	.0571	.0096	5.9287	-.0230	.0009	.0009	2.013	458.51
2.70	.0900	.0076	.0895	.0118	7.5759	-.0350	.0009	.0009	2.007	457.05
3.71	.1225	.0073	.1218	.0152	8.0123	-.0459	.0009	.0009	2.000	455.39
4.71	.1538	.0072	.1527	.0198	7.7117	-.0559	.0009	.0009	2.008	457.21
5.68	.1824	.0071	.1808	.0251	7.1954	-.0642	.0009	.0009	2.010	457.76
6.69	.2132	.0070	.2109	.0318	6.6370	-.0726	.0009	.0009	2.011	458.00
7.69	.2402	.0069	.2372	.0389	6.0912	-.0798	.0009	.0009	2.011	457.88
-.31	-.0036	.0082	-.0035	.0082	-.4308	-.0003	.0008	.0008	2.012	458.19

SMOOTH DIHEDRAL

PROJECT 1298 RUN 152 MACH 2.00

ALPHA	CN	CA	CL	CD	L/D	CM	CAC	CDC	R/FT	DYN PRS
-5.47	-.1620	.0060	-.1607	.0214	-7.4958	.0558	.0008	.0008	2.004	449.36
-4.46	-.1303	.0063	-.1295	.0164	-7.8840	.0455	.0008	.0008	2.001	448.64
-3.46	-.0992	.0067	-.0986	.0126	-7.8067	.0349	.0008	.0008	2.001	448.75
-2.46	-.0689	.0070	-.0685	.0100	-6.8591	.0239	.0008	.0008	1.999	448.21
-1.46	-.0374	.0076	-.0372	.0085	-4.3637	.0122	.0008	.0008	2.009	450.46
-.45	-.0083	.0079	-.0082	.0079	-1.0369	.0016	.0008	.0008	2.001	448.71
.55	.0194	.0079	.0193	.0081	2.3736	-.0087	.0008	.0008	2.005	449.57
1.53	.0472	.0077	.0470	.0089	5.2575	-.0186	.0008	.0008	2.003	449.11
2.56	.0804	.0074	.0800	.0110	7.2867	-.0304	.0008	.0008	2.004	449.32
3.57	.1099	.0072	.1092	.0140	7.7844	-.0405	.0008	.0008	2.001	448.78
4.53	.1363	.0070	.1354	.0178	7.6121	-.0483	.0008	.0008	1.997	447.89
5.55	.1653	.0070	.1638	.0229	7.1509	-.0565	.0008	.0008	2.004	449.32
6.54	.1919	.0069	.1899	.0287	6.6107	-.0636	.0008	.0008	2.002	448.96
7.53	.2179	.0068	.2151	.0353	6.0924	-.0703	.0008	.0008	1.999	448.17
-.45	-.0092	.0079	-.0091	.0079	-1.1469	.0020	.0008	.0008	1.998	447.96

SMOOTH DIHEDRAL

PROJECT 1298 RUN 154 MACH 2.16

ALPHA	CN	CA	CL	CD	L/D	CM	CAC	CDC	R/FT	DYN PRS
-5.35	-.1505	.0061	-.1493	.0201	-7.4173	.0498	.0007	.0007	2.007	440.27
-4.35	-.1210	.0064	-.1202	.0155	-7.7373	.0405	.0007	.0007	2.002	439.10
-3.36	-.0922	.0067	-.0917	.0121	-7.5899	.0310	.0007	.0007	2.007	440.20
-2.34	-.0618	.0070	-.0614	.0096	-6.4203	.0204	.0007	.0007	2.010	440.82
-1.35	-.0328	.0075	-.0327	.0083	-3.9464	.0101	.0007	.0007	2.004	439.65
-.36	-.0059	.0078	-.0058	.0078	-.7438	.0004	.0007	.0007	2.009	440.59
.65	.0218	.0078	.0217	.0080	2.6983	-.0093	.0007	.0007	2.006	439.94
1.66	.0504	.0075	.0501	.0090	5.5704	-.0194	.0007	.0007	2.010	440.95
2.66	.0802	.0073	.0798	.0110	7.2408	-.0299	.0007	.0007	2.005	439.85
3.66	.1088	.0071	.1081	.0141	7.6885	-.0393	.0007	.0007	2.006	440.07
4.65	.1362	.0070	.1351	.0180	7.5060	-.0474	.0008	.0007	2.010	440.98
5.64	.1612	.0069	.1597	.0227	7.0409	-.0539	.0008	.0008	2.005	439.72
6.65	.1872	.0068	.1851	.0285	6.5055	-.0606	.0008	.0008	2.004	439.62
7.66	.2123	.0067	.2095	.0350	5.9895	-.0667	.0008	.0008	2.011	441.15
-.34	-.0040	.0078	-.0040	.0078	-.5070	-.0001	.0007	.0007	2.004	439.55

SMOOTH DIHEDRAL

PROJECT 1298 RUN 157 MACH 2.40

ALPHA	CN	CA	CL	CD	L/D	CM	CAC	CDC	R/FT	DYN PRS
-5.14	-.1359	.0060	-.1348	.0181	-7.4275	.0441	.0006	.0006	2.000	418.89
-4.20	-.1102	.0063	-.1094	.0143	-7.6413	.0360	.0006	.0006	1.992	417.32
-3.09	-.0783	.0066	-.0778	.0108	-7.2117	.0260	.0006	.0006	1.997	418.40
-2.16	-.0534	.0070	-.0531	.0090	-5.9020	.0174	.0006	.0006	2.000	418.84
-1.17	-.0300	.0072	-.0299	.0078	-3.8426	.0091	.0006	.0006	1.998	418.67
-.22	-.0077	.0074	-.0077	.0074	-1.0337	.0013	.0006	.0006	1.998	418.53
.85	.0269	.0074	.0268	.0078	3.4246	-.0106	.0006	.0006	1.997	418.34
1.85	.0541	.0072	.0539	.0089	6.0205	-.0201	.0006	.0006	2.000	418.86
2.86	.0839	.0069	.0835	.0111	7.5181	-.0301	.0006	.0006	2.001	419.14
3.87	.1070	.0068	.1063	.0140	7.5729	-.0377	.0006	.0006	2.000	418.84
4.90	.1355	.0067	.1344	.0182	7.3711	-.0460	.0006	.0006	2.002	419.31
5.85	.1563	.0065	.1548	.0224	6.8989	-.0517	.0006	.0006	2.001	419.14
6.80	.1756	.0066	.1736	.0273	6.3458	-.0569	.0006	.0006	2.001	419.06
7.81	.1995	.0065	.1967	.0335	5.8651	-.0625	.0006	.0006	2.001	419.14
-.16	.0017	.0074	.0018	.0074	.2355	-.0020	.0006	.0006	2.001	419.11

SMOOTH DIHEDRAL

PROJECT 1298 RUN 162 MACH 2.60

ALPHA	CN	CA	CL	CD	L/D	CM	CAC	CDC	R/FT	DYN PRS
-5.13	-.1267	.0059	-.1257	.0172	-7.2923	.0413	.0006	.0006	1.999	399.54
-4.18	-.1058	.0061	-.1051	.0138	-7.6148	.0346	.0006	.0006	1.999	399.45
-3.17	-.0766	.0064	-.0761	.0106	-7.1862	.0250	.0006	.0006	1.999	399.47
-2.12	-.0511	.0066	-.0509	.0085	-6.0075	.0168	.0005	.0005	1.998	399.33
-1.17	-.0279	.0068	-.0278	.0074	-3.7484	.0083	.0005	.0005	2.000	399.59
-.12	.0030	.0071	.0031	.0071	.4308	-.0021	.0005	.0005	1.998	399.26
.86	.0227	.0071	.0226	.0075	3.0305	-.0093	.0005	.0005	1.999	399.42
1.85	.0472	.0069	.0469	.0084	5.5905	-.0176	.0005	.0005	1.999	399.57
2.86	.0719	.0067	.0715	.0102	6.9810	-.0260	.0005	.0005	1.999	399.45
3.83	.0958	.0065	.0952	.0129	7.3843	-.0341	.0005	.0005	1.999	399.38
4.86	.1231	.0064	.1221	.0168	7.2587	-.0415	.0006	.0006	1.999	399.49
5.89	.1465	.0063	.1451	.0213	6.8047	-.0481	.0006	.0006	1.999	399.52
6.89	.1677	.0063	.1657	.0263	6.2934	-.0541	.0006	.0006	1.999	399.42
7.85	.1893	.0063	.1867	.0321	5.8194	-.0590	.0006	.0006	1.999	399.40
-.12	-.0012	.0071	-.0012	.0071	-.1652	-.0009	.0005	.0005	1.999	399.47

SMOOTH DIHEDRAL

PROJECT 1298 RUN 164 MACH 2.80

ALPHA	CN	CA	CL	CD	L/D	CM	CAC	CDC	R/FT	DYN PRS
-5.18	-.1222	.0057	-.1211	.0167	-7.2427	.0387	.0005	.0005	2.002	379.11
-4.16	-.0960	.0059	-.0953	.0129	-7.4021	.0311	.0005	.0005	2.002	379.07
-3.13	-.0725	.0061	-.0720	.0101	-7.1549	.0234	.0005	.0005	2.001	379.05
-2.12	-.0473	.0064	-.0471	.0081	-5.8034	.0153	.0005	.0005	2.001	379.01
-1.15	-.0236	.0066	-.0235	.0071	-3.3341	.0075	.0005	.0005	2.001	378.95
-.14	-.0017	.0068	-.0016	.0068	-.2439	-.0002	.0005	.0005	2.004	379.45
.84	.0216	.0068	.0215	.0071	3.0263	-.0081	.0005	.0005	2.002	379.23
1.87	.0467	.0066	.0465	.0081	5.7371	-.0166	.0005	.0005	2.002	379.09
2.87	.0692	.0064	.0688	.0099	6.9660	-.0242	.0005	.0005	2.001	378.95
3.86	.0904	.0063	.0898	.0123	7.2682	-.0308	.0005	.0005	2.002	379.07
4.87	.1150	.0062	.1141	.0159	7.1516	-.0377	.0005	.0005	2.001	378.87
5.84	.1343	.0062	.1329	.0198	6.7234	-.0434	.0005	.0005	2.004	379.53
6.83	.1555	.0061	.1537	.0246	6.2565	-.0492	.0005	.0005	2.001	379.01
7.84	.1743	.0061	.1719	.0298	5.7712	-.0542	.0005	.0005	2.001	378.89
-.15	-.0023	.0068	-.0023	.0068	-.3330	-.0001	.0005	.0005	2.001	378.95

SMOOTH DIHEDRAL

PROJECT 1482 RUN 1 MACH 2.00

ALPHA	CN	CA	CL	CD	L/D	CM	CAC	CDC	R/FT	DYN PRS
-4.83	-.1318	.0050	-.1309	.0161	-8.1276	.0445	.0008	.0008	6.010	1347.74
-3.79	-.1022	.0054	-.1016	.0122	-8.3449	.0346	.0008	.0008	6.006	1346.31
-2.86	-.0754	.0059	-.0751	.0097	-7.7751	.0252	.0008	.0008	6.005	1346.49
-1.89	-.0475	.0064	-.0473	.0079	-5.9723	.0151	.0008	.0008	6.006	1346.81
-.85	-.0186	.0068	-.0185	.0071	-2.6136	.0049	.0008	.0008	6.007	1347.03
.16	.0082	.0069	.0082	.0069	1.1851	-.0048	.0008	.0008	6.008	1347.28
1.12	.0354	.0067	.0353	.0074	4.7638	-.0144	.0008	.0008	6.007	1347.06
2.18	.0652	.0064	.0650	.0089	7.3366	-.0249	.0008	.0008	6.006	1346.71
3.27	.0966	.0060	.0961	.0115	8.3521	-.0354	.0008	.0008	6.005	1346.56
4.18	.1212	.0057	.1205	.0145	8.2808	-.0429	.0008	.0008	6.008	1347.28
5.15	.1476	.0055	.1465	.0188	7.8115	-.0506	.0008	.0008	6.006	1346.81
6.20	.1753	.0053	.1737	.0242	7.1681	-.0579	.0008	.0008	6.007	1347.10
.10	.0074	.0069	.0074	.0069	1.0682	-.0045	.0008	.0008	6.006	1346.73

SMOOTH DIHEDRAL

PROJECT 1482 RUN 4 MACH 2.40

ALPHA	CN	CA	CL	CD	L/D	CM	CAC	CDC	R/FT	DYN PRS
-5.08	-.1303	.0048	-.1294	.0163	-7.9486	.0409	.0007	.0007	5.996	1333.01
-4.18	-.1079	.0054	-.1072	.0133	-8.0872	.0343	.0007	.0007	5.996	1333.07
-2.39	-.0556	.0054	-.0553	.0078	-7.1350	.0176	.0007	.0007	5.992	1332.32
-1.73	-.0381	.0061	-.0379	.0073	-5.2215	.0116	.0007	.0007	5.992	1332.19
-.97	-.0225	.0059	-.0224	.0062	-3.5821	.0063	.0007	.0007	5.992	1332.27
.22	.0098	.0064	.0098	.0065	1.5087	-.0045	.0007	.0007	5.996	1333.04
1.22	.0341	.0062	.0339	.0069	4.9015	-.0129	.0007	.0007	6.002	1334.42
2.03	.0518	.0061	.0515	.0079	6.5253	-.0192	.0007	.0007	5.997	1333.26
3.20	.0847	.0057	.0842	.0104	8.0943	-.0298	.0007	.0007	5.995	1332.85
4.12	.1071	.0055	.1065	.0131	8.0976	-.0367	.0007	.0007	5.998	1333.59
4.99	.1259	.0053	.1249	.0162	7.7053	-.0422	.0007	.0007	6.002	1334.36
5.68	.1412	.0051	.1400	.0191	7.3417	-.0466	.0007	.0007	5.993	1332.35
.37	.0143	.0062	.0142	.0063	2.2534	-.0060	.0006	.0006	5.995	1332.87

MEDIUM DIHEDRAL

PROJECT 1482 RUN 17 MACH 1.80

ALPHA	CN	CA	CL	CD	L/D	CM	CAC	CDC	R/FT	DYN PRS
-4.90	-.1553	.0073	-.1541	.0205	-7.5235	.0588	.0007	.0007	2.000	455.51
-3.92	-.1250	.0075	-.1242	.0160	-7.7717	.0478	.0008	.0008	2.002	455.91
-2.89	-.0910	.0078	-.0905	.0123	-7.3270	.0354	.0008	.0008	2.004	456.42
-1.88	-.0581	.0081	-.0578	.0100	-5.7568	.0229	.0008	.0008	2.004	456.38
-.90	-.0288	.0084	-.0287	.0089	-3.2283	.0117	.0008	.0008	2.004	456.38
.09	.0009	.0085	.0009	.0085	.1017	.0007	.0008	.0008	2.005	456.50
1.11	.0302	.0083	.0301	.0089	3.3839	-.0104	.0008	.0008	2.006	456.85
2.13	.0603	.0079	.0600	.0101	5.9337	-.0214	.0009	.0009	2.004	456.42
3.13	.0915	.0074	.0910	.0124	7.3337	-.0330	.0009	.0009	2.003	456.22
4.15	.1242	.0070	.1234	.0160	7.7203	-.0443	.0009	.0009	2.004	456.26
5.15	.1539	.0067	.1527	.0205	7.4333	-.0539	.0009	.0009	2.005	456.50
6.12	.1824	.0065	.1807	.0259	6.9632	-.0624	.0009	.0009	2.004	456.34
7.16	.2120	.0063	.2095	.0327	6.4085	-.0702	.0009	.0009	2.003	456.18
8.16	.2396	.0062	.2363	.0402	5.8822	-.0772	.0009	.0009	2.003	456.14
.13	.0018	.0084	.0018	.0084	.2109	.0001	.0008	.0008	2.005	456.54

MEDIUM DIHEDRAL

PROJECT 1482 RUN 24 MACH 2.00

ALPHA	CN	CA	CL	CD	L/D	CM	CAC	CDC	R/FT	DYN PRS
-4.86	-.1435	.0071	-.1424	.0193	-7.3970	.0527	.0007	.0007	2.001	448.78
-3.80	-.1117	.0073	-.1110	.0147	-7.5511	.0420	.0007	.0007	2.002	448.96
-2.82	-.0824	.0075	-.0819	.0115	-7.0977	.0313	.0007	.0007	2.003	449.18
-1.88	-.0541	.0078	-.0538	.0095	-5.6435	.0207	.0007	.0007	2.003	449.14
-.87	-.0249	.0080	-.0248	.0084	-2.9466	.0099	.0007	.0007	2.003	449.18
.12	.0019	.0080	.0019	.0080	.2314	-.0001	.0008	.0008	2.002	449.03
1.13	.0291	.0078	.0289	.0084	3.4349	-.0100	.0008	.0008	2.002	448.89
2.19	.0598	.0074	.0595	.0097	6.1371	-.0209	.0008	.0008	2.002	448.93
3.18	.0892	.0071	.0387	.0120	7.4037	-.0314	.0008	.0008	2.003	449.07
4.17	.1181	.0067	.1173	.0153	7.6803	-.0412	.0008	.0008	2.004	449.32
5.15	.1445	.0065	.1434	.0194	7.3774	-.0493	.0008	.0008	2.003	449.14
6.14	.1716	.0063	.1700	.0246	6.9081	-.0563	.0008	.0008	2.003	449.14
7.19	.1994	.0061	.1971	.0310	6.3489	-.0634	.0008	.0008	2.002	448.93
8.17	.2239	.0061	.2208	.0378	5.8410	-.0696	.0008	.0008	2.002	448.96
.15	.0032	.0080	.0032	.0080	.3970	-.0006	.0008	.0008	2.003	449.25

MEDIUM DIHEDRAL

PROJECT 1482 RUN 26 MACH 2.16

ALPHA	CN	CA	CL	CD	L/D	CM	CAC	CDC	R/FT	DYN PRS
-4.62	-.1298	.0071	-.1288	.0175	-7.3586	.0463	.0007	.0007	2.002	439.16
-3.61	-.1012	.0072	-.1005	.0136	-7.4132	.0368	.0007	.0007	2.005	439.75
-2.60	-.0727	.0074	-.0723	.0107	-6.7851	.0268	.0007	.0007	2.005	439.68
-1.59	-.0438	.0076	-.0436	.0088	-4.9407	.0164	.0007	.0007	2.003	439.39
-.61	-.0177	.0078	-.0177	.0080	-2.2095	.0068	.0007	.0007	2.002	439.23
.39	.0086	.0077	.0086	.0078	1.1017	-.0027	.0007	.0007	2.002	439.13
1.37	.0343	.0075	.0341	.0083	4.0956	-.0117	.0007	.0007	2.002	439.13
2.40	.0632	.0071	.0629	.0097	6.4565	-.0220	.0007	.0007	2.002	439.23
3.44	.0930	.0068	.0924	.0124	7.4787	-.0323	.0007	.0007	2.003	439.33
4.41	.1197	.0065	.1188	.0157	7.5779	-.0407	.0007	.0007	2.001	439.00
5.41	.1454	.0063	.1442	.0200	7.2179	-.0484	.0007	.0007	2.001	438.87
6.39	.1705	.0061	.1688	.0251	6.7345	-.0549	.0007	.0007	2.001	438.90
7.38	.1938	.0060	.1914	.0308	6.2119	-.0606	.0007	.0007	2.002	439.03
8.40	.2190	.0059	.2158	.0378	5.7037	-.0666	.0007	.0007	2.003	439.26
.41	.0095	.0077	.0095	.0078	1.2143	-.0031	.0007	.0007	2.002	439.16

MEDIUM DIHEDRAL

PROJECT 1482 RUN 6 MACH 2.40

ALPHA	CN	CA	CL	CD	L/D	CM	CAC	CDC	R/FT	DYN PRS
-5.00	-.1325	.0070	-.1314	.0186	-7.0753	.0461	.0006	.0006	2.003	419.69
-4.08	-.1093	.0071	-.1086	.0149	-7.2982	.0385	.0006	.0006	2.001	419.28
-3.05	-.0797	.0073	-.0792	.0115	-6.8909	.0289	.0006	.0006	2.004	419.91
-1.98	-.0525	.0074	-.0522	.0092	-5.6597	.0190	.0006	.0006	2.001	419.25
-.98	-.0259	.0075	-.0258	.0079	-3.2583	.0099	.0006	.0006	2.002	419.44
.02	.0008	.0076	.0008	.0076	.1016	.0005	.0006	.0006	2.004	419.83
1.03	.0259	.0074	.0257	.0079	3.2528	-.0084	.0006	.0006	2.002	419.50
2.04	.0529	.0071	.0527	.0090	5.8682	-.0182	.0006	.0006	2.002	419.42
3.04	.0753	.0068	.0748	.0108	6.9123	-.0257	.0006	.0006	2.004	419.94
4.10	.1060	.0065	.1053	.0141	7.4783	-.0359	.0006	.0006	2.001	419.25
5.12	.1330	.0063	.1320	.0181	7.2828	-.0434	.0006	.0006	2.005	420.08
6.05	.1512	.0061	.1497	.0220	6.8090	-.0489	.0006	.0006	1.998	418.56
7.01	.1727	.0060	.1707	.0270	6.3166	-.0549	.0006	.0006	2.003	419.77
7.99	.1965	.0059	.1937	.0331	5.8500	-.0605	.0006	.0006	2.003	419.77
.06	.0019	.0076	.0019	.0076	.2463	-.0002	.0006	.0006	2.004	419.88

MEDIUM DIHEDRAL

PROJECT 1482 RUN 10 MACH 2.60

ALPHA	CN	CA	CL	CD	L/D	CM	CAC	CDC	R/FT	DYN PRS
-4.89	-.1212	.0068	-.1202	.0171	-7.0415	.0428	.0005	.0005	2.004	400.44
-3.87	-.0988	.0068	-.0981	.0135	-7.2879	.0353	.0005	.0005	2.003	400.32
-2.85	-.0716	.0069	-.0712	.0104	-6.8300	.0262	.0005	.0005	2.004	400.40
-1.84	-.0460	.0070	-.0458	.0084	-5.4209	.0175	.0005	.0005	2.003	400.37
-.90	-.0217	.0071	-.0215	.0074	-2.8930	.0089	.0005	.0005	2.004	400.51
.07	-.0006	.0071	-.0006	.0071	-.0895	.0013	.0005	.0005	2.004	400.47
1.06	.0218	.0070	.0217	.0074	2.9412	-.0066	.0005	.0005	2.004	400.47
2.12	.0522	.0066	.0519	.0086	6.0667	-.0167	.0005	.0005	2.004	400.40
3.09	.0728	.0064	.0723	.0103	7.0200	-.0242	.0005	.0005	2.003	400.30
4.11	.0982	.0062	.0975	.0132	7.3938	-.0325	.0005	.0005	2.003	400.25
5.15	.1230	.0060	.1219	.0170	7.1593	-.0399	.0005	.0005	2.004	400.42
6.12	.1430	.0059	.1416	.0211	6.7159	-.0458	.0005	.0005	2.005	400.61
7.15	.1661	.0057	.1641	.0263	6.2401	-.0517	.0005	.0005	2.006	400.80
8.06	.1836	.0056	.1810	.0313	5.7881	-.0563	.0005	.0005	2.006	400.89
.07	-.0018	.0071	-.0018	.0071	-.2507	.0013	.0005	.0005	2.004	400.40

MEDIUM DIHEDRAL

PROJECT 1482 RUN 11 MACH 2.80

ALPHA	CN	CA	CL	CD	L/D	CM	CAC	CDC	R/FT	DYN PRS
-4.87	-.1131	.0065	-.1121	.0161	-6.9603	.0403	.0004	.0004	2.001	378.95
-3.88	-.0898	.0065	-.0892	.0126	-7.0729	.0327	.0004	.0004	2.000	378.70
-2.89	-.0708	.0065	-.0703	.0101	-6.9586	.0261	.0004	.0004	2.000	378.83
-1.87	-.0438	.0067	-.0436	.0081	-5.3817	.0175	.0004	.0004	2.000	378.72
-.89	-.0205	.0067	-.0204	.0071	-2.8898	.0096	.0004	.0004	1.999	378.56
.08	-.0025	.0067	-.0025	.0067	-.3776	.0028	.0004	.0004	2.000	378.83
1.10	.0241	.0065	.0240	.0070	3.4196	-.0057	.0004	.0004	1.999	378.66
2.07	.0452	.0063	.0449	.0080	5.6392	-.0133	.0004	.0004	2.000	378.76
3.07	.0678	.0062	.0674	.0098	6.8911	-.0207	.0004	.0004	1.998	378.38
4.07	.0886	.0059	.0880	.0122	7.2004	-.0276	.0004	.0004	1.999	378.50
5.09	.1127	.0058	.1117	.0158	7.0795	-.0345	.0004	.0004	1.999	378.62
6.10	.1345	.0056	.1331	.0199	6.6863	-.0406	.0004	.0004	1.999	378.66
7.11	.1564	.0056	.1545	.0249	6.2086	-.0465	.0005	.0004	2.001	379.01
8.10	.1768	.0055	.1743	.0304	5.7405	-.0518	.0005	.0004	2.001	378.89
.10	.0010	.0067	.0010	.0067	.1459	.0020	.0004	.0004	2.000	378.78

MEDIUM DIHEDRAL

PROJECT 1570 RUN 3 MACH 2.00

ALPHA	CN	CA	CL	CD	L/D	CM	CAC	CDC	R/FT	DYN PRS
-6.50	-.1986	.0067	-.1966	.0291	-6.7517	.0724	.0008	.0008	2.001	448.60
-4.56	-.1409	.0070	-.1399	.0182	-7.7015	.0533	.0008	.0008	2.000	448.46
-2.50	-.0774	.0074	-.0770	.0108	-7.1236	.0306	.0008	.0008	2.002	449.03
-.50	-.0173	.0080	-.0172	.0082	-2.1108	.0082	.0008	.0008	2.006	449.82
1.46	.0361	.0078	.0359	.0087	4.1384	-.0116	.0008	.0008	2.008	450.25
3.55	.0993	.0070	.0987	.0131	7.5275	-.0342	.0008	.0008	2.010	450.68
5.50	.1546	.0065	.1533	.0213	7.2093	-.0515	.0008	.0008	2.012	451.18
7.51	.2085	.0062	.2059	.0334	6.1617	-.0655	.0008	.0008	2.014	451.72
1.09	.0265	.0079	.0263	.0084	3.1440	-.0078	.0008	.0008	1.997	447.75

MEDIUM DIHEDRAL

PROJECT 1570 RUN 4 MACH 2.40

ALPHA	CN	CA	CL	CD	L/D	CM	CAC	CDC	R/FT	DYN PRS
-6.30	-.1732	.0066	-.1715	.0256	-6.7095	.0582	.0007	.0006	2.003	419.64
-4.26	-.1122	.0069	-.1114	.0152	-7.3227	.0399	.0007	.0006	2.002	419.55
-2.27	-.0592	.0071	-.0589	.0094	-6.2605	.0222	.0006	.0006	2.002	419.53
-.28	-.0077	.0075	-.0077	.0075	-1.0223	.0036	.0006	.0006	2.002	419.53
1.66	.0377	.0071	.0374	.0082	4.5541	-.0124	.0007	.0007	2.002	419.39
3.78	.1007	.0066	.1000	.0132	7.5851	-.0328	.0007	.0007	2.002	419.42
5.75	.1505	.0061	.1491	.0212	7.0400	-.0474	.0007	.0007	2.002	419.53
7.86	.2004	.0059	.1977	.0332	5.9489	-.0593	.0007	.0007	2.002	419.53
-.21	-.0028	.0075	-.0028	.0075	-.3769	.0025	.0006	.0006	2.002	419.47

MEDIUM DIHEDRAL

PROJECT 1570 RUN 7 MACH 2.80

ALPHA	CN	CA	CL	CD	L/D	CM	CAC	CDC	R/FT	DYN PRS
-6.04	-.1451	.0063	-.1436	.0216	-6.6608	.0491	.0005	.0005	2.002	379.13
-4.09	-.1007	.0064	-.0999	.0136	-7.3469	.0354	.0005	.0005	2.000	378.76
-2.14	-.0538	.0065	-.0536	.0085	-6.2736	.0200	.0005	.0005	2.001	378.99
-.14	-.0065	.0067	-.0065	.0067	-.9725	.0037	.0005	.0005	2.001	378.89
2.01	.0470	.0063	.0468	.0079	5.8975	-.0146	.0005	.0005	2.001	378.97
4.00	.0927	.0059	.0921	.0124	7.4349	-.0298	.0005	.0005	2.001	378.89
5.99	.1365	.0056	.1351	.0199	6.8038	-.0422	.0005	.0005	2.001	378.93
7.88	.1734	.0055	.1710	.0292	5.8540	-.0523	.0005	.0005	2.000	378.85
-.05	-.0010	.0067	-.0010	.0067	-.1510	.0018	.0005	.0005	2.001	378.91

MEDIUM DIHEDRAL

PROJECT 1570 RUN 8 MACH 2.40

ALPHA	CN	CA	CL	CD	L/D	CM	CAC	CDC	R/FT	DYN PRS
-6.33	-.1642	.0058	-.1625	.0239	-6.8035	.0524	.0007	.0007	2.003	419.66
-4.28	-.1138	.0062	-.1131	.0147	-7.7171	.0376	.0007	.0007	2.000	418.95
-2.34	-.0609	.0068	-.0605	.0093	-6.5356	.0197	.0007	.0007	2.000	419.00
-.28	-.0067	.0072	-.0067	.0072	-.9236	.0012	.0006	.0006	2.001	419.25
1.78	.0503	.0070	.0500	.0086	5.8204	-.0184	.0006	.0006	2.001	419.17
3.82	.1039	.0068	.1032	.0137	7.5582	-.0360	.0007	.0007	1.999	418.81
5.76	.1495	.0066	.1480	.0215	6.8735	-.0490	.0007	.0007	2.001	419.28
7.82	.2025	.0063	.1998	.0338	5.9096	-.0612	.0007	.0007	1.999	418.78
-.33	-.0067	.0073	-.0066	.0074	-.9015	.0013	.0006	.0006	2.000	419.11

MEDIUM DIHEDRAL

PROJECT 1570 RUN 9 MACH 2.80

ALPHA	CN	CA	CL	CD	L/D	CM	CAC	CDC	R/FT	DYN PRS
-6.05	-.1412	.0057	-.1398	.0205	-6.8126	.0448	.0005	.0005	1.999	378.50
-4.02	-.0911	.0059	-.0905	.0123	-7.3733	.0300	.0005	.0005	2.000	378.74
-2.04	-.0489	.0061	-.0486	.0079	-6.1794	.0159	.0005	.0005	2.000	378.76
.02	.0015	.0066	.0015	.0066	.2208	-.0011	.0005	.0005	2.001	378.91
1.95	.0466	.0064	.0464	.0080	5.8287	-.0167	.0005	.0005	2.002	379.15
3.95	.0921	.0062	.0914	.0125	7.3189	-.0314	.0005	.0005	2.000	378.76
5.94	.1363	.0061	.1349	.0201	6.7035	-.0437	.0005	.0005	2.000	378.85
7.95	.1776	.0060	.1751	.0305	5.7433	-.0549	.0005	.0005	2.001	378.95
-.04	.0011	.0066	.0011	.0066	.1695	-.0011	.0005	.0005	2.000	378.78

MEDIUM DIHEDRAL

PROJECT 1570 RUN 10 MACH 2.00

ALPHA	CN	CA	CL	CD	L/D	CM	CAC	CDC	R/FT	DYN PRS
-6.54	-.1879	.0058	-.1860	.0272	-6.8459	.0651	.0008	.0008	1.998	448.00
-4.54	-.1282	.0063	-.1273	.0164	-7.7600	.0460	.0008	.0008	1.999	448.35
-2.54	-.0680	.0069	-.0676	.0099	-6.8258	.0247	.0008	.0008	1.999	448.28
-.54	-.0107	.0077	-.0106	.0078	-1.3615	.0037	.0008	.0008	2.001	448.71
1.52	.0462	.0076	.0460	.0088	5.2335	-.0171	.0008	.0008	2.001	448.64
3.50	.1053	.0071	.1047	.0135	7.7387	-.0378	.0008	.0008	2.001	448.60
5.48	.1591	.0068	.1577	.0220	7.1718	-.0537	.0008	.0008	2.001	448.64
7.52	.2138	.0067	.2111	.0346	6.0969	-.0681	.0008	.0008	2.001	448.60
-.52	-.0086	.0077	-.0086	.0078	-1.0942	.0030	.0008	.0008	1.999	448.35

NASA
National Aeronautics and Space Administration

Report Documentation Page

1. Report No. NASA TP-2918	2. Government Accession No.	3. Recipient's Catalog No.
4. Title and Subtitle Effect of Milling Machine Roughness and Wing Dihedral on the Supersonic Aerodynamic Characteristics of a Highly Swept Wing		5. Report Date August 1989
		6. Performing Organization Code
7. Author(s) Christine M. Darden		8. Performing Organization Report No. L-16546
9. Performing Organization Name and Address NASA Langley Research Center Hampton, VA 23665-5225		10. Work Unit No. 505-69-01-01
		11. Contract or Grant No.
12. Sponsoring Agency Name and Address National Aeronautics and Space Administration Washington, DC 20546-0001		13. Type of Report and Period Covered Technical Paper
		14. Sponsoring Agency Code

15. Supplementary Notes

16. Abstract

An experimental investigation was conducted to assess the effect of surface finish on the longitudinal and lateral aerodynamic characteristics of a highly swept wing at supersonic speeds. The investigation also included a study of the effects of wing dihedral. Included in the tests were four wing models: three models having 22.5° of outboard dihedral, identical except for surface finish, and a zero-dihedral, smooth model of the same planform for reference. Of the three dihedral models, two were taken directly from the milling machine without smoothing—one having a maximum scallop height of 0.002 in. and the other a maximum scallop height of 0.005 in. The third dihedral model was hand finished to a smooth surface. Tests were conducted in Test Section 1 of the Langley Unitary Plan Wind Tunnel over a range of Mach numbers from 1.8 to 2.8, a range of angles of attack from $-5°$ to $8°$, and at a Reynolds number per foot of 2×10^6. Selected data were also taken at a Reynolds number per foot of 6×10^6. Drag coefficient increases, with corresponding lift-drag ratio decreases, were the primary aerodynamic effects attributed to increased surface roughness due to milling machine grooves. These drag and lift-drag ratio increments due to roughness increased as Reynolds number increased.

17. Key Words (Suggested by Authors(s)) Wind-tunnel testing, Numerical control milling, Supersonic speeds, Surface roughness, Wing dihedral	18. Distribution Statement Unclassified—Unlimited. Subject Category 02

19. Security Classif. (of this report) Unclassified	20. Security Classif. (of this page) Unclassified	21. No. of Pages 88	22. Price A05

NASA FORM 1626 OCT 86 NASA-Langley, 1989

For sale by the National Technical Information Service, Springfield, Virginia 22161-2171